On the evolution of an ice shelf melt channel at the base of Filchner Ice Shelf, from observations and viscoelastic modeling

Angelika Humbert[1,2], Julia Christmann[1], Hugh F. J. Corr[3], Veit Helm[1], Lea-Sophie Höyns[1,4], Coen Hofstede[1], Ralf Müller[5,6], Niklas Neckel[1], Keith W. Nicholls[3], Timm Schultz[5,6], Daniel Steinhage[1], Michael Wolovick[1], and Ole Zeising[1,2]

[1]Alfred-Wegener-Institut Helmholtz-Zentrum für Polar- und Meeresforschung, Bremerhaven, Germany
[2]University of Bremen, Department of Geosciences, Bremen, Germany
[3]British Antarctic Survey, Natural Environment Research Council, Cambridge, UK
[4]University of Bremen, Department of Mathematics and Computer Science, Bremen, Germany
[5]Institute of Applied Mechanics, University of Kaiserslautern, Kaiserslautern, Germany
[6]Division of Continuum Mechanics, Technical University of Darmstadt, Darmstadt, Germany

Correspondence: Angelika Humbert (angelika.humbert@awi.de)

Abstract. Ice shelves play a key role in the stability of the Antarctic Ice Sheet due to their buttressing effect. A loss of buttressing as a result of increased basal melting or ice shelf disintegration will lead to increased ice discharge. Some ice shelves exhibit channels at the base that are not yet fully understood. In this study, we present in-situ melt rates of a channel which is up to $330\,\mathrm{m}$ high and located in the southern Filchner Ice Shelf. Maximum observed melt rates are $2\,\mathrm{m\,a^{-1}}$. Melt rates

5　inside the channel decrease in the direction of ice flow and turn to freezing $\sim 55\,\mathrm{km}$ downstream of the grounding line. While closer to the grounding line melt rates are higher within the channel than outside, this relationship reverses further downstream. Comparing the modeled evolution of this channel under present-day climate conditions over 250 years with its present geometry reveals a mismatch. Melt rates twice as large as the present-day values are required to fit the observed geometry. In contrast, forcing the model with present-day melt rates results in a closure of the channel, which contradicts observations. Time series of melt rate measurements show strong tidally-induced variability in vertical strain-rates. We found no evidence of seasonality,

10　but discrete pulses of increased melting occurred throughout the measurement period. The type of melt channel in this study diminishes in height with distance from the grounding line and are hence not a destabilizing factor for ice shelves.

1 Introduction

Melt channels carved upward into the base of ice shelves have been hypothesized to destabilize ice shelves and are often linked

15　to enhanced basal melt (Le Brocq et al., 2013; Langley et al., 2014; Drews, 2015; Marsh et al., 2016; Dow et al., 2018; Hofstede et al., 2021a). At some locations, these channels increase in height with distance from the grounding line, thus reducing the structural strength of the ice shelf, while at other locations they diminish downstream, minimizing their influence on shelf integrity. It remains unknown why some channels diminish downstream and whether channels that diminish downstream are also locations of enhanced basal melt.

Channels at the base of ice shelves may form where subglacial channels beneath the inland grounded ice discharge fresh water into the ocean (Le Brocq et al., 2013), or they may arise arise from topographic features or from shear margins developing surface troughs when adjusting to flotation (Alley et al., 2019). Features like bedrock undulations or eskers underneath the grounded ice may also leave a channel-like imprint in the geometry of the floating shelf (Drews et al., 2017; Jeofry et al., 2018). In all cases, the geometry of the channel at the ice base will be altered by two factors: incision due to basal melt arising from oceanic heat and closure due to viscoelastic creep.

Surface troughs on ice shelves are linked to incisions at the ice base, thus either to melt channels (e.g. Le Brocq et al., 2013; Langley et al., 2014) or to basal crevasses (e.g. Humbert et al., 2015). The surface troughs are formed by viscoelastic deformations in the transition to buoyancy and buoyancy equilibrium itself. Channels at the ice base have been surveyed using radio echo sounding (Rignot and Steffen, 2008; Vaughan et al., 2012; Le Brocq et al., 2013; Dutrieux et al., 2014; Langley et al., 2014; Dow et al., 2018). Their typical dimensions range from $300 - 500 \, \mathrm{m}$ wide and up to $50 \, \mathrm{m}$ high (Langley et al., 2014) to $1 - 3 \, \mathrm{km}$ wide and $200 - 400 \, \mathrm{m}$ high (Rignot and Steffen, 2008). Channel flanks are not necessarily smooth but may form terrace structures in the lateral (across ice flow) dimension as shown by Dutrieux et al. (2014) for Pine Island Glacier, Antarctica. These terraces are separated by up to $50 \, \mathrm{m}$ high walls with steep slopes between $40°$ and $60°$.

Hofstede et al. (2021a) found a basal channel on Support Force Glacier at the transition to the Filchner Ice Shelf attributed to the outflow of subglacial water. The channel increases in height close to the grounding line and widens downstream. Between 7 and $14 \, \mathrm{km}$ from the grounding line, the flanks of the channel become steeper and terraces form on its sides, which are sustained over $38 \, \mathrm{km}$ from the grounding line, but with decreasing height between $14–38 \, \mathrm{km}$. Within this distance, the height of the channel varies only slightly from 170 to $205 \, \mathrm{m}$. This particular channel is the focus of this study.

Basal melt rates inside a channel underneath Ross Ice Shelf, Antarctica were found by Marsh et al. (2016) to be up to $22.2 \, \mathrm{m \, a^{-1}}$ near the grounding line and only $2.5 \, \mathrm{m \, a^{-1}}$ for observations $40 \, \mathrm{km}$ downstream. In the lateral direction, the melt rate is only $0.82 \, \mathrm{m \, a^{-1}}$ demonstrating enhanced melt inside the channel compared to its surroundings. At Pine Island Glacier, Antarctica, Stanton et al. (2013) found basal melt rates of up to $24 \, \mathrm{m \, a^{-1}}$ and an across-channel variability that they suggested to be related to channelized flow. The decrease of channel melt rates with distance downstream is likewise described by Le Brocq et al. (2013). Buoyant fresh water initially enhances basal melting inside the channel by increasing the vigor of the turbulent plume at the ice base and entraining more ambient warm water Jenkins and Doake (1991). However, at some point the rising plume can become super-cooled due to the falling pressure, which leads to the formation of frazil ice and freeze-on. This is a general feature of the thermohaline circulation underneath ice shelves (e.g. MacAyeal, 1984). Similar to Le Brocq et al. (2013), Marsh et al. (2016) assumed that the channel at Ross Ice Shelf is formed by the outflow of subglacial meltwater. Washam et al. (2019) found high seasonal variability in basal melting within a channel at Petermann Gletscher, Greenland. In summer, melt rates reached a maximum of $80 \, \mathrm{m \, a^{-1}}$, whereas in winter, melt rates were below $5 \, \mathrm{m \, a^{-1}}$. They suggested that increased subglacial discharge during summer strengthens ocean currents under the ice which drives the high melt rates. Besides seasonal variability, melt rates also change within smaller periods. Vaňková et al. (2020) identified melt rate variations at the semi-diurnal $\mathrm{M_2}$ tidal constituent at six of 17 locations at Filchner-Ronne Ice Shelf, Antarctica. In-situ observations of

melt rates in sub ice shelf channels are often conducted with a phase sensitive Radio Echo Sounder (pRES), which is described
55 in more detail below.

Modeling basal melt rates adequately requires fully coupled ice-ocean models, that evaluate the energy balance at the ice-ocean transition to compute basal melt rates. While none of the global circulation models deals with ice shelf cavities, there are some coupled ice-sheet-ocean models simulating large scale basal melt rates (Gwyther et al., 2020; Dinniman et al., 2016; Jourdain et al., 2017; Seroussi et al., 2017; Timmermann and Hellmer, 2013; Galton-Fenzi et al., 2012). However, only a few
60 of them incorporate melt channels as this requires very high horizontal resolution: Gladish et al. (2012) showed that channels confine the warm water and stabilize the ice shelf by preventing melt on broader spatial scales. This conclusion is affirmed by Millgate et al. (2013) who found that an increasing number of melt channels lead to a decreasing overall mean melt rate. Our study will provide an observational dataset of basal melt rates that allows understanding these types of modeling results.

The change in geometry due to mechanical deformation is another important contribution to the evolution of basal channels.
65 The spatial gradients in displacement u lead to strain ε that causes a change in ice thickness. This process is governed by the viscoelastic nature of a Maxwell fluid for ice. While ice is reacting purely viscously on long time scales, its behavior on short time scales is elastic (Reeh et al., 2000; Gudmundsson, 2011; Sergienko, 2013; Humbert et al., 2015; Christmann et al., 2016; Schultz, 2017; Christmann et al., 2019). The transition from grounded to floating ice and short term geometry changes due to basal melt or accumulation are examples of ice affected by the elastic response. Over time scales of years, viscous creep
70 becomes more relevant. As a consequence, the geometry of melt channels needs to be modeled using viscoelastic material models based on a characteristic Maxwell time of $153\,\mathrm{d}$ (deduced in the model section) arising from the material parameters used for this study.

In this study, we present in-situ melt rates of a large melt channel feature in the southern Filchner Ice Shelf at the inflow from Support Force Glacier (SFG). Field measurements and satellite-borne data provide constraints to investigate how this feature
75 evolves using numerical modeling. In addition to the spatial distribution of basal melt, we analyze the temporal evolution of melt rates. We split this manuscript into two main parts, starting with observations followed by a modeling section. We present the methodology and the results in each part separately. A synthesis then follows focusing on the evolution of the melt channel.

2 Observations

2.1 Data acquisition

80 We acquired data at a melt channel on the southern Filchner Ice Shelf under the framework of the Filchner Ice Shelf Project (FISP). We performed 44 phase-sensitive radar (pRES) measurements (locations are shown in Fig. 1) in the season 2015/16, that have been repeated in 2016/17 as Lagrangian-type measurements. These measurements were taken in 13 cross-sections ranging from 14 to $61\,\mathrm{km}$ downstream from the grounding line (Fig. 1). This allows us to investigate the spatial variability of basal melt rates. At each cross-section, up to four measurements were performed at different locations: at the steepest western
85 flank (SW), at the lowest surface elevation (L), at the steepest eastern flank (SE) and outside east of the channel (OE; Fig. 1b). In order to achieve an all-year time series, one autonomous pRES (ApRES) station was installed (Fig. 1b). This instrument

3
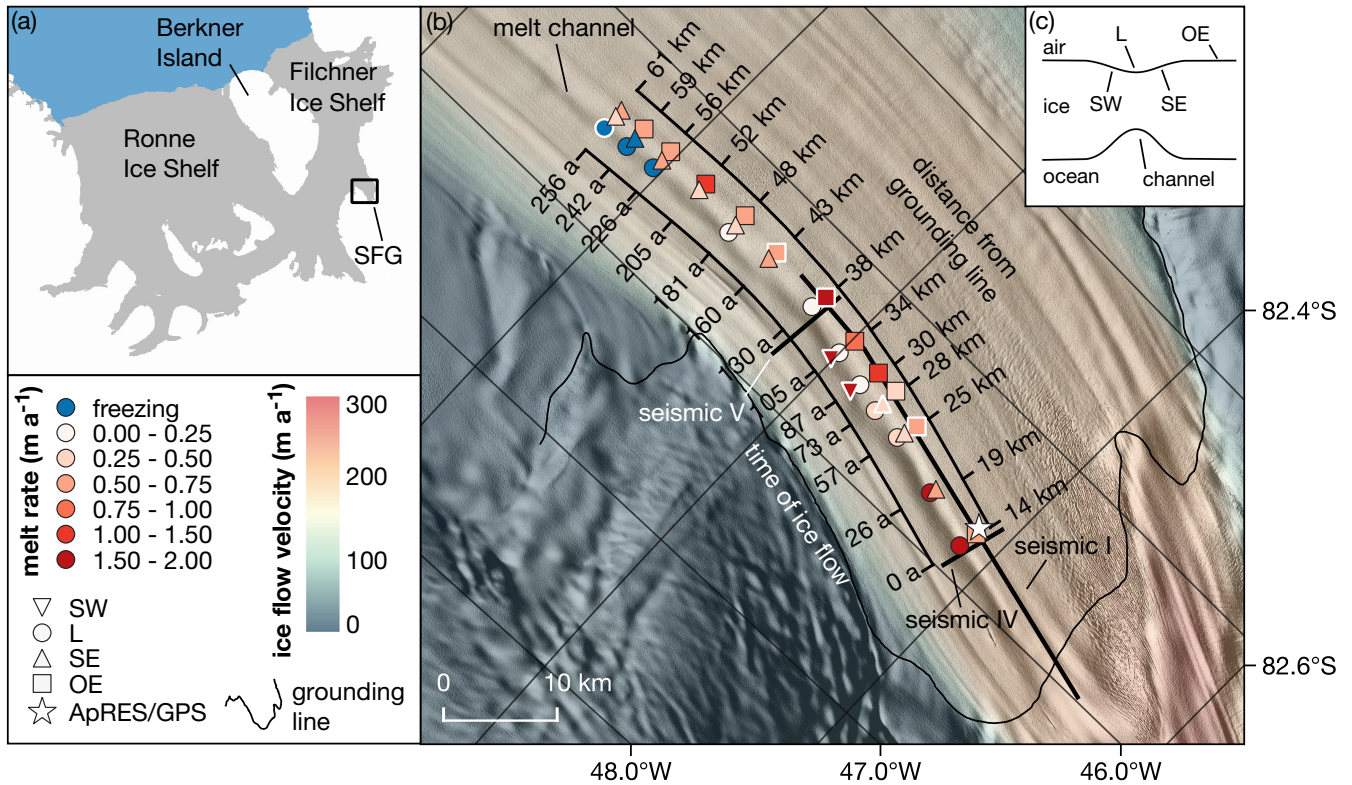
Figure 1. (a) Map of the Ronne and Filchner ice shelves. The study area near the Support Force Glacier (SFG) is marked with a black box. (b) Study area with pRES-derived basal melt rates at 13 cross-sections of the melt channel. The different symbols indicate the position relative to the channel, as shown in (c). Those melt rates derived from a nadir and an off-nadir basal return are marked with a white outline. For each cross-section, the distance from the grounding line and the duration of ice flow from the location furthest upstream are given. The location of an ApRES/GPS station is shown by a star. The seismic I, IV and V lines mark the location of active seismic profiles (Hofstede et al., 2021a, b). The background is a hillshade of the Reference Elevation Model of Antarctica (Howat et al., 2018, 2019) overlaid by the ice flow velocity (Hofstede et al., 2021a). (c) Sketch of a cross-section of the channel with measurement locations on the steepest western surface flank (SW), at the lowest surface elevation (L), on the steepest eastern surface flank (SE) and outside east of the channel (OE).

performed autonomous measurements every two hours resulting in 4342 measurements between 10 January 2017 and 6 January 2018. One year earlier, a GPS station was also in operation at this point from December 24, 2015 to May 5, 2016, the data of which we use for tidal analysis. To distinguish the single-repeated measurements from the autonomous measurements, we

90   refer to them as *pRES* and *ApRES* measurements, respectively.

4

2.2 Materials and methods

2.2.1 pRES device and processing

The pRES device is a low-power, ground-based radar that allows for estimating displacement of layers from repeated measurements with a precision of millimeters (Brennan et al., 2014). This accuracy enables the investigation of even small basal melt rates, taking into account snow accumulation together with firn compaction and strain in the vertical direction (Corr et al., 2002; Jenkins et al., 2006). The pRES is a frequency modulated continuous wave (FMCW) radar that transmits a sweep, called *chirp*, over a period of one second with a center frequency of $300\,\text{MHz}$ and bandwidth of $200\,\text{MHz}$ (Nicholls et al., 2015). For a better signal to noise ratio, the single-repeated measurements were performed with 100 chirps per measurement and the measurements of the time series with 20 chirps due to memory and power limitations. After collecting the data, anomalous chirps within each burst were removed and the remaining chirps were stacked. Anomalous chirps were identified by correlating each chirp with every other chirp of the burst. Those with a low correlation coefficient on average were rejected.

We followed Brennan et al. (2014) and Stewart et al. (2019) for data processing to get amplitude- and phase-depth profiles. The final profile that contains the amplitude and phase information as a function of two-way travel time was obtained from a Fourier transformation. To convert two-way travel time into depth, the propagation velocity of the radar wave is computed following Kovacs et al. (1995). For this the vertical ice/firn density profile is required. Here we use a model described by Herron and Langway (1980). As input parameters, accumulation rate and mean annual temperature are needed, for which we use data from the regional climate model RACMO 2.3/ANT (van Wessem et al., 2014, multi-annual mean 1979 – 2011). Despite the correction of higher propagation velocities in the firn, the uncertainty of the velocity and thus of the depth is 1% (Fujita et al., 2000).

2.2.2 Basal melt rates from repeated pRES measurements

The method for determining basal melting rates, previously described by e.g. Nicholls et al. (2015) and Stewart et al. (2019), is based on the ice thickness evolution equation. The change in ice thickness over time $\partial H / \partial t$ consists of components arising from deformation and accumulation/ablation at both interfaces (e.g. Zeising and Humbert, 2021). As our observations are discrete in time, the change of ice shelf thickness ΔH within the time period Δt, that is caused by changes at the surface and in the firn ΔH_s (e.g. snow accumulation/ablation and firn compaction), by strain in vertical direction ΔH_ε and by thickness changes due to basal melt ΔH_b is considered:

$$\frac{\Delta H}{\Delta t} = \frac{\Delta H_s}{\Delta t} + \frac{\Delta H_\varepsilon}{\Delta t} + \frac{\Delta H_b}{\Delta t} \tag{1}$$

(Vaňková et al., 2020; Zeising and Humbert, 2021). In order to obtain the basal melt rate, the change in ice thickness must be adjusted for the other contributions. Snow accumulation/ablation, firn compaction but also changes in radar hardware or settings (a different pRES instrument was used for the revisit) can cause a vertical offset near the surface that cannot be distinguished from one another. Following Jenkins et al. (2006), we aligned both measurements below the firn-ice transition. To this end, we computed the depth of pore closure h_{pc} takes place, i.e. the depth at which a density of $830\,\text{kg}\,\text{m}^{-3}$ is reached.

We apply the densification model (Herron and Langway, 1980) and mean annual accumulation rate and temperature from the multi-year mean RACMO2.3 product (van Wessem et al., 2014). In our study area, h_{pc} varies between $62\,\mathrm{m}$ and $71\,\mathrm{m}$. The actual alignment is based on a correlation of the amplitudes for a window of $6\,\mathrm{m}$ around h_{pc}. No reliable alignment could be obtained from the correlation for nine stations because the correlations of the surrounding depths resulted in ambiguous alignments. As a consequence, these stations were not considered.

After the alignment, the change in the ice thickness H_i below the pore closure depth h_{pc} is only affected by vertical strain and basal melt. Thus the basal melt rate a_b (positive for melting, negative for freezing) is

$$a_b = -\frac{\Delta H_b}{\Delta t} = -\left(\frac{\Delta H_i}{\Delta t} - \frac{\Delta H_\varepsilon}{\Delta t}\right) \tag{2}$$

with ΔH_ε being the thickness change due to vertical strain $\varepsilon_{zz}^{\mathrm{obs}}$. ΔH_ε is derived from integrating $\varepsilon_{zz}^{\mathrm{obs}}$ from the aligned reflector at h_{pc} to the ice base h_b

$$\Delta H_\varepsilon = \int_{\overline{h_b}}^{h_{\mathrm{pc}}} \varepsilon_{zz}^{\mathrm{obs}}\,\mathrm{d}z. \tag{3}$$

Here, $\overline{h_b}$ denotes the average depth of the ice base of the measurements. The vertical strain is defined as

$$\varepsilon_{zz}^{\mathrm{obs}} = \frac{\partial u_z}{\partial z} \tag{4}$$

with the displacement in vertical direction u_z.

In order to determine u_z, we followed the method described by Stewart et al. (2019). We divided the first measurement in segments of $6\,\mathrm{m}$ width with $3\,\mathrm{m}$ overlap from a depth of $20\,\mathrm{m}$ below the surface to $20\,\mathrm{m}$ above the ice base. To determine vertical displacements, we cross-correlated each segment of the first measurement with the repeated measurement. The lag of the largest amplitude correlation coefficient was used to find the correct minimum phase difference, from which we derived the vertical displacement. Since noise prevents the reliable estimation of the vertical displacement from a certain depth on, we calculated the depth at which the averaged correlation of unstacked chirps undercuts the empirical value of 0.65. We name this the noise-level depth limit h_{nl}, which is $743\,\mathrm{m}$ on average in this study area. Only those segments located below h_{pc} and above h_{nl} were used to avoid densification processes and noise to influence the strain estimation. A linear regression was calculated from the shifts of the remaining segments, assuming a constant vertical strain distribution over depth as the overall trend. However, at six stations, all in the hinge zone where the ice is bent by tides, we observed a slight deviation from a linear trend at deeper layers (Fig. A1a). A depth-dependent tidal vertical strain caused by tidal bending near the grounding line was also found by e.g. Jenkins et al. (2006) and Vaňková et al. (2020), although the long-term vertical strain was found to be depth independent (Vaňková et al., 2020). The segments that indicate a non-linear distribution are located below h_{nl} and are hence not taken into account for the regression. Nevertheless, we want to provide a lower limit of $|\Delta H_\varepsilon|$ considering other forms of strain-depth relations (Jenkins et al., 2006). For this purpose, we use a strain model that is decreasing linearly from half the ice

thickness (approximately h_{nl}) to the depth of at which $\varepsilon_{zz}^{\mathrm{obs}} = 0$ (Fig. A1b). This serves as a lower limit of $|\Delta H_\varepsilon|$, whereas a linear $\varepsilon_{zz}^{\mathrm{obs}}(z)$ gives the upper limit. The average of both gives ΔH_ε and the difference the <mark>uncertainty.</mark>

In order to derive ΔH_i, we used a wider segment of $10\,\mathrm{m}$ around the basal return, which was identified by a strong increase
155 in amplitude. Its upper limit is located $9\,\mathrm{m}$ above the basal return, while the lower limit is defined $1\,\mathrm{m}$ below the basal return. The vertical displacement of the ice base and thus the change in ice thickness was obtained from the cross-correlation of the basal segment. However, more than one strong basal reflection occurred at 7 sites. For these sites, we averaged the melt rates we derived from both basal segments. In Appendix A1 we discuss the identification of the basal reflection and the influence of off-nadir basal returns on the estimation of basal melt rates (Tab. A1, Figs. A2 and A3).

160 The uncertainty of the melt rate results mainly from the alignment of the repeated measurement and the uncertainty of ΔH_ε. This leads to uncertainties in the melt rate of up to $0.26\,\mathrm{m\,a^{-1}}$ for locations in the hinge zone, while at other locations the uncertainty is predominantly in the range of $< 0.05\,\mathrm{m\,a^{-1}}$. At those stations where the melt rate was averaged, the error represents the difference of the two melt rates. Since this difference is up to $1.34\,\mathrm{m\,a^{-1}}$, the error significantly exceeds $0.26\,\mathrm{m\,a^{-1}}$ in some cases.

165 In order to classify how representative the melt rates are for the past, we reconstructed the ice thickness based on the values derived from the pRES measurements. First, we linearly interpolated a_b, ΔH_ε and ΔH_s along the distance of the channel to get continuous values between the cross-sections and smoothed the results in order to obtain a trend for each process. We converted the distance from the upstream-most cross-section to an age beyond this cross-section by assuming the mean flow velocity is constant in time and space. Next, we treat the change in ice thickness as a transport equation. To this end, we
170 compute the advection of the ice thickness along the flowline under present day climate conditions (H_{PDadv}). For this we use interpolated functions of $a_b(t)$, $\Delta H_\varepsilon(t)$ and $\Delta H_s(t)$. The expected ice thickness at H_{PDadv} is then the thickness at $t_0 = 0\,\mathrm{a}$ plus the cumulative change in ice thickness:

$$H_{\mathrm{PDadv}}(t) = H(t_0) + \int_{t_0}^{t} \left(\Delta H_s(t') + \Delta H_\varepsilon(t') + a_b(t') \right) dt'. \tag{5}$$

We can invert this and calculate a synthetic melt rate $a_b^{\mathrm{syn}}(t)$ that reconstructs the observed ice thickness H:

$$175 \quad H(t) = H(t_0) + \int_{t_0}^{t} \left(\Delta H_s(t') + \Delta H_\varepsilon(t') + a_b^{\mathrm{syn}}(t') \right) dt'. \tag{6}$$

Descriptions of the symbols are given in Tab. A2.

2.2.3 Basal melting from ApRES time series

The processing of the autonomous measured time series with a 2-hour measurement interval differs slightly from the single-repeated measurements. For the ApRES time series, the instrument was located below the surface, thus snow accumulation had
180 no influence on the measured ice thickness and an alignment of the measurements is not necessary. This gives the possibility to determine the firn compaction ΔH_f. Without the alignment, thickness change due to strain needs to be considered for the

whole ice thickness H

$$\Delta H_\varepsilon = \int\limits_0^H \varepsilon_{zz}^{\text{obs}} \, \mathrm{d}z. \tag{7}$$

For processing, we followed the method described by Zeising and Humbert (2021), which differs slightly from the processing applied by Vaňková et al. (2020). Similar to processing of the single-repeated measurements, we divided the first measurement into the same segments and calculated the cross-correlation of the first measurement (t_1) with each repeated measurement (t_i). The displacement was obtained by the lag of the minimum phase difference. To avoid half-wavelength ambiguity due to phase wrapping, we limited the range of expected lag based on the displacement derived for the period $t_1 - t_{i-1}$.

The estimation of the vertical strain for the period $t_1 - t_i$ is based on a regression analysis of the vertical displacements for chosen segments. Only those segments located below a depth of $70 \, \mathrm{m}$ and above the noise-level depth limit of $h \approx 600 \, \mathrm{m}$ were used to avoid densification processes and noise influencing the strain estimation. Assuming constant strain over depth, the regression analysis gives the vertical strain and the cumulative displacement $u_z(z)$ is

$$u_z(z) = \varepsilon_{zz}^{\text{obs}} z + \Delta H_f \tag{8}$$

where the intercept at the surface is the firn compaction ΔH_f. Similar to determination of ΔH_i of the single-repeated measurements, we derived the change in ice thickness ΔH for a wider segment of $10 \, \mathrm{m}$. The cumulative melt of the ApRES time series was finally derived by

$$\Delta H_b(t) = -\int\limits_{t_1}^t \left(\Delta H(t') - \Delta H_\varepsilon(t') - \Delta H_f(t') \right) dt'. \tag{9}$$

In order to investigate if the basal melt is affected by tides, we first de-trended the cumulative melt time series and computed the frequency spectrum afterwards.

Subsequently, we used the time series of $\Delta H(t)$ to investigate the occurrence of melt events. We de-tided $\Delta H(t)$ by subtracting a harmonic fit based on frequencies up to the solar annual constituent and calculated the thinning rate afterwards. Assuming that basal melt causes changes on short time scales of several days, we attribute abrupt increases in the thinning rate to basal melt anomalies.

2.2.4 Global Positioning System (GPS) processing

The GPS processing is similar to the method used by Christmann et al. (2021). With the Waypoint GravNav 8.8 processing software, we applied a kinematic precise point positioning (PPP) processing for the GPS data that were stored in daily files. We merged three successive daily solutions to enable full day overlaps avoiding jumps between individual files. Afterwards, we combined the files in the middle of each 1-day overlap using relative point to point distances and removed outliers. The data has been low-pass filtered for frequencies higher than $1/3600 \, \mathrm{Hz}$. For tidal analysis, we calculated the power spectrum of the vertical displacement.

8

2.2.5 Digital Elevation Model (DEM)

We use the TanDEM-X PolarDEM 90m Digital Elevation data product provided by the German Aerospace Center (DLR) as reference elevation model (DLR, 2020). As the elevation values represent ellipsoidal heights relative to the WGS84 ellipsoid we refer the PolarDEM to the EIGEN-6C4 Geoid (Foerste et al., 2014). In the following, we refer the DEM heights above Geoid as observed surface elevation h_{TDX}. The absolute vertical height accuracy of the PolarDEM is validated against ICESat data and given to be $< 10\,\mathrm{m}$ (Rizzoli et al., 2017). For our region of interest the accuracy is given to be $< 5\,\mathrm{m}$ as shown in Fig. 16 of Rizzoli et al. (2017).

2.3 Results and discussion of observations

2.3.1 Spatial melt rate distribution around basal channel

We were able to determine basal melt rates at 34 of the 44 single-repeated pRES measurements. At some of the excluded stations, low correlation values prevented the alignment at the firn-ice transition or the estimation of the vertical strain. At others, a change in the shape of the first basal return prevented the determination of the change in ice thickness.

The estimated basal melt rates range from 0 to $2\,\mathrm{m\,a^{-1}}$, with the largest melt rates on the steepest western flank (SW) of the channel (Fig. 2a). A trend of decreasing melt rates in the along channel direction was found at the highest part (L) of the channel. Here, melt rates decrease from $1.8\,\mathrm{m\,a^{-1}}$ to basal freezing, measured at the three most downstream cross-sections. Outside of the channel (OE), basal melt rates are more variable without a trend. Stations at the eastern flank (SE) show a lower range of variability. Here, a_b varies between basal freezing and $0.8\,\mathrm{m\,a^{-1}}$.

The height of the channel (difference in ice thickness between L and OE; Fig. 2b) increases from about $200\,\mathrm{m}$ at the southernmost cross-section to a maximum of about $330\,\mathrm{m}$ over a distance of $20\,\mathrm{km}$ in ice flow direction. At this location the melt rates within the channel fall below those outside the channel and the height of the channel decreases, reaching $\sim 100\,\mathrm{m}$ at the northernmost cross-section.

In Fig. 2c we display the melt rates as a function of ice-shelf draft, derived from the TanDEM-X surface elevation and the pRES ice thickness. The melt rates outside the channel (OE) seem to be independent of the ice-shelf draft, while inside the channel (L) the melt rates decrease with reduced draft. However, melt rates at the largest draft inside the channel are approx. three times larger than those outside the channel or at the steepest eastern flank (SE) at similar draft.

The distribution of ΔH_ε shows a significant thickening of more than $1\,\mathrm{m\,a^{-1}}$ at the most upstream cross-section at L and OE (Fig. A4). In the ice flow direction, ΔH_ε declines, reaching about zero above the channel at the cross-section furthest downstream. In contrast, outside the channel, strain-thinning occurred from $30\,\mathrm{km}$ downstream the grounding line. The change in ice thickness due to firn compaction and accumulation is close to zero in the entire study area (Fig. A4).

However, the measurements only show a snapshot, as the variability on longer time scales is unknown. Based on the interpolated melt rates, ΔH_ε and ΔH_s along the channel (solid lines in Fig. 3a and A4), we computed the advected ice thickness under present day climate conditions H_{PDadv} (solid lines in Fig. 3b). The comparison of H_{PDadv} with the measured ice thickness
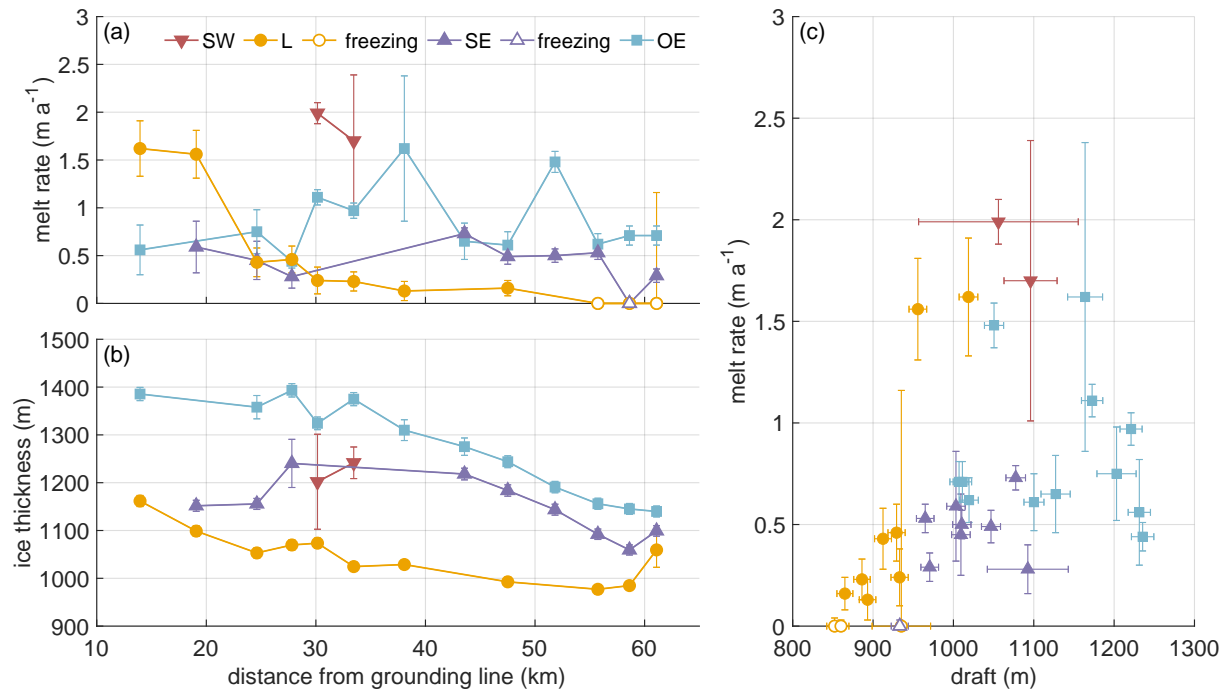
Figure 2. Spatial distribution of pRES-derived (a) basal melt rates (positive a_b represents melting) and (b) ice thickness at the locations SW (red), L (yellow), SE (purple) and OE (blue) around the channel as a function of distance from the grounding line. (c) Melt rate as a function of ice draft obtained from pRES-derived ice thickness and h_{TDX}.

245   (dashed lines) shows large differences of up to $185\,\text{m}$ above the channel. While the observed ice thickness decreases rapidly above the channel, H_{PDadv} remains almost constant. In contrast, no significant differences between the observed ice thickness and H_{PDadv} can be identified outside the channel. If the present day melt rates were representative of the long-term mean, the channel would close within 250 years, as the difference in H_{PDadv} above and outside the channel reaches zero. However, since the channel still exists beyond the northern end of our study area, it can be concluded that the melt rates in the channel must

250   have been higher in the past. How large the melt rates must have been on average can be deduced from the reconstruction of the existing ice thickness. The resulting synthetic average melt rate in the channel is about twice as high as the observed melt rates, reaching $3.5\,\text{m}\,\text{a}^{-1}$ in the upstream area (yellow dashed line in Fig. 3a). Assuming a steady state ice thickness upstream of the study area (supported by low elevation change found in (Helm et al., 2014)) and constant vertical strain and accumulation in the past, this indicates that melt rates in the last 250 years have been significantly higher than observed now.

255   In addition to the observations we have presented in this section, we show the pRES-derived vertical displacement profiles in section 3.2.2 together with simulations.
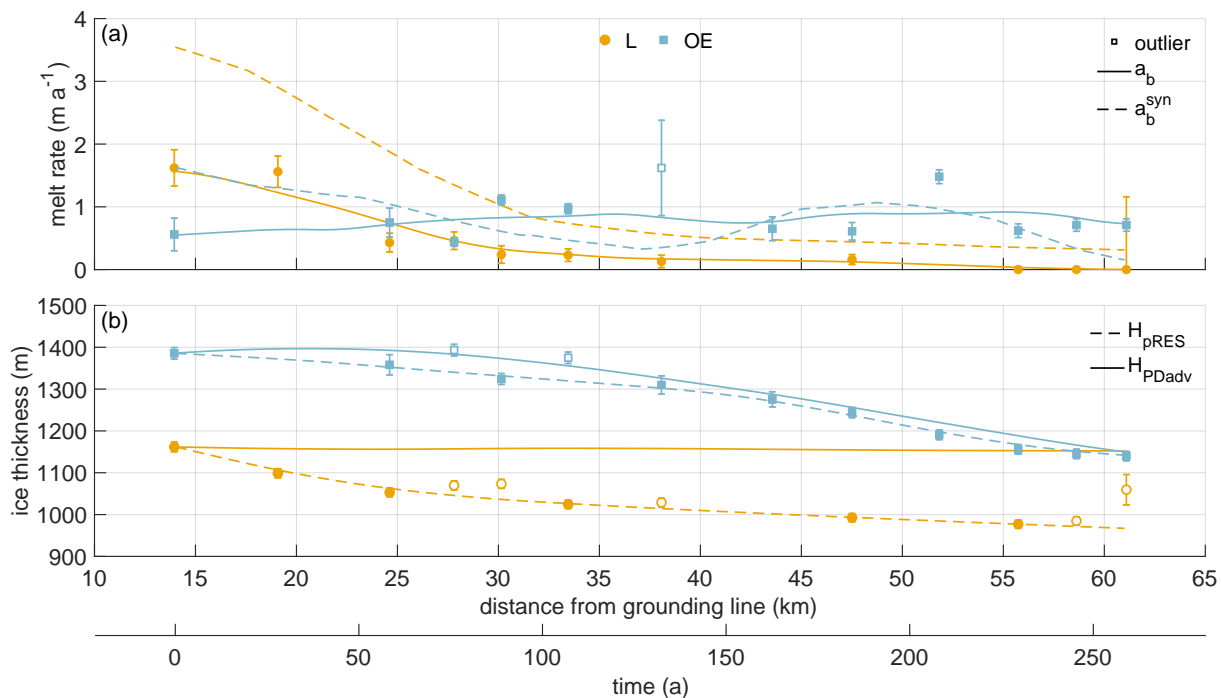
Figure 3. (a) Melt rates at locations L (yellow) and OE (blue) are shown by dots (L) and squares (OE). The interpolated melt rates (a_b) are shown by solid lines and synthetic melt rates (a_b^{syn}) that are necessary to reproduce H_{pRES} at L and OE are shown by dashed lines. (b) Ice thickness at locations L (yellow) and OE (blue) are shown by dots (L) and squares (OE). The interpolated ice thicknesses (H_{pRES}) are shown by dashed lines and the advected ice thicknesses under present day climate conditions (H_{PDadv}) from the observed melt rates at L and OE are shown by solid lines. The two x-axes show the distance from the grounding line in kilometers and the duration of ice flow in years from the measurement location furthest upstream. Unconsidered observations were marked as outliers. Error bars mark the uncertainties of the pRES-derived values.

2.3.2 Time series of basal melting

The ApRES time series outside the melt channel reveals an average melt rate of $0.23\,\mathrm{m\,a^{-1}}$ (Fig. 4a). A look at the monthly mean melt rates shows increased melt during the summer months (January, February and November, December) in comparison with the winter season. In these months the melt rates show values from more than $0.3\,\mathrm{m\,a^{-1}}$ up to $0.62\,\mathrm{m\,a^{-1}}$. The spectral analysis of the unfiltered cumulative melt time series shows all main diurnal and semi-diurnal constituents, which is in accordance with the frequencies observed from the GPS station (Fig. A5).

The presence of the tidal induced signal prevents a robust analysis of the basal melt rate as a high resolution time series. Nevertheless, to investigate the occurrence of non-tidal melt anomalies, we analyzed the time series of $\Delta H(t)$ after it was de-tided. The resulting de-tided thinning rate shows several melt anomalies distributed over the entire measurement period (Fig. 4b). These events lasted from a several hours to a few days and melted up to $1.5\,\mathrm{cm}$ of ice.

11
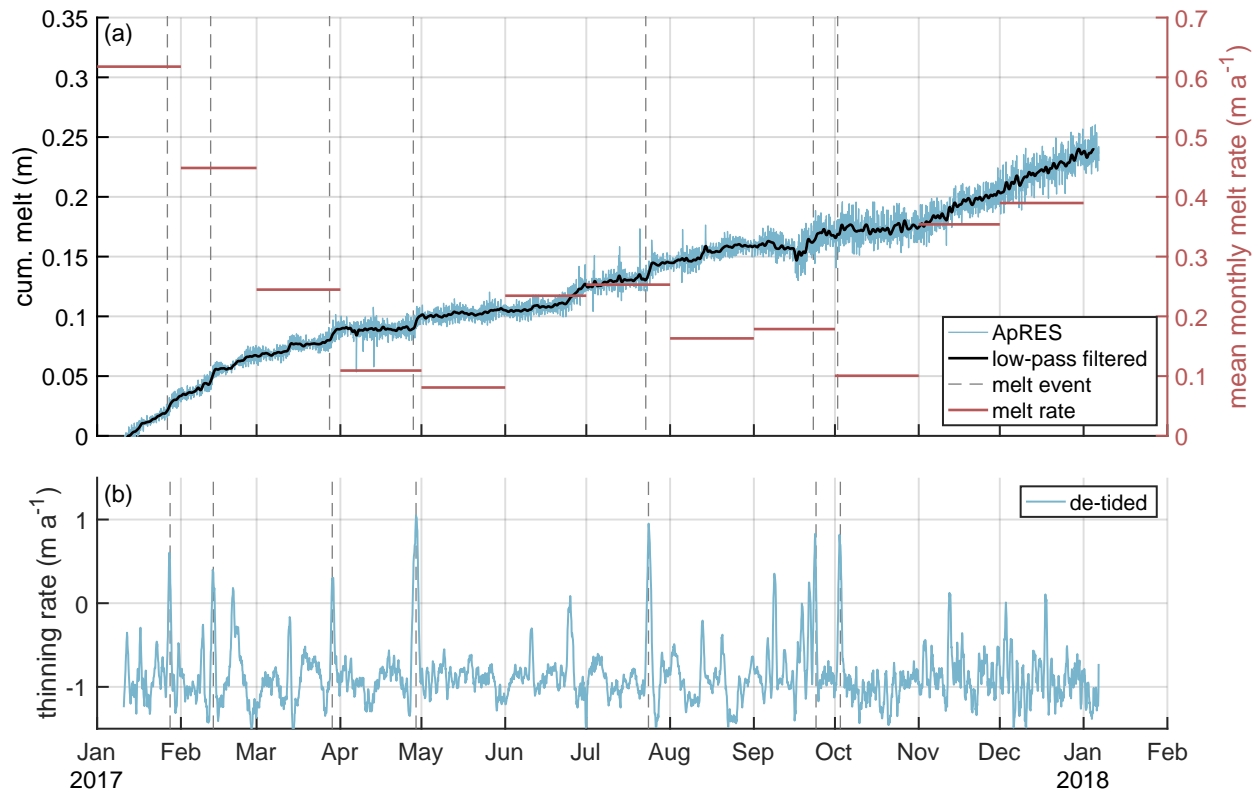
Figure 4. Time series of basal melting at ApRES location outside the channel. (a) Cumulative melt (blue line, left y-axis) over measurement period from 10 January 2017 to 6 January 2018 with low-pass filtered time series (black line). In September 2017, a malfunction of the ApRES caused a change of the attenuation which resulted in a noisier time series. Monthly mean melt rates are shown by red lines on the right y-axis. (b) Thinning rate after subtracting of the tidal signal (blue line). The dashed gray lines in (a) and (b) mark stronger melt events.

The unfiltered time series of the cumulative melt indicates a tidal signal with amplitudes of $\sim 1\,\mathrm{cm}$ within $12\,\mathrm{h}$ around the low-pass filtered cumulative melt. However, we found evidence that this tidal signal is due to the inaccuracy in the determination of the strain and not a true tidal melt amplitude: We found a clear accordance of the strain in the upper ice column with the tidal signal as recorded by GPS measurements, however, we are lacking tidal vertical strain in the lower column of the ice due to the noise. As the tidal variation of $\Delta H / \Delta t$ is by far lower than the observed $\Delta H_\varepsilon / \Delta t$, either deformation in the upper and lower parts compensates each other, or basal melt/freeze takes this role. We can exclude freezing, as we do not find jumps in the amplitude of the basal return in the ApRES signal (Vaňková et al., 2021) over tidal time scales. Consequently, we infer that strain in the lower half compensates that in the upper part and there is only a small variation of basal melt on tidal time scales.

As our location is close to two hinge zones, upstream and west of the melt channel, only a full three-dimensional model could shed light on the vertical strain in the lower part of the ice column. This is numerically costly for the required non-linear

12

strain theory and beyond the scope of the project. With melt channels being located (or initiated) in the hinge zone, any kind of ApRES time series performed at thick ice columns might be affected by the unclear strain-depth profile in the lower part of the ice column. This may be overcome by a radar device with higher transmission power, that allows the detection of vertical displacement of layers down to the base. The observed tidal dependency of the vertical strain is consistent with the finding from other ApRES locations at the Filchner-Ronne Ice Shelf by Vaňková et al. (2020). They found the strongest dependency, even of the basal melt rate at some stations, on the semidiurnal (M_2) constituent. Besides depth-independent tidal vertical strain, (Vaňková et al., 2020) found tidal deformation from elastic bending at ApRES stations located near grounded ice.

For an ice shelf such as the Filchner we expect the principal drivers of basal melting to be the water speed and its temperature above the in situ freezing point (e.g. Holland and Jenkins, 1999). For much of the ice shelf the water speed is dominated by tidal activity (Vaňková et al., 2020), but near the grounding line of SFG we expect the tidal currents to be low, consistent with the evidence from the ApRES thinning rate time series. It is likely that the anomalously high melting events seen in the record result from the passage of eddies, with their associated water speed and temperature anomalies.

3 Viscoelastic modeling

To obtain a more profound understanding of the evolution of the channel, we conduct transient simulations and analyze the change in geometry of 2D cross-sections (x, z direction) over time, as well as the simulated strain-field. The simulations are forced with the basal melt rates (both interpolated and synthetic) obtained in this study (Fig. 3). We transform distance (y-direction) to time in along flow direction of the ice shelf (Fig. 1) using present day velocities. This enables us to study under which conditions the channel is stable or vanishes.

Ideally, we would have observations of ice geometry and basal melt rates from the grounding line onward, but our first cross-section with observations is located $14\,\text{km}$ downstream of the grounding line (Fig. 1). The initial elastic response of the grounded ice becoming afloat has faded away. Further elastic contributions to the deformation originate from in-situ melt at the base and accumulation at the surface. To best fit the stress-state at the first cross-section, we conduct a spin-up.

3.1 Model

The model comprises non-linear strain theory, as there is no justification to expect a priori the simplified, linearized strain description for simulation times longer than $200\,\text{a}$ (e.g. Haupt, 2000). We treat the ice as a viscoelastic fluid and solve the system of equations for displacements using the commercial finite element software COMSOL (Appendix Sec. B1; Fig. B1 Christmann et al., 2019). The constitutive relation corresponds to a Maxwell material with an elastic response on short time scales and viscous response on long time scales. For homogeneous, isotropic ice, two elastic material parameters exist (Young's modulus E and Poisson's ratio ν). We conduct all viscoelastic simulations with commonly used values for ice of $E = 1\,\text{GPa}$ and $\nu = 0.325$ (Christmann et al., 2019). Another material parameter of the viscoelastic Maxwell material is the viscosity. It controls the viscous flow of ice. We use a constant viscosity of $\eta = 5 \times 10^{15}\,\text{Pa\,s}$ and discuss the influence of this material parameter later on. This constant viscosity is at the upper limit of the viscosity distribution derived by an inversion for the

rheological rate factor in the floating part of the Filchner-Ronne Ice Shelf (Appendix Sec. B2 and Fig. B2). This inversion has been conducted using the Ice Sheet and Sea-Level System Model (ISSM) (Larour et al., 2012) in higher-order Blatter-Pattyn approximation (Blatter, 1995; Pattyn, 2003), using BedMachine geometry (Morlighem, 2020; Morlighem et al., 2020), the velocity field of Mouginot et al. (2019b, a), and a temperature field presented in Eisen et al. (2020), based on the geothermal heat flux of Martos et al. (2017). For the assumed material parameters, we obtain a characteristic Maxwell time of $\tau = 153\,\mathrm{d}$ by $\tau = (2 + 2\nu)\eta/E$ (Haupt, 2000).

The model geometry represents a cross-section through the melt channel (Fig. 5) with the x-direction being across channel and resembling the seismic IV profile (Fig. 1) for $t = 0\,\mathrm{a}$. By assuming plane strain, the shape and the loading do not vary in the along-flow direction (width is sufficiently large). The stress state is independent of the third dimension, the displacement u_y in flow direction is zero and hence all strain components in the direction of the width vanish

$$\varepsilon_{yy} = \varepsilon_{xy} = \varepsilon_{yz} = 0. \tag{10}$$

The computational domain is discretized by an unstructured mesh using prisms with a triangular basis involving a refined resolution near the channel. We use the direct MUMPS solver and backward differentiation formula with automatic time step control and quadratic Lagrange polynomials as shape functions for the displacements. The viscous strain is an additional internal variable in the Maxwell model and we use shape functions of linear Lagrange type. In some cases, the geometry evolution leads to degraded mesh elements, which requires automated remeshing from time to time.

In this study, the ice density is $910\,\mathrm{kg\,m^{-3}}$ and the seawater density is $1028\,\mathrm{kg\,m^{-3}}$. At the upper and lower boundaries, we apply stress boundary conditions: for the ice-ocean interface, a traction boundary condition specifies the water pressure by a Robin-type condition. The ice-atmosphere interface is traction-free. Laterally, we apply displacement boundary conditions. As we take a plane strain approach, we can neglect deformation in the along-flow direction. To obtain realistic lateral boundary conditions, we transform observed vertical strain and hence, vertical displacements, at the location OE in horizontal displacements. First, we assume incompressibility

$$\varepsilon_{zz}^{\mathrm{obs}} = -(\varepsilon_{xx}^{\mathrm{obs}} + \varepsilon_{yy}^{\mathrm{obs}}) \tag{11}$$

and compute the sum of the horizontal strain. We integrate this strain to get a horizontal displacement. Therefore, we assume a homogeneous material, no additional forces in horizontal direction and a constant ice thickness. The last assumption is not valid inside the channel. However with a channel of $300\,\mathrm{m}$ maximum height over $1\,\mathrm{km}$ width, the deviation from outside to inside the channel is small for a computational domain of around $10\,\mathrm{km}$ width and an ice thickness around $1300\,\mathrm{m}$. With these assumptions we get a constant strain and integrate this strain to get a horizontal displacement. As we additionally assume plane strain, we can only apply this displacement to the lateral boundary in the across-flow direction. To model the compression and extension of the ice flow through the embayment, we apply the horizontal displacement to each lateral side so that u_x becomes

$$u_x = \frac{1}{2} \int_0^W \left(\varepsilon_{xx}^{\mathrm{obs}} + \varepsilon_{yy}^{\mathrm{obs}} \right) dx = \frac{\left(\varepsilon_{xx}^{\mathrm{obs}} + \varepsilon_{yy}^{\mathrm{obs}} \right) W}{2}, \tag{12}$$

14

with W the width of the simulated cross-section (Fig. 5). We assume that the horizontal displacements are depth-independent at lateral boundaries, resulting in a compression or elongation perpendicular to the channel (Fig. B3a).

The climate forcing consists of SMB and basal melt rate. Technically, both are applied by changing the geometry of the reference configuration with the respective cumulative quantities (Fig. B3b,c). For the SMB, we used multi-year mean RACMO2.3
345   data (van Wessem et al., 2014) ranging from 0.15 to $0.17\,\mathrm{m\,a}^{-1}$ for a density of $910\,\mathrm{kg\,m}^{-3}$, that we slightly modified to account for the surface depression over the channel: accumulation measurements at the pRES locations indicated higher accumulation in the channel than outside by a factor of roughly 1.5. Thus, we used 50% higher accumulation rates above the basal channel and a smooth cosine-shaped transition in the x-direction. A crucial forcing is of course the basal melt rate. Here we conduct individual experiments that are based on our observed melt rates and their variations. As this data is spatially
350   sparse, we need to interpolate those values in the across-channel (x) direction. We assume a smooth cosine-shaped transition between the observed basal melt rates outside east (OE) and inside the channel (L). For melt rates outside west, we do not have any observations and assume them to be time-independent. With 10% lower melt rates than for OE during the spin-up and a smooth cosine-shaped transition between outside west and lowest, we get a good agreement of the ice base geometry for outside west with seismic IV and V. For the first $20\,\mathrm{a}$ after the spin-up, the melt rate outside east is higher than outside west.
355   While afterwards, the melt rates in the western part are higher than in the eastern part outside the channel.

As we conduct Lagrangian experiments, we computed the time between the observed measurements through their distance divided by flow velocity. We define $t_0 = 0\,\mathrm{a}$ at the pRES measurements furthest upstream (Fig. 1) that is also the location of the seismic observation IV by Hofstede et al. (2021a, b). To evaluate our simulations, we compare the simulated surface topography and ice thickness, as well as $u_z(z)$ with the observed one for the considered time interval of $250\,\mathrm{a}$.
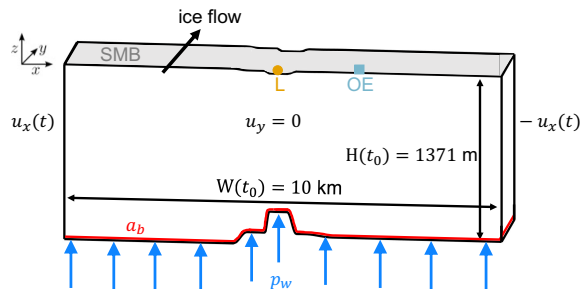
Figure 5. The cross-section of the model geometry at the end of the spin-up (t_0) of the first experiment shows its corresponding width and ice thickness outside east. The boundary conditions of the viscoelastic model are the water pressure p_w acting perpendicular to the ice base, the displacement in the flow direction u_y, which is zero due to plane strain assumptions, and the time-dependent displacement $u_x(t)$ acting in the lateral direction derived by pRES observations. The locations of the pRES station at the lowest point (L) of the channel and outside east (OE) are shown at their position on the surface in addition to the SMB (mass increase) and the melt rate a_b (mass decrease) at the base of the geometry.

We performed a spin-up to avoid model shocks, introduced by the transient behavior of a Maxwell material, that could be falsely interpreted as the response to geometry changes, for instance, caused by basal melt rates. The main goal here is to have the geometry after spin-up fit reasonably to the geometry measured at the seismic IV line (see Fig. 1) that we denote as time t_0. The spin-up covers 75 years, which corresponds to the time from the grounding line to that profile under present day flow speeds. To this end, we take a constant melt rate equal to the melt rate at t_0 and adjust the geometry at the grounding line to match the geometry at t_0 of the seismic IV profile reasonably well. After the spin-up, the width $W(t_0)$ of the simulated geometry is $10\,\mathrm{km}$. With this procedure the initial elastic deformation at the beginning of the transient simulation vanished and the viscoelastic geometry evolution of the melt channel can be evaluated for different melt scenarios and SMB forcings.

Short-term forces like the time-varying climate forcing as well as the lateral extension or compression demand the usage of a viscoelastic instead of a viscous model to simulate the temporal evolution of the basal channel shown later on. First, we conduct a series of simulations with different material parameters and identify the best match of observed and simulated ice thickness above (L) and outside east (OE) of the channel. At these two positions most of the pRES measurements were done and the distribution of the melt rates gives an adequate basis to force the model. Due to the sparsity of observations at the western side, we apply a forcing in the model based only on melt rates at L and OE.

In the first experiment, we use an interpolation of the observed melt rates as forcing and compare the results with H_{PDadv} (solid lines in Fig. 3). The second experiment aims to derive the best match between simulated and observed geometry. For this experiment, we use synthetic melt rates (dashed lines in Fig. 3a).

3.2 Results and discussion of simulations

3.2.1 First experiment: pRES-derived melt rate

The spin-up for this experiment starts with a manually adjusted geometry (including the channel at the base) at $t = -75\,\mathrm{a}$ to fit seismic IV profile at t_0. We applied a constant melt rate of $1.5\,\mathrm{m\,a^{-1}}$ at L and $0.5\,\mathrm{m\,a^{-1}}$ at OE. This forcing enlarges the melt channel during the spin-up as the ice thickness OE increases due to the prescribed displacement representing compression caused by the lateral boundaries moving towards the center of the channel. The general shape of the base matches the seismic profile IV reasonably well (Fig. 1 and Fig. B4). After the spin-up, we force the base with a_b (solid line in Fig. 3a).

The results of this experiment are displayed in Fig. 6. For both locations, L and OE, the simulated and observed geometry differ significantly. The simulated ice thickness above the channel declines by $21\,\mathrm{m}$ in $250\,\mathrm{a}$, while the observed thickness is $191\,\mathrm{m}$ thinner than the simulated one. Outside the channel, the simulated trend shows thinning. This thinning begins after $50\,\mathrm{a}$, whereas we find continuous thinning in the observations. This delayed onset of thinning is also represented in the simulated surface topography. Most notable is the match between simulated H_{sim} and advected H_{PDadv} ice thickness under present day climate conditions at the center of the channel (L). This match confirms that present day melt rates would not lead to the observed channel evolution over $250\,\mathrm{a}$.
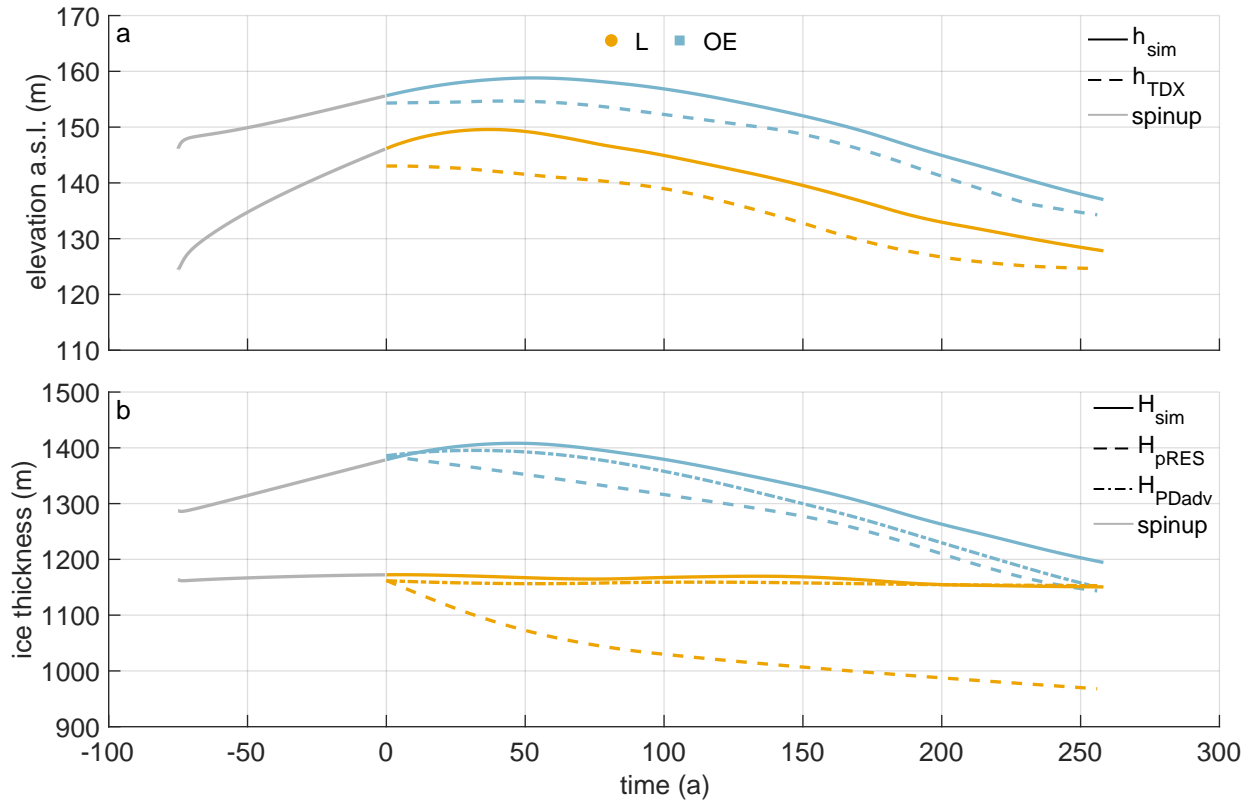
Figure 6. First experiment: Simulated surface elevation (a) and ice thickness (b) using the pRES-derived melt rate. Colors denote quantities above the channel (yellow) and outside the channel (blue). (a) Simulated surface elevation h_sim (solid lines) and observed h_TDX (dashed lines). (b) Simulated ice thickness H_sim (solid lines), under present day climate conditions advected H_PDadv (dashed-dotted lines) and observed H_pRES (dashed lines). Gray lines represent the spin-up.

3.2.2 Second experiment: Synthetic melt rate

The spin-up for the second experiment also starts with a geometry that has been manually adjusted at $t = -75\,\mathrm{a}$ to fit seismic IV profile at t_0. In the second simulation experiment, we force the base with the synthetic melt rate (Fig. 3a) that is inside the channel larger than the observed met rate. Again, the melt rate has been kept constant over the spin-up with $a_b^\mathrm{syn}(t_0)$. The synthetic melt rate leads to a cumulative melt after $250\,\mathrm{a}$ of $290\,\mathrm{m}$ (Fig. B3a) with $184\,\mathrm{m}$ more ice melted at L than in the first experiment and hence, the initial geometry has to be different to the first experiment.

The modeled geometry of this experiment is presented in Fig. 7. The simulated ice thickness at L is in very good agreement with H_pRES. There is some mismatch at OE, but the simulated trend of thinning is synchronous to the observations. After $250\,\mathrm{a}$ the deviation from the observed ice thickness at OE reaches $+53\,\mathrm{m}$. The simulated base for the second experiment shows a persistent basal channel (Fig. B5). The mismatch of the surface elevation at L and OE reverses over time: while the simulated

17

surface topography at OE is first too low, it is too high in the second half of the transient simulation (Fig. 7). However, the trend of the observed h_{TDX} and simulated h_{sim} elevation behave similarly. While ice thickness is in good agreement, surface elevation above the channel is overestimated by $4\,\mathrm{m}$ at the end of the spin-up. After $57\,\mathrm{a}$, it turns from an over- to underestimation that results in an $8\,\mathrm{m}$ lower h_{sim} than the observed h_{TDX} after $250\,\mathrm{a}$. To understand if the ice is in hydrostatic equilibrium, we compute the freeboard at the position L for an ice density of $910\,\mathrm{kg\,m^{-3}}$. The surface elevation is $133\,\mathrm{m}$ at t_0 and decreases to $112\,\mathrm{m}$ after $250\,\mathrm{a}$. Although h_{TDX} is larger than this, the ice is approaching flotation in the downstream direction. One could take another approach and estimate the mean density under the assumption of buoyancy equilibrium: at t_0 this corresponds to $901\,\mathrm{kg\,m^{-3}}$ and after $250\,\mathrm{a}$ to $896\,\mathrm{kg\,m^{-3}}$. As more ice is melted from below and with higher snow accumulation at L, the density decreases, which is to be expected.

After $250\,\mathrm{a}$, the simulated freeboard at OE is $1\,\mathrm{m}$ higher than the surface elevation of $138\,\mathrm{m}$ inferred by buoyancy equilibrium using an ice density of $910\,\mathrm{kg\,m^{-3}}$ and at OE the discrepancy is $3\,\mathrm{m}$. Overall, we see convergence to equilibrium state at OE and the simulated surface elevation at L. At the end of the simulation, only h_{TDX} above the channel does not reach buoyancy equilibrium, which leads to the justifiable assumption that the mean ice density at L is lower than OE.

At the position of the furthest upstream pRES observations we know from interferometry shown in Hofstede et al. (2021a) that the location is still in the hinge zone. The assumption of buoyant equilibrium is therefore likely to be flawed. At the end of the simulation, the geometry should be close to buoyancy equilibrium despite melting and a 50% higher SMB at L than OE. Hence, simulations carried out using a higher SMB within the channel would result in better agreement with the observed values of h_{TDX}.

Next, we consider the variation of the vertical displacement with depth. The results are presented in Fig. 8. For this purpose, we calculated the cumulative vertical displacement in one year. For comparability, the vertical displacements due to accumulation and snow compaction were removed from the observed distributions. Most notably, we move from a vertically extensive regime to a compressive regime with increasing distance from the grounding line. Given the complexity of the problem, the simulations show a reasonable agreement with the observations. The best match is reached at OE, which is not that surprising. The generally good agreement of the simulated displacements outside the channel comes from tuning u_x at the lateral boundary to match u_z from the pRES measurements at OE. A schematic illustration of first principal strains and their directions shows a closure of the channel for lateral compression and simultaneously a thickening of the ice shelf that is larger inside the channel than outside (Fig. B6). For lateral extension, we conversely get a thinning of the ice shelf that is smaller inside the channel than outside. Both simulated and observed vertical displacement distributions show that the strain decreases from L to OE (Fig. 8). The only exception here is $t = 57\,\mathrm{a}$, where the vertical strain at SE is larger than the one at L, in the observations. While at $0\,\mathrm{a}$ and $26\,\mathrm{a}$ the deviation of the simulated displacements between L and OE is small, it increases afterwards. From $105\,\mathrm{a}$, the simulated vertical displacements agree very well with those of the pRES-measurements, where a displacement distribution was derivable at L and OE. The same comparison for the first experiment (Fig. B7) shows similar results, with significantly less pronounced differences between L and OE. Hence, the mismatch to the observed vertical displacements for this experiment using the measured melt rates is higher than for the second experiment with the synthetic melt rates.
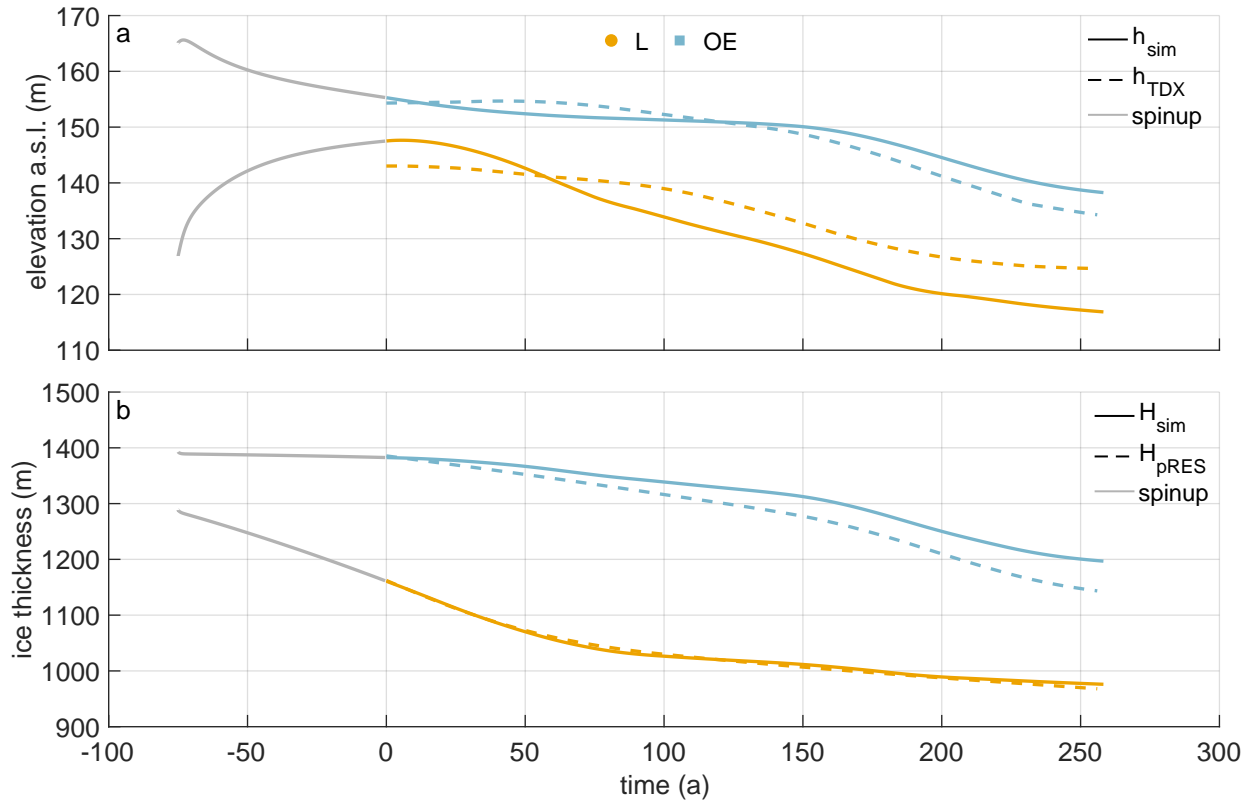
Figure 7. Second experiment: simulated surface elevation (a) and ice thickness (b) using the synthetic melt rate. Colors denote quantities above the channel (yellow) and outside the channel (blue). (a) Simulated surface elevation h_{sim} (solid lines) and observed h_{TDX} (dashed lines). (b) Simulated ice thickness H_{sim} (solid lines) and observed H_{pRES} (dashed lines). Gray lines represent the spin-up.

As the last point of this second experiment, we consider the influence of the viscosity on the evolution of the melt channel (Fig. B8). To reach the ice thickness of seismic IV, the simulation applying the smallest viscosity needs a higher initial channel at the beginning of the spin-up (Appendix Sec. B3). The channel thickness of the pRES-measurement is modeled best using a viscosity of $5 \times 10^{15}\,\mathrm{Pa\,s}$. A two times higher viscosity leads to a geometry where the ice is $42\,\mathrm{m}$ thinner in the center of the channel after $250\,\mathrm{a}$, while a five times lower viscosity results in $116\,\mathrm{m}$ thicker ice above the channel due to more viscous flow into the channel. The simulated ice thickness OE is similar for all three different viscosities. The distributions of vertical displacement with depth illustrate that the difference between L and OE is larger for smaller viscosity values (Fig. B9). Often the viscosity of $5 \times 10^{15}\,\mathrm{Pa\,s}$ fits quite well to obtain the observations by the simulation but for some a slightly (Fig. B9a) or a considerably lower viscosity (Fig. B9c) would be needed.
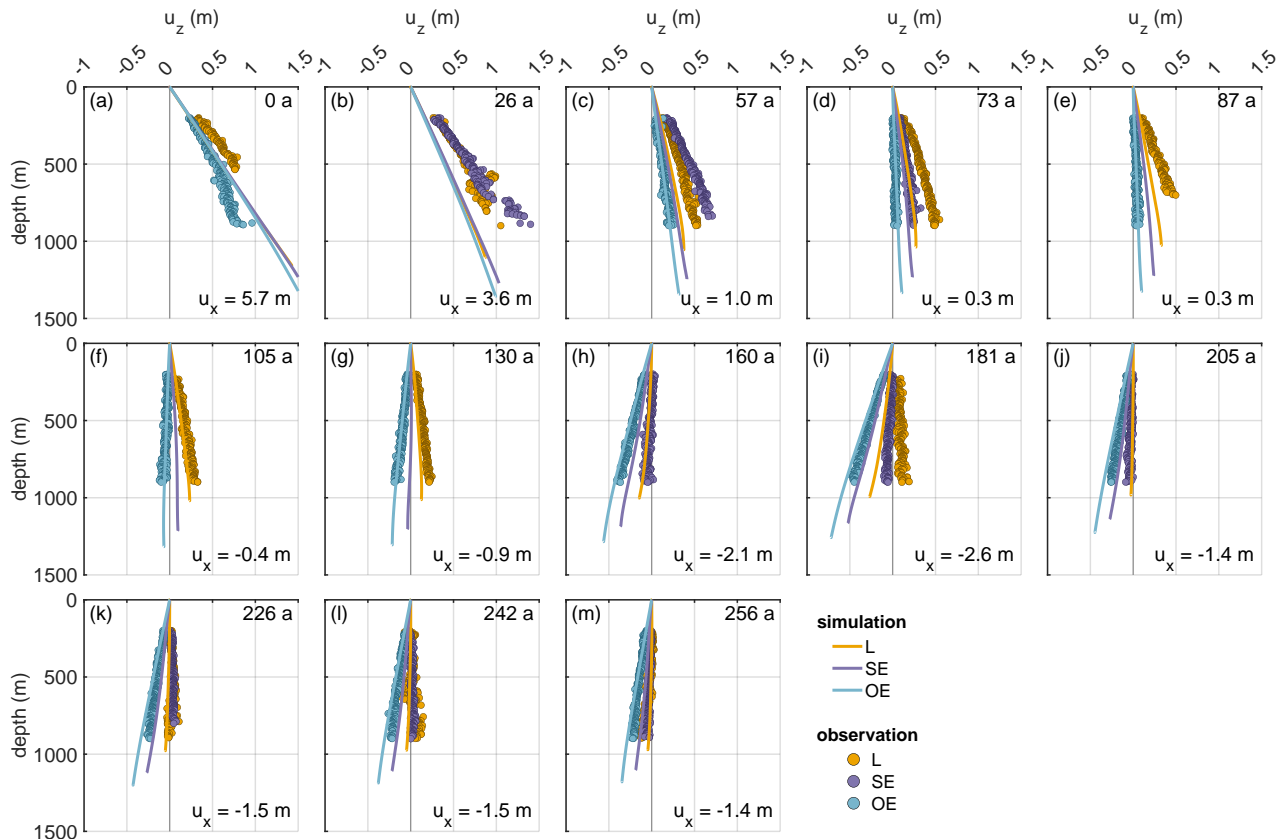
Figure 8. Second experiment: comparison of displacements (u_z) derived from observations (dots) and the simulations (lines). The different panels show the displacement for $\Delta t = 1\,$a allocated to the simulation time (upper right corner). The numbers in the lower right corners give horizontal displacement u_x derived from ε_{zz} of the pRES measurements outside the channel (OE) with positive values representing compression and negative values extension.

4 Discussion

Observed melt rates inside the channel are in general rather modest, $< 2\,\mathrm{m\,a^{-1}}$. For comparison, values retrieved at a channel $1.7\,\mathrm{km}$ from the grounding line of the Ross Ice Shelf at the inflow of the Mercer and Whillans ice streams were $22.2\,\mathrm{m\,a^{-1}}$ (Marsh et al., 2016). These values dropped to below $4\,\mathrm{m\,a^{-1}}$ over a distance of $10\,\mathrm{km}$ and reached $2.5\,\mathrm{m\,a^{-1}}$ after $40\,\mathrm{km}$. We also find that the melt rates decrease by a factor of five in the center of the channel over a distance of $11\,\mathrm{km}$, however, this takes place between 14 and $25\,\mathrm{km}$ downstream the grounding line. At the Ross Ice Shelf, the ratio between the melt rates inside the channel and $1\,\mathrm{km}$ outside it is about 27, whereas we find only a factor of 3, with the distance between L and OE being $1.8\,\mathrm{km}$.

Zeising et al. (2022) presented pRES-derived basal melt rates downstream of our study area. Roughly $40\,\mathrm{km}$ downstream the northernmost cross-section ($\sim 200\,\mathrm{a}$ of ice flow), these measurements show that the channel still exists, but with a small height of $\sim 16\,\mathrm{m}$. Inside the channel, Zeising et al. (2022) determined a melt rate $\sim 0.20\,\mathrm{m\,a^{-1}}$ lower than outside. The larger melt rates outside the channel compared to inside is in agreement with the finding of our study. In general, the channel height declines, so the channel fades out. The channel diminishes because melt rates inside the channel fall below those outside the channel. The trend in vertical strain has only a minor contribution to this evolution. We thus do not find any evidence that such channels are a cause for instabilities of ice shelves as suggested by Dow et al. (2018).

One of the main findings of our study is that the present geometry can only be formed with considerable higher melt rates in the past (see Fig. 3). This finding is based on the assumption that the strain-rates were in the past similar to present day and that melt on both flanks of the channel are similar. This is justified, as significant changes in strain would require a change in the system that would cause other characteristics to change, like the main flow direction, for which we do not find any indication. However, in our setting, we are in a compressive regime. A similar assumption may at other locations not be possible.

The pRES melt rate observations covered only one year. As the ocean conditions within the sub-ice shelf cavity are known to respond to the ocean forcing from the ice front (e.g. Nicholls, 1997), we would expected them to be subject to significant interannual variability. Underlying any interannual variability, a long-term reduction in basal melt rates would be the expected response to a reduction in production of dense shelf waters north of the ice front, resulting from a reduction in sea ice formation (Nicholls, 1997), resulting in turn from a reduction in the southerly winds that blow freshly produced sea ice to the north. A decrease in northward motion of sea ice has been observed in the satellite record (e.g. Holland and Kwok, 2012). The modeling experiments by Naughten et al. (2021) also find decreasing ice-shelf basal melt rates. This reduction is therefore consistent with higher basal melt rates in the past. However, our model results suggest that the mismatch between the past melt rates needed to explain the channel geometry and the present-day observed melt rates applies only to the channel, and not to the ambient ice. This could be explained by historically higher levels of subglacial outflow at the grounding line, or anomalously low levels during the observation period. Subglacial outflow contributes to the buoyant flow up the basal slope and therefore the shear-induced turbulence that raises warm water from deeper in the water column towards the ice base. Variations in the subglacial outflow could be caused by variations in subglacial storage, as Smith et al. (2009) found an active subglacial lake at the transition between Academy Glacier and SFG, and Humbert et al. (2018) also suggest the presence of a subglacial lake in the upstream area of SFG.

Hofstede et al. (2021a) showed that the subglacial channel appears $7\,\mathrm{km}$ upstream of the grounding line increasing its height to $280\,\mathrm{m}$ at the grounding line. The location of the channel corresponds with increased subglacial flux found by Humbert et al. (2018) using a simple routing scheme. Once this topographic feature reaches the ocean, it serves to focus the buoyant plume and enhance shear-driven vertical mixing, bringing heat and salt to the ice base leading to higher basal melt rates.

However, with increasing distance along the channel, the basal gradient, and therefore the speed of the buoyant flow, is reduced, which also reduces the entrainment of warm water from beneath. Coupled with the pressure-induced increase in the freezing point with decreasing depth, this leads to a gradual reduction of the melt rate in the channel. From Fig. 2a, the melt rate in the channel reduces below that of the ambient ice base by about $30\,\mathrm{km}$ distance from the grounding line, suggesting that

the effect of focused meltwater outflow thereafter is to suppress the channel.

The cause of the strong melt anomalies identified in the ApRES measurements remains unclear as no direct ocean observation exists near SFG. However, the time scale of the events is consistent with the passage of warm cored eddies. Such features have been observed in the ocean cavity beneath the neighboring Ronne Ice Shelf (Nicholls, 2018).

The channel height is found to increase until 30–$35\,\mathrm{km}$ downstream of the grounding line. Further downstream, the channel begins to close. Our modeling results show that less viscous ice ($1 \times 10^{15}\,\mathrm{Pa\,s}$) would tend to shut the channel faster than the rate we observe (Fig. B8). For the best match between observed and modeled geometry, we need viscosities around $5 \times 10^{15}\,\mathrm{Pa\,s}$ to prevent closure by deformation (Fig. 7). This viscosity value is also supported by an inversion of ice rheology to fit observed surface velocities in the melt channel region (Appendix Sec. B2). With a viscosity of $5 \times 10^{15}\,\mathrm{Pa\,s}$, we can use a viscoelastic model to simulate the channel evolution in both experiments to match the observations: (i) pRES-derived melt rates result in an ice thickness fitting the present day advected ice thickness H_{PDadv} (Fig. 6), and (ii) synthetic melt rates lead to the observed ice thickness H_{pRES} (Fig. 7). The channel vanishes for the pRES-derived melt rates as those are unable to maintain the channel geometry open against viscoelastic deformation (Fig. B4). Based on the higher synthetic melt rates, the simulated basal channel remains open and we get a similar basal appearance to that found by the seismic measurements (Fig. B5). However, if we would want to match the observed basal geometry at seismic profile V more precisely, we would have to spatially vary the basal melt rate in the across-flow direction, enlarge the transition between L and OE, and thus extend the channel to the eastern side.

To evaluate the importance of using a viscoelastic and not a purely viscous material law, we compute the logarithmic Hencky strain (Appendix Sec. B4). With this strain measure, an additive decomposition of the strain into an elastic and viscous part is possible. After the spin-up, the elastic strain components in the across-flow and thickness direction are in the order of permille and one order of magnitude higher than the shear component (Fig. B10). Christmann et al. (2021) derived similar magnitudes in the viscoelastic simulation of 79° North Glacier considering linearized strains. The magnitude of elastic strain in the across-flow direction is caused by the lateral compression and varies slightly to higher values around the channel due to the dent of the channel. However, the highest elastic strain values are reached outside the channel and decrease with time (Fig. B11). It is likely that the elastic deformation slightly increases especially inside the channel if the lateral compression changes into tension or vice versa. In the thickness direction, the elastic strain is decreasing towards the channel (Fig. B10b). This causes the difference in geometry change, due to different values of the viscosity, to be larger inside the channel rather than outside (Fig. B8). The simulated geometry change is mainly due to the elastic response to thinning by basal melt and ice accumulation. Any purely viscous simulation would overrate the deformation in the vertical direction as the elastic strain has the opposite sign as the viscous one (Fig. B12d-f). Higher melt rates were needed to compensate for this. Wearing et al. (2021) presents a full Stokes simulation of a comparable melt channel and indeed needs higher melt rates to keep the channel open. The relative amount of elastic strain shows values up to 8% of the total strain for high lateral compression or extension and is hence not negligible (Fig. B10). It is important to keep this result in mind for future inverse modeling of melt rates in melt channels.

We find a difference ($-4\,\mathrm{m}$ to $8\,\mathrm{m}$) between simulated and observed surface elevation at L (Fig. 7). The elevation difference is most likely caused by the constant density that we used for the simulations, as the ice thickness matches well. For the

thinner ice above the channel, this could be achieved by an ice density decreasing from outside to inside and from upstream to downstream in the channel. However, one has to keep in mind that the accuracy of the surface elevation product is only $5\,\mathrm{m}$, so the differences in surface elevation may not be significant.

In general, we benefited highly from having measurements of vertical strain available. This opens new possibilities to identify weaknesses in the modeling, such as limited knowledge on lateral boundary conditions and rheological parameters, and gave us useful insight into the spatial variation of the vertical strain across such a topographic feature (Figs. 8 and B7). Although the pRES surveys only about half the ice thickness, the slope of $u_z(z)$ in the upper half is distinct for the positions L, SE and OE and greatly varies with distance from the grounding line, and is also influenced by the embayment of the ice shelf. Simulated u_z at L starts to match well with observations after about $100\,\mathrm{a}$, which could result from the first few cross-sections still being influenced by the hinge zone (Fig. 8). Tidal bending was not taken into account here, due to the 2D setting. This could in future be investigated, if repeated pRES measurements would be conducted up to the grounding line covering the entire hinge zone, in which case it would also be extremely advantageous to obtain basal melt rates at tidal time scales.

Our study demonstrates that viscoelastic simulations can be a useful but complex tool to analyze melt channel evolution. In an inverse approach, viscoelastic models could also give more insights into basal melt rates of channel systems of ice shelves in general, given that satellite-borne surface elevation is available in high resolution. However, the fact that large deformations require non-linear strain theory will make this a challenging endeavor. As changes in basal melt rates will inevitably lead to surface elevation changes of channel systems, systematic monitoring of the surface topography from space can serve as an early warning system and trigger further in-situ observation similar to this study.

5 Conclusions

We find basal melt rates in a melt channel and its surroundings on Filchner Ice Shelf to be up to $2\,\mathrm{m\,a^{-1}}$. Basal melt rates inside the channel drop with distance down-flow, even turning into freezing $55\,\mathrm{km}$ downstream of the grounding line. Close to the grounding line, melt rates are larger inside the channel than outside, while further downstream this relationship reverses. Along flow, the channel height decreases from a maximum of $330\,\mathrm{m}$ to below $100\,\mathrm{m}$. The channel diminishes because the reduced melt rate is unable to maintain the channel geometry against viscoelastic deformation. Analysis of the predicted ice thickness from advection of present-day thickness with present-day melt rates revealed large differences compared to the observed ice thickness above the channel, which indicates that melt rates have been about twice as large in the last $250\,\mathrm{a}$. The viscoelastic simulation confirms this statement and indicates that basal melt channels need high basal melt rates and relatively cold ice to persist. The deformation of the basal melt channel is mainly driven by the elastic response to the basal melt rate. The observed and simulated evolution of this melt channel demonstrates that melt channels of this kind are not a destabilizing element of ice shelves. The ApRES time series showed brief melt anomalies distributed over the entire measurement period and slightly increased melt rates in summer.

Appendix A: Observations

A1 Basal reflections and the influence of off-nadir returns

The identification of the basal reflections in both measurements, the first and the repeat measurement, is important in order to determine the change in ice thickness and thus the basal melt rate. Due to a high contrast in relative permittivity, the ice—ocean interface is a particularly strong reflector. Accordingly, the reflection at the ice base in the echogram is characterized by a sharp increase in amplitude. After identifying the first basal reflection in both measurements, the vertical displacement can be determined by means of a cross-correlation of the basal segment, provided that the shape of the basal reflector has not changed significantly. However, this was not the case at five of the 44 stations in our study area. At these, the basal return had changed significantly and thus prevented an unequivocally match. We therefore excluded these stations from the melt rate analysis. At all other stations, the reflection had changed only slightly, so that the vertical displacement could be reliably determined. Figure A2 shows three examples (OE, SE and L) from a cross-section 48 km downstream of the grounding line. In all of these measurements, a strong increase in amplitude was found between 992 m (L) and 1244 m (OE), which represents the first onset of the basal reflections. While the shape of the basal return changed only slightly, there was a change in amplitude, which is lower in the repeat measurement, especially in Fig. A2e,f. One potential reason for this was different measurement settings that influenced the amplification of the signal, but imprecise alignment of the transmitting and receiving antennas can also be responsible for this.

However, at 7 of the 44 stations more than one strong and clear defined basal reflection was found, raising the question of which is the nadir and which is the off-nadir reflection. The reason for this is that a steep base, such as on the flanks of the channel, creates strong off-nadir reflections. Depending on the basal gradient, this off-nadir reflection may also arrive before the nadir reflection. As pRES data represent point measurements, they cannot be used to constrain the local shape of the ice base and thus distinguishing nadir from off-nadir returns is difficult. One possible indicator of the nadir reflection can be the reflection amplitude, since the antenna radiates most of its energy in the nadir direction. However, in certain basal geometries off-nadir reflections can still be stronger than the nadir reflection, even accounting for the antenna beam pattern. Figure A3 shows two examples of stations with off-nadir reflections. In the measurements at the pRES029 station (OE; Fig. A3a,b), the basal reflection with the largest amplitude appeared with a range 11 m greater than the first basal reflection. This could be an indication that the first basal reflection is an off-nadir return. The analysis of the vertical displacement of both basal reflections shows a deviation of 0.13 m. The second example from station pRES019 (SW; Fig. A3c-e) shows two basal reflections of approximately equal strength, separated by about 175 m. At this station, the deviation of the vertical displacement of both basal returns was only 0.01 m. Which of these reflections is the nadir and which is the off-nadir reflection cannot be reliably determined from the pRES measurement. Only by analyzing the basal geometry, e.g. by airborne radar or seismic profiles, can the reflection be assigned to its place of origin by determining the basal distances from the measurement location. However, since seismic profiles are only available in the vicinity of two cross-sections, this method cannot be used for all stations. Thus, we calculated the displacement of the second and strongest basal return of those 7 stations where more than one strong basal return occurred. The melt rates derived from the first and the second basal return are shown in Tab. A1. While at 3 sites the

difference in melt rate is below $0.1\,\mathrm{m\,a^{-1}}$, at others, the melt rate difference exceeds $1\,\mathrm{m\,a^{-1}}$. Since we cannot distinguish between nadir and off-nadir solely from our pRES measurements, we have averaged the two derived melt rates and take into account the difference in the error. However, at station pRES042 (L) we found basal freezing by analyzing the first basal return but derived a melt rate of $1.09\pm0.07\,\mathrm{m\,a^{-1}}$ from the second, stronger basal return. We designate this location as a basal freezing station and state the range of melt rate as an error.

A2 Additional table

Table A1. Melt rates determined from different basal returns.

pRES station	location	basal return #1 range (m)	a_b ($\mathrm{m\,a^{-1}}$)	basal return #2 range (m)	a_b ($\mathrm{m\,a^{-1}}$)	Average range (m)	a_b ($\mathrm{m\,a^{-1}}$)
pRES016	SW	1221.0±12.21	1.09±0.08	1262.3±12.62	2.32±0.07	1241.7±33.04	1.70±0.69
pRES019	SW	1114.6±11.15	1.97±0.09	1289.3±12.89	2.02±0.09	1202.0±99.36	1.99±0.11
pRES020	SE	1202.4±12.02	0.28±0.12	1278.3±12.78	0.27±0.12	1240.3±50.37	0.28±0.12
pRES025	OE	1347.2±13.47	0.89±0.10	1368.8±13.69	0.61±0.09	1358.0±24.38	0.75±0.23
pRES028	OE	1301.3±13.01	2.29±0.09	1318.6±13.18	0.95±0.09	1310.0±21.75	1.62±0.76
pRES029	OE	1269.9±12.70	0.60±0.13	1280.8±12.80	0.70±0.14	1275.4±18.18	0.65±0.19
pRES042	L	1033.6±10.34	freezing	1085.2±10.85	1.09±0.07	1059.4±36.39	freezing – 1.09±0.07

Table A2. Description of symbols

Symbol	Description	Unit
u_x	horizontal displacement in across flow	m
u_y	horizontal displacement in along flow	m
u_z	vertical displacement	m
$\varepsilon_{xx}^{\mathrm{obs}}$	horizontal strain in across flow	
$\varepsilon_{yy}^{\mathrm{obs}}$	horizontal strain in along flow	
$\varepsilon_{zz}^{\mathrm{obs}}$	vertical strain	
$\overline{h_b}$	averaged depth of the ice base	m
h_{pc}	depth of the pore closure relative to surface	m
h_{nl}	noise-level depth limit relative to surface	m
h_{sim}	simulated surface elevation	m
h_{TDX}	TanDEM-X surface elevation	m
H	ice thickness	m
H_{pRES}	pRES derived ice thickness	m
H_{sim}	simulated ice thickness	m
H_{PDadv}	advection of the ice thickness under present day climate conditions	m
t	time	a
t_0	$t = 0\,\mathrm{a}$, defined at the most upstream pRES measurement location	a
t_1	1st measurement of ApRES time series	
t_i	i-th measurement of ApRES time series	
Δt	time period between repeated measurements	a
ΔH	change in ice thickness	m
ΔH_i	change in ice thickness below the depth of the pore close	m
ΔH_s	change in ice thickness at the surface and in the firn	m
ΔH_f	change in ice thickness due to firn compaction	m
ΔH_ε	change in ice thickness due strain	m
ΔH_b	change in ice thickness due to basal melt	m
a_b	basal melt rate	$\mathrm{m\,a^{-1}}$
a_b^{syn}	synthetic basal melt rate	$\mathrm{m\,a^{-1}}$
W	width of the cross-section in simulations	m

A3 Additional figures
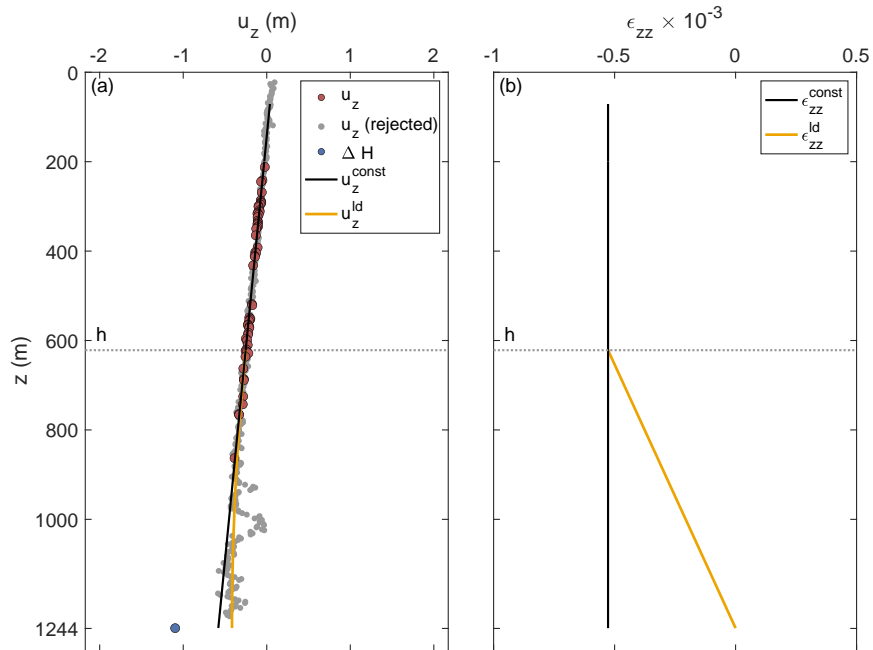
Figure A1. Strain analysis of a pRES measurement at location OE (pRES30; 48 km from grounding line). (a) Derived vertical displacements u_z for $\Delta t = 1\,\mathrm{a}$ of the ice base (ΔH; blue dot) and internal layers (red and gray dots). Displacements used for the linear regression u_z^{const} (black line) are colored in red and rejected displacements are shown in gray. The second model u_z^{ld} with a linear decreases (ld) from depth h (dotted line) to zero at the ice base is shown in orange. (b) Vertical strain for $\Delta t = 1\,\mathrm{a}$ of both models whose displacement is shown in (a).
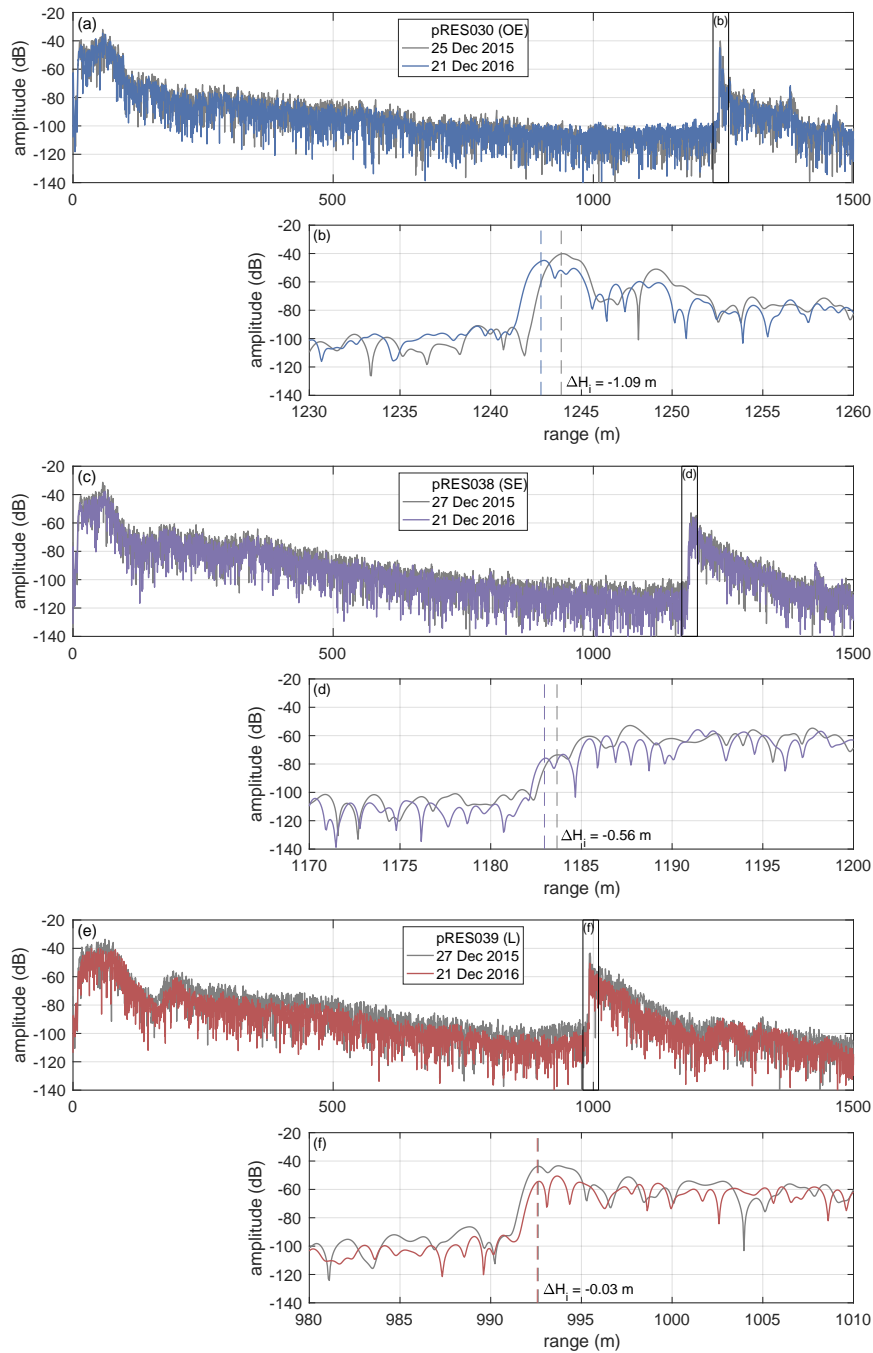
Figure A2. Amplitude profiles of first (gray line) and repeated pRES measurements at locations OE (a, b; blue), SE (c, d; purple) and L (e, f; red), all at the cross-section with a distance of 48 km from the grounding line. (b, d, f) Enlarged basal section, visualized by black boxes in (a), (c) and (e). Vertical dashed lines mark the ice thickness and ΔH_i the change in ice thickness between both visits.
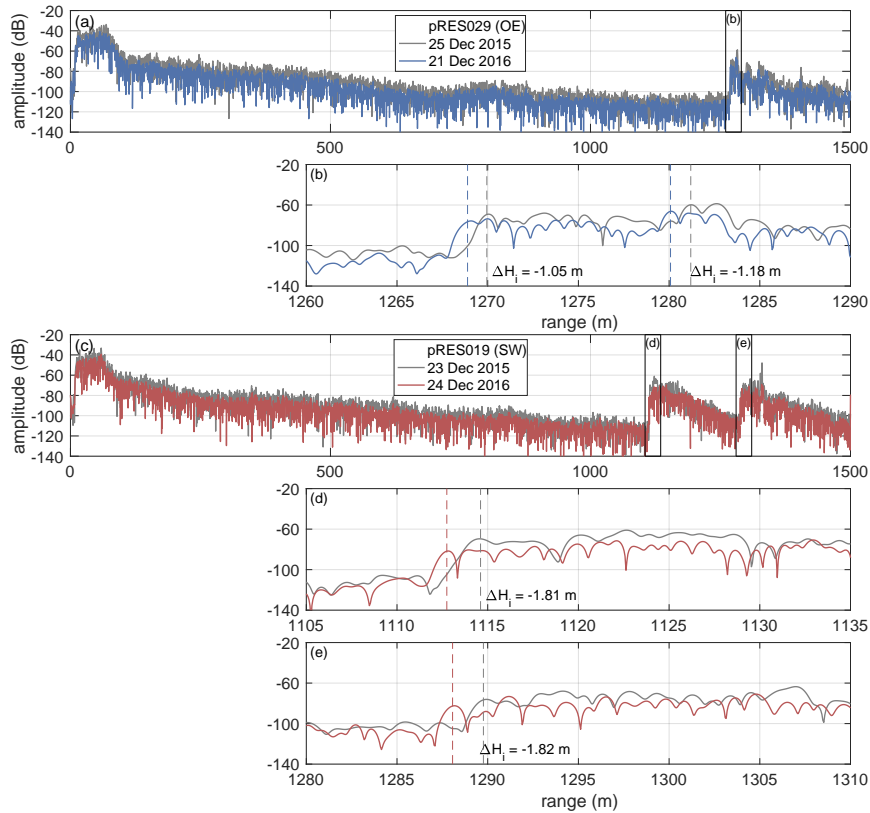
Figure A3. Amplitude profiles of two measurements indicating off-nadir basal reflections. (a, b) First (gray line) and repeated pRES measurement (blue) at location OE at the cross-section with a distance of 43 km from the grounding line. (b) Enlarged basal section, visualized by black boxes in (a). Vertical dashed lines mark the ice thickness and ΔH_i the change in ice thickness between both visits for the first and second strong increase in amplitude. (c–e) First (gray line) and repeated pRES measurement (red) at location SW at the cross-section with a distance of 28 km from the grounding line. (d, e) Enlarged basal sections, visualized by black boxes in (c). Vertical dashed lines mark the ice thickness and ΔH_i the change in ice thickness between both visits for the first and second strong increase in amplitude.
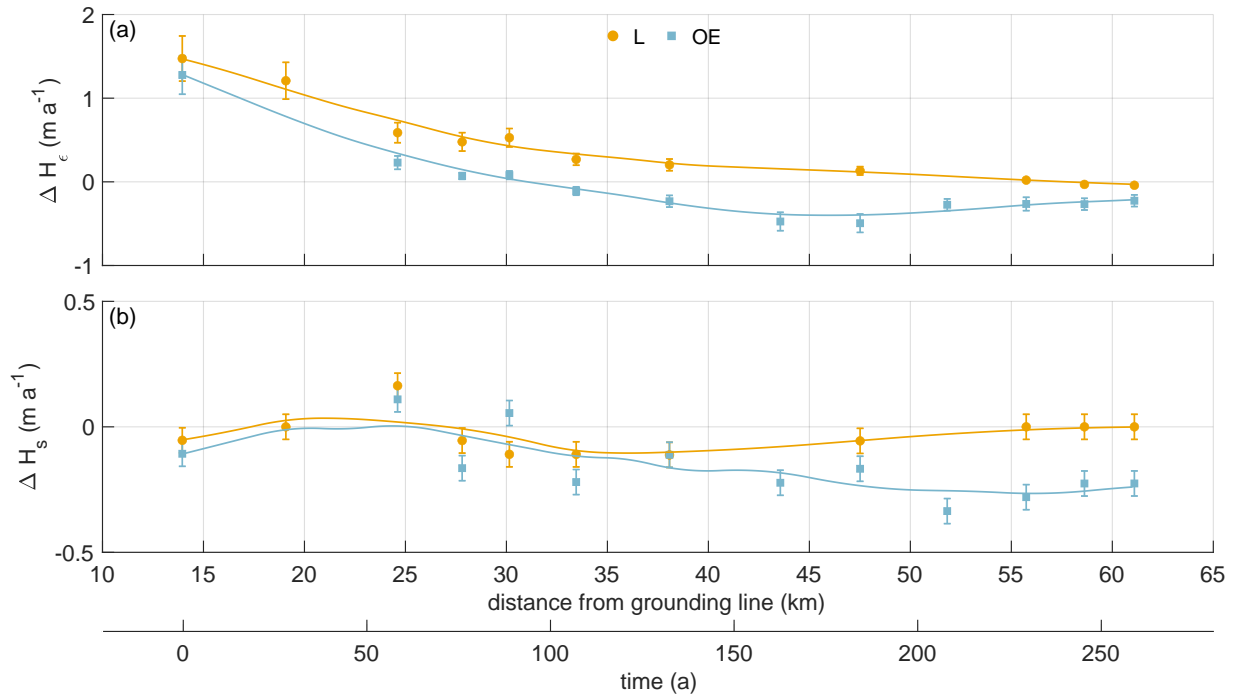
Figure A4. Distribution of pRES-derived (a) change in ice thickness due to strain and (b) ice thickness change due to surface process (firn compaction and accumulation) above the channel (yellow dots) and outside east of the channel (blue squares). The solid lines represent a smoothed fit. Error bars mark the uncertainties of the pRES-derived values.
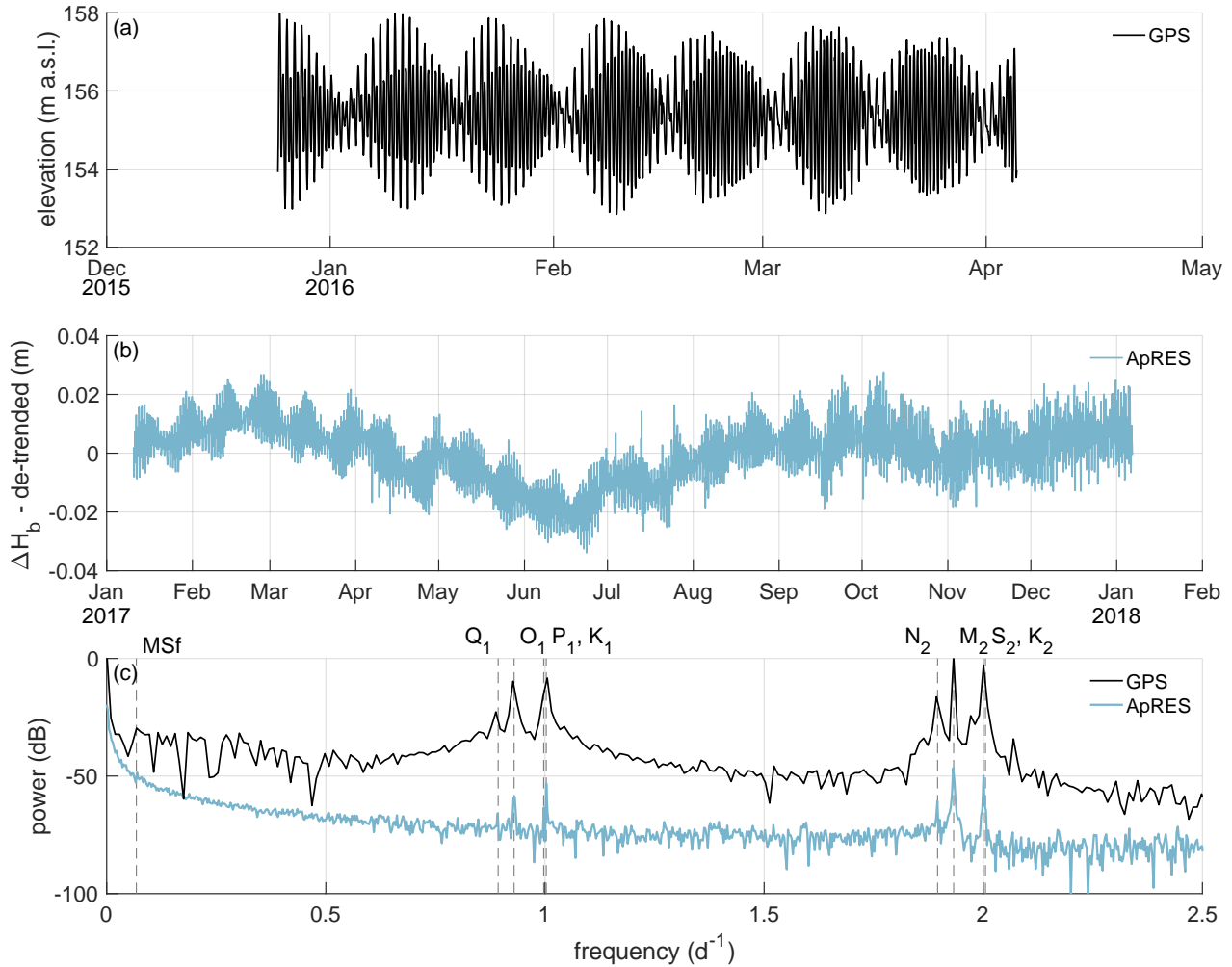
Figure A5. (a) Surface elevation recorded by the GPS station from end of December 2015 to early April 2016. (b) Linear de-trended cumulative melt (ΔH_b) from ApRES observations between January 2017 and January 2018. (c) Frequency spectrum from data shown in (a) and (b). Vertical gray dashed lines mark the constituents with half day periods ($N_2 = 12.66$ h, $M_2 = 12.42$ h, $S_2 = 12.00$ h, $K_2 = 11.97$ h), daily periods ($Q_1 = 26.87$ h, $O_1 = 25.82$ h, $P_1 = 24.07$ h, $K_1 = 23.93$ h), and Fortnightly period (MSf = 14.76 d). Notice, due to a shorter measuring period of the GPS, the resolution in frequency space is lower than of the ApRES.

Appendix B: Modeling

B1   Viscoelastic model for nonlinear strains

605   This section presents the basic equations for a viscoelastic Maxwell model applicable for finite strains. To consider finite deformations, we need to distinguish different configurations (Fig. B1). The reference configuration (stresses and strains denoted by the subscript 0) includes all positions $\boldsymbol{X}$ of material points in an initially undeformed domain. The displacement vector field $\boldsymbol{u} = \boldsymbol{x} - \boldsymbol{X}$ relates the particle position vector $\boldsymbol{X}$ in the reference configuration to its spatial position $\boldsymbol{x}$ in the current configuration depending on the external load and the time passed (Fig. B1). To formulate differential equations for finite vis-

610   coelasticity, we focus on the system of equations with respect to the reference configuration, which is frequently applied in solid mechanics Haupt (2000).

In the reference configuration, the quasi-static momentum balance reads

$$\mathrm{Div}\,\boldsymbol{\sigma}_0 + \boldsymbol{f}_0 = \boldsymbol{0} \tag{B1}$$

with $\mathrm{Div}(\cdot)$ the divergence with respect to the reference configuration. The tensor $\boldsymbol{\sigma}_0 = J\boldsymbol{\sigma}\boldsymbol{F}^{-T}$ is the first Piola-Kirchhoff

615   stress containing the Jacobian determinant $J = \det(\boldsymbol{F})$, the Cauchy stress $\boldsymbol{\sigma}$ of the current configuration and the transposed inverse of the deformation gradient

$$\boldsymbol{F} = \frac{\partial \boldsymbol{x}}{\partial \boldsymbol{X}} = \frac{\partial \boldsymbol{u}}{\partial \boldsymbol{X}} + \boldsymbol{I} \tag{B2}$$

characterizing the material gradient of motion in which $\boldsymbol{I}$ is the second order identity tensor. The volume force $\boldsymbol{f}_0 = -(J\rho_{\mathrm{ice}}g)\boldsymbol{e}_z$ accounts for the gravitational force in the thickness direction using the ice density $\rho_{\mathrm{ice}} = 910\,\mathrm{kg\,m}^{-3}$, the acceleration due to

620   gravity g, and the upward pointing unit vector $\boldsymbol{e}_z = (0,0,1)^T$. The formulation for finite viscoelasticity uses the conceptual multiplicative decomposition of the deformation gradient

$$\boldsymbol{F} = \boldsymbol{F}_{\mathrm{e}}\boldsymbol{F}_{\mathrm{v}} \tag{B3}$$

into rate-independent elastic (e) and rate-dependent viscous (v) parts (Lee, 1969). All material equations are formulated in the intermediate configuration (stresses and strains denoted by $\tilde{(\cdot)}$) as an additive decomposition of the strain (similar to linearized

625   strain; Christmann et al., 2019) is feasible in the intermediate configuration

$$\tilde{\boldsymbol{\epsilon}} = \tilde{\boldsymbol{\epsilon}}_{\mathrm{e}} + \tilde{\boldsymbol{\epsilon}}_{\mathrm{v}}. \tag{B4}$$

The elastic strain is given by $\tilde{\boldsymbol{\epsilon}}_{\mathrm{e}} = \frac{1}{2}\left(\boldsymbol{F}_{\mathrm{e}}^T\boldsymbol{F}_{\mathrm{e}} - \boldsymbol{I}\right)$ and the viscous strain by $\tilde{\boldsymbol{\epsilon}}_{\mathrm{v}} = \frac{1}{2}\left(\boldsymbol{I} - \boldsymbol{F}_{\mathrm{v}}^{-T}\boldsymbol{F}_{\mathrm{v}}^{-1}\right)$. For a viscoelastic Maxwell model, the viscous stress is equal to the elastic stress in the intermediate configuration. If we assume a Saint-Venant-Kirchhoff material for the elastic material, we get

630    $$\tilde{\boldsymbol{\sigma}}^D = 2\mu\tilde{\boldsymbol{\epsilon}}_{\mathrm{e}}^D = 2\eta\overset{\Delta}{\tilde{\boldsymbol{\epsilon}}}_{\mathrm{v}} \tag{B5}$$

with the viscosity η, the first Lamé constant $\mu = E/\left[2(1+\nu)\right]$ and the deviatoric part of the elastic strain $\tilde{\boldsymbol{\epsilon}}_{\mathrm{e}}^{D} = \tilde{\boldsymbol{\epsilon}}_{\mathrm{e}} - \frac{1}{3}\mathrm{tr}(\tilde{\boldsymbol{\epsilon}}_{\mathrm{e}})\boldsymbol{I}$. The viscous strain rate is defined using the objective lower Oldroyd rate $\overset{\Delta}{\tilde{\boldsymbol{\epsilon}}}_{\mathrm{v}} = \dot{\tilde{\boldsymbol{\epsilon}}}_{\mathrm{v}} + \boldsymbol{l}_{\mathrm{v}}^{T}\tilde{\boldsymbol{\epsilon}}_{\mathrm{v}} + \tilde{\boldsymbol{\epsilon}}_{\mathrm{v}}\boldsymbol{l}_{\mathrm{v}}$ with the viscous deformation rate $\boldsymbol{l}_{\mathrm{v}} = \dot{\boldsymbol{F}}_{\mathrm{v}}\boldsymbol{F}_{\mathrm{v}}^{-1}$ and the time derivative $\mathrm{d}(\cdot)/\mathrm{d}t$ denoted by the superimposed dot.

635 For the viscoelastic simulation, we have to formulate all equations and boundary conditions in the same configuration; here, we choose the reference configuration. Beside solving the momentum balance (B1), we solve the material law

$$\boldsymbol{\sigma}_0^S = \frac{\lambda + \frac{2}{3}\mu}{2}\left[\mathrm{tr}\boldsymbol{C}\boldsymbol{C}_{\mathrm{v}}^{-1} - 3\right]\boldsymbol{C}_{\mathrm{v}}^{-1} + \mu\left[\boldsymbol{C}_{\mathrm{v}}^{-1}\boldsymbol{C}\boldsymbol{C}_{\mathrm{v}}^{-1} - \frac{1}{3}\mathrm{tr}\left(\boldsymbol{C}\boldsymbol{C}_{\mathrm{v}}^{-1}\right)\boldsymbol{C}_{\mathrm{v}}^{-1}\right] \tag{B6}$$

with the symmetric second Piola-Kirchhoff stress $\boldsymbol{\sigma}_0^S = \boldsymbol{F}^{-1}\boldsymbol{\sigma}_0$, the second Lamé constant $\lambda = \frac{E\nu}{(1+\nu)(1-2\nu)}$ and the right Cauchy-Green tensor $\boldsymbol{C} = \boldsymbol{F}^T\boldsymbol{F}$. For a viscoelastic Maxwell material, we either have to compute elastic or viscous deformations through an internal variable in the reference configuration. The evolution equation for the internal variable $\boldsymbol{C}_{\mathrm{v}} = \boldsymbol{F}_{\mathrm{v}}^T\boldsymbol{F}_{\mathrm{v}}$

640 reads

$$\eta\dot{\boldsymbol{C}}_{\mathrm{v}} = \mu\left(\boldsymbol{C} - \frac{1}{3}\mathrm{tr}(\boldsymbol{C}\boldsymbol{C}_{\mathrm{v}}^{-1})\boldsymbol{C}_{\mathrm{v}}\right). \tag{B7}$$

At last, we have to define the boundary conditions in the reference configuration. Dirichlet conditions are the same in reference and current configuration, while traction boundary conditions change due to adjusting normal vectors for the different configurations. To model compression and extension, the horizontal displacements acting on the lateral boundaries are com-
645 puted out of the observed strain at the position OE

$$u_{\mathrm{left}} = u_x(t), \qquad u_{\mathrm{right}} = -u_x(t) \tag{B8}$$

with u_x the displacement component in across-flow direction (Eq. 12, Fig. 5). The upper surface is traction-free and the base perceive the depth-increasing water pressure of the current configuration

$$p = \begin{cases} \rho_{\mathrm{sw}}g(-z - u_z) & \text{for } z + u_z \leq 0 \\ 0 & \text{else} \end{cases} \tag{B9}$$

650 in normal direction with sea water density $\rho_{\mathrm{sw}} = 1028\,\mathrm{kg\,m^{-3}}$ and u_z the displacement component in the thickness direction. Hence, we have to compute the water pressure in the reference configuration

$$\boldsymbol{t}_0 = P_0\boldsymbol{N} = pJ\boldsymbol{F}^{-T}\boldsymbol{N} = p\boldsymbol{n} \tag{B10}$$

with the pressure P_0 and the normal vector $\boldsymbol{N}$ in the reference configuration as well as the pressure p and the normal vector $\boldsymbol{n}$ in the current configuration. Additionally, we deform the geometry by temporally and spatially variable fields of basal melt
655 subtracted at the lower boundary and SMB added to the upper boundary.

B2 Viscosity from inverse modeling

For estimating the viscosity distribution in the Filchner-Ronne Ice Shelf, we conduct a control-method inversion for the rheology parameter in the floating part. We use the Ice Sheet and Sea Level System Model (Larour et al., 2012) applied to the
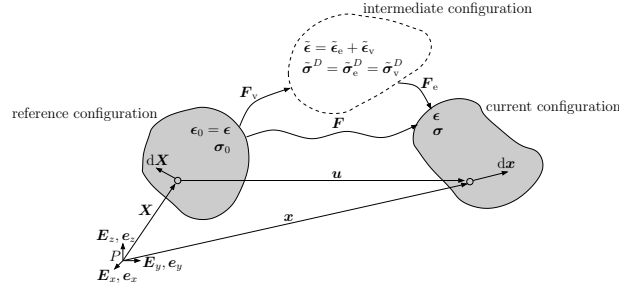
Figure B1. Reference, current and intermediate configurations and their corresponding strain and stress denotation for the finite viscoelastic Maxwell model. In the intermediate configuration (dashed line) the viscoelastic material equations are defined.

Filchner-Ronne Ice Shelf using the Blatter-Pattyn higher-order approximation (Blatter, 1995; Pattyn, 2003). The calculation is done on an unstructured finite element grid with a refined resolution of $2\,\mathrm{km}$ at the grounding line, in the shear margins as well as at other regions of faster ice flow. In the melt channel domain we further refine the resolution of the grid to $0.5\,\mathrm{km}$.

To generate the geometry of the ice shelf the BedMachine Antarctica v2 data set is used (Morlighem et al., 2020; Morlighem, 2020). For the ice rigidity in the grounded region, as well as an initial guess of ice rigidity in the floating shelf, we assume the results of a long-term thermal spin-up also used in Eisen et al. (2020) based on the geothermal flux from Martos et al. (2017). We constrain ice surface velocities to fit the MEaSUREs data set (Mouginot et al., 2019b, a).

Our optimization approach infers iteratively two parameters – the basal friction parameter in the grounded area and the ice rheology parameter in the floating area. For this purpose two cost functions are built. Each cost function consists of two at the surface S evaluated data misfits, linear and logarithmic, as well as a Tikhonov regularization term:

$$J(\boldsymbol{v},p) = \gamma_1 \int\limits_S \frac{(v_x - v_x^{\mathrm{obs}})^2 + (v_y - v_y^{\mathrm{obs}})^2}{2}\,\mathrm{d}S + \gamma_2 \int\limits_S \left(\log\left(\frac{||\boldsymbol{v}|| + \xi}{||\boldsymbol{v}^{\mathrm{obs}}|| + \xi}\right)\right)^2\,\mathrm{d}S + \gamma_t\,J_{\mathrm{reg}}(p) \tag{B11}$$

with $\boldsymbol{v}^{\mathrm{obs}}$ the observed surface velocity, $\boldsymbol{v}$ the modeled velocity, p the respective control parameter for the inversion and a added minimal velocity ξ to avoid singularities. The first term will be most sensitive to velocity observations in fast-flowing areas, the second term will be most sensitive to velocity observations in slow-floating areas, while the third term $J_{\mathrm{reg}}(p)$ penalizes oscillations in the optimization parameter p. We performed an L-curve analysis to find suitable weights $\gamma_1, \gamma_2, \gamma_t$ for both cost functions. With this trade-off curve, we can make sure that we find a regularization term that fits the data well without overfitting noise. For the basal friction inversion, we found best weights $\gamma_1 = 1$, $\gamma_2 = 5 \times 10^{-6}$ and $\gamma_t = 1 \times 10^{-8}$, while for the ice rigidity inversion the optimal weights were $\gamma_1 = 1, \gamma_2 = 0.8$ and $\gamma_t = 4 \times 10^{-17}$.

We linearize and solve the optimization problem using the M1QN3 algorithm with an incomplete adjoint (Larour et al., 2012). For this inversion setting we apply a gradient relative convergence criterion $\varepsilon_{\mathrm{gttol}} = 10^{-6}$ and two points which are less then $\mathrm{dxmin} = 10^{-4}$ from each other are considered identical. Besides we used a maximum number of iterations and function evaluations of 1000. We show our best-fit results for ice viscosity in the region around the melt channel in Fig. B2. The range of the viscosity is between 5.0563×10^{13} and $2.6656 \times 10^{15}\,\mathrm{Pa\,s}$.
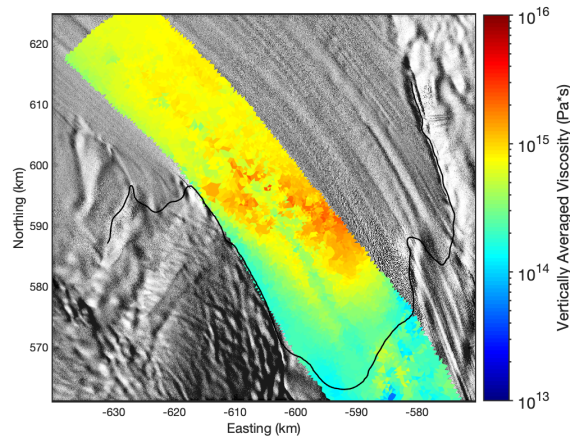
Figure B2. Ice viscosity in the melt channel area obtained from inverse modeling. The map extent is the same as in Fig. 1. The background image is a hillshade of the Reference Elevation Model of Antarctica (Howat et al., 2018, 2019).

B3 Sensitivity of experiment 2 on viscosity

To capture the influence of the viscosity, different constant values (one smaller and one higher as in the second experiment) are investigated in a further experiment. The spin-up for each viscosity starts at $t = -75\,\mathrm{a}$ with an arbitrary basal geometry that should fit seismic IV profile at the end of the spin-up (t_0). The melt rate $a_b^{\mathrm{syn}}(t_0)$ is again assumed to be constant over the spin-up for all different viscosity values. We force the base with the synthetic melt rate (Fig. 3a), the same melt rate we already used in the second experiment. The initial base for the middle and high viscosity is nearly the same as $5 \times 10^{15}\,\mathrm{Pa\,s}$ is for ice a rather high value requiring cold ice (Fig. B8). For the smallest viscosity, a deeper channel at the beginning of the spin-up is needed.

B4 Elastic strain measure

For the concept of nonlinear strain, strain measures are defined and valid in particular configurations. However, the commonly used strain measures, like the Green-Lagrange strain in the reference configuration or the Euler-Almansi strain in the actual configuration, always have combined viscoelastic parts that cannot be split into viscous and elastic parts separately due to the multiplicative decomposition of the deformation gradient (Eq. B3). To quantify the elastic contribution of the melt channel evolution, we consider the Hencky strain, often called true strain, a logarithmic strain measure introduced in more detail by (Cuitino and Ortiz, 1992). Xiao (2005) and Neff et al. (2015) showed an extensive overview of the logarithmic strain properties and its applications. The advantage of the Hencky strain is an additive decomposition of the strain into an elastic and viscous part comparable to the procedure assuming a linearized strain for the linear strain theory. Furthermore, the Hencky strain is identical in the reference and current configuration.

36

700   The Hencky strain is defined by

$$\epsilon^H = \frac{1}{2}\ln(\boldsymbol{F}^T\boldsymbol{F}) = \frac{1}{2}\ln(\boldsymbol{C}). \tag{B12}$$

We can compute the logarithm of the right Cauchy- Green tensor $\boldsymbol{C}$ by logarithmizing the eigenvalues derived by a spectral decomposition. For rigid body motions when $\boldsymbol{C} = \boldsymbol{I}$, the Hencky strain is zero. The eigenvalues of $\boldsymbol{F}^T\boldsymbol{F}$ for the Lagrangian perspective are the same as the eigenvalues of $\boldsymbol{F}\boldsymbol{F}^T$ in the Eulerian sense. Hence, the Hencky strain in the reference configu-
705 ration is the same as in the current configuration and, for simplicity, we call it strain ϵ here.

    In the viscoelastic Maxwell model considering finite strains, we have a multiplicative decomposition of the deformation gradient $\boldsymbol{F}$ in an elastic and viscous part (Eq. B3) and it holds

$$\boldsymbol{C} = \boldsymbol{F}^T\boldsymbol{F} = \boldsymbol{F}_\mathrm{v}^T\boldsymbol{F}_\mathrm{e}^T\boldsymbol{F}_\mathrm{e}\boldsymbol{F}_\mathrm{v} = \boldsymbol{F}_\mathrm{v}^T\boldsymbol{C}_\mathrm{e}\boldsymbol{F}_\mathrm{v} \tag{B13}$$

with $\boldsymbol{C}_\mathrm{e} = \boldsymbol{F}_\mathrm{e}^T\boldsymbol{F}_\mathrm{e}$. Furthermore, we can split the deformation gradient in a rotation $\boldsymbol{R}$ and a stretching $\boldsymbol{U}$ ($\boldsymbol{F} = \boldsymbol{R}\boldsymbol{U}$). The
710 rotation has to be orthogonal, hence, we arbitrarily choose the viscous rotation as the identity tensor ($\boldsymbol{R}_\mathrm{v} = \boldsymbol{I}$) and get

$$\boldsymbol{C} = \boldsymbol{U}_\mathrm{v}^T\boldsymbol{C}_\mathrm{e}\boldsymbol{U}_\mathrm{v} \quad \Rightarrow \quad \ln(\boldsymbol{C}) = \ln(\boldsymbol{U}_\mathrm{v}^T) + \ln(\boldsymbol{C}_\mathrm{e}) + \ln(\boldsymbol{U}_\mathrm{v}). \tag{B14}$$

The stretching is symmetric ($\boldsymbol{U}_\mathrm{v}^T = \boldsymbol{U}_\mathrm{v}$) and we get $2\ln(\boldsymbol{U}_\mathrm{v}) = \ln(\boldsymbol{U}_\mathrm{v}^2) = \ln(\boldsymbol{C}_\mathrm{v})$ based on the relation $\boldsymbol{C}_\mathrm{v} = \boldsymbol{U}_\mathrm{v}^2$. In the end, we can split the strain additive into

$$\underbrace{\ln(\boldsymbol{C})}_{2\epsilon} = \underbrace{\ln(\boldsymbol{C}_\mathrm{e})}_{2\epsilon^\mathrm{e}} + \underbrace{\ln(\boldsymbol{C}_\mathrm{v})}_{2\epsilon^\mathrm{v}} \tag{B15}$$

715 and get the elastic strain

$$\epsilon^\mathrm{e} = \epsilon - \epsilon^\mathrm{v} = \frac{1}{2}\ln(\boldsymbol{C}) - \frac{1}{2}\ln(\boldsymbol{C}_\mathrm{v}), \tag{B16}$$

where $\boldsymbol{C}_\mathrm{v}$ is the internal variable of the viscoelastic material model.

B5 Additional figures
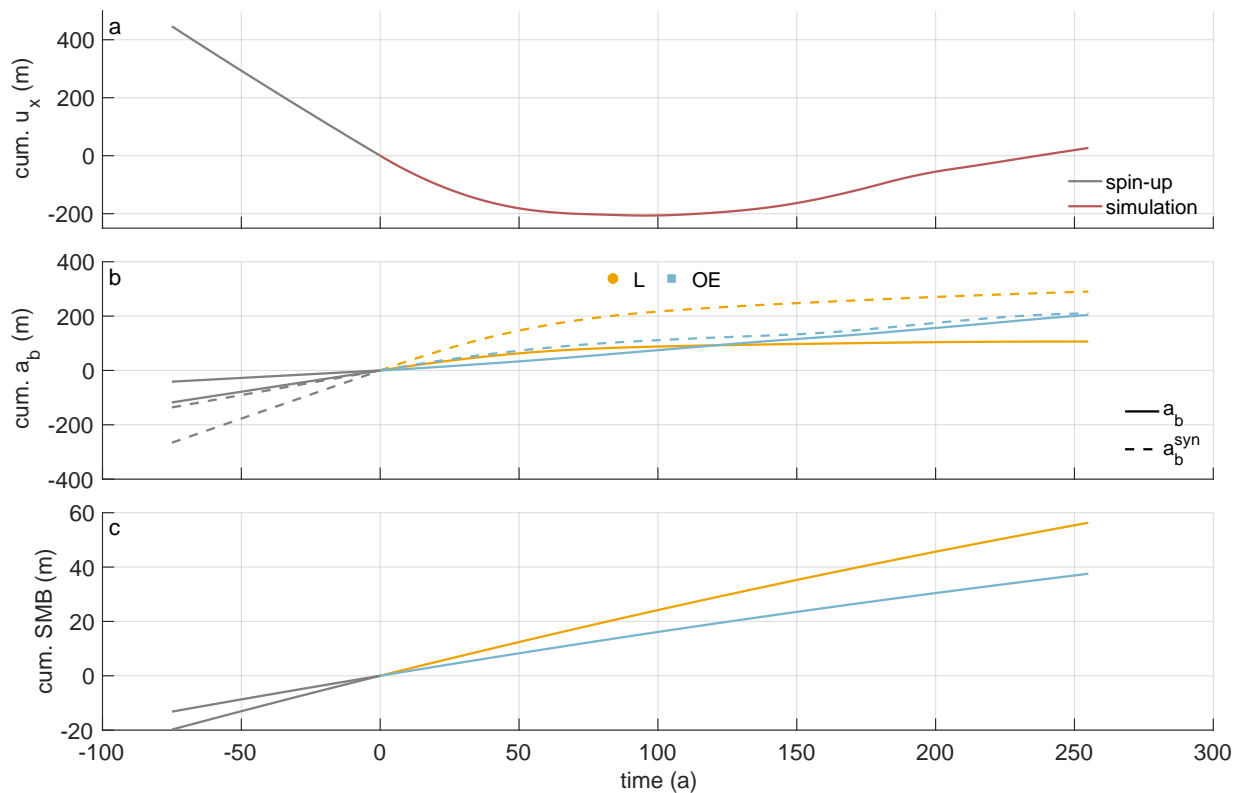
Figure B3. Model input derived from pRES measurements and RACMO (van Wessem et al., 2014). (a) Cumulative horizontal displacement calculated from pRES-derived vertical strain rates outside of the channel. (b) Cumulative basal melt rates above (yellow) and outside the channel (blue). Solid lines are derived from the pRES measurements and dashed lines are synthetic melt rates that are necessary to reproduce the measured ice thickness distribution. (c) Cumulative surface mass balance (SMB) derived from multi-year mean RACMO2.3 data (van Wessem et al., 2014) for a density of $910\,\mathrm{kg\,m^{-3}}$ outside the channel (blue) and above the channel (yellow), 50% larger. Gray lines represent values used in the spin-up and colored lines values used in the simulation of the evolution of the channel.
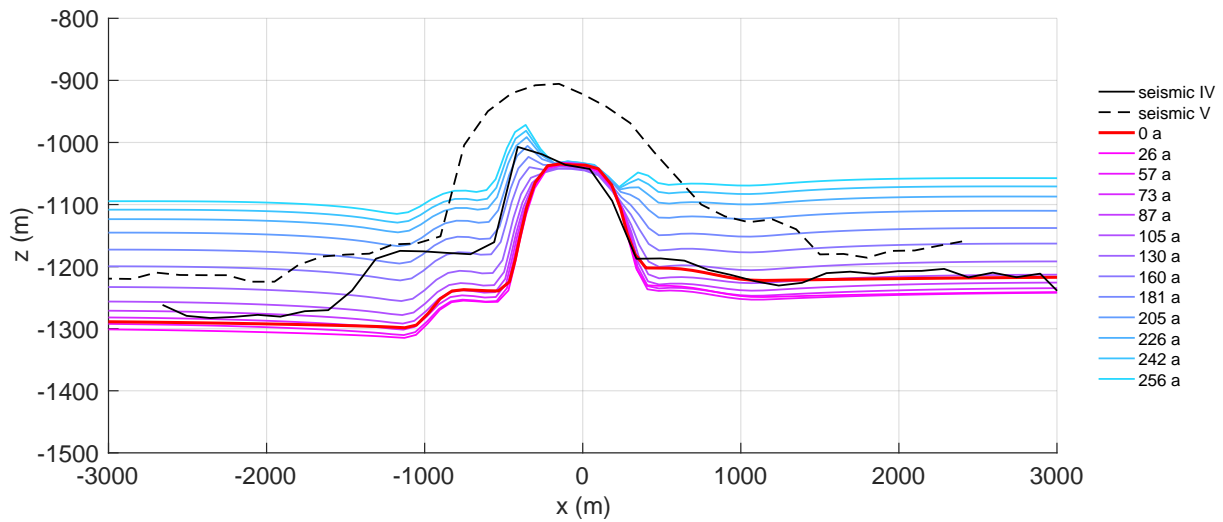
Figure B4. Evolution of the base for the first experiment applying pRES-derived melt rates in the viscoelastic simulation. The black curve shows seismic profile IV (Hofstede et al., 2021b) and the red line the simulated base after the spin-up. For each position of pRES observations, the simulated base is shown using a color distribution ranging from red (furthest upstream) to blue (furthest downstream). The dashed black line is the base of seismic profile V (Hofstede et al., 2021b) near the pRES observation fitting to 130 a
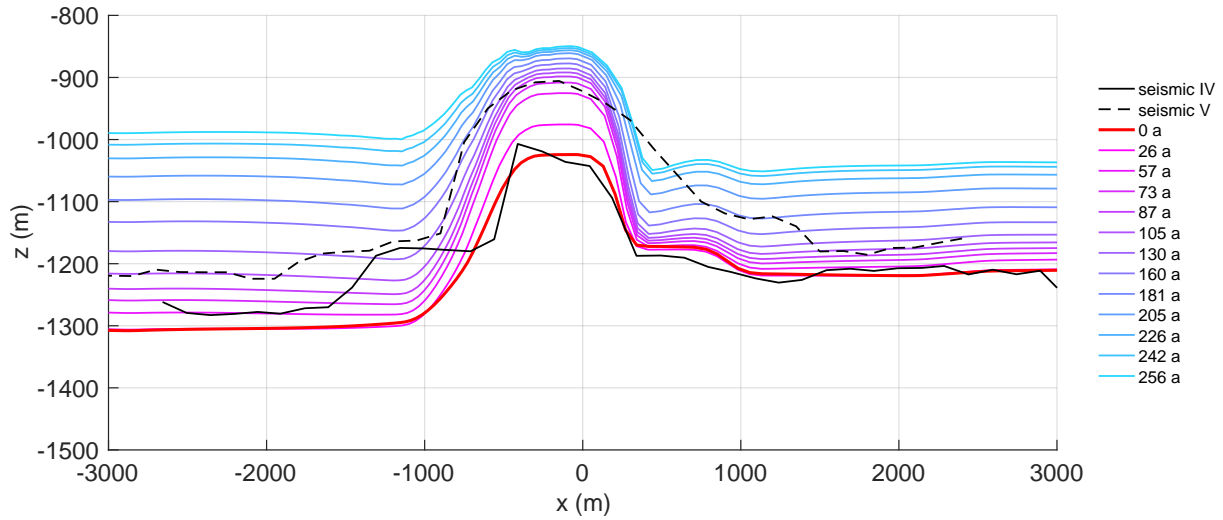
Figure B5. Evolution of the base for the second experiment applying synthetic melt rates in the viscoelastic simulation.The black curve shows seismic profile IV (Hofstede et al., 2021b) and the red line is the simulated base after the spin-up. For each position of pRES observations, the simulated base is shown using a color distribution ranging from red (furthest upstream) to blue (furthest downstream). The dashed black line is the base of seismic profile V (Hofstede et al., 2021b) near the pRES observation fitting to 130 a. The opening of the basal channel cannot be rebuilt with the model as the melt rate inside the channel is only applied to constant channel width. The basal channel stays open during the simulation time of 256 a.
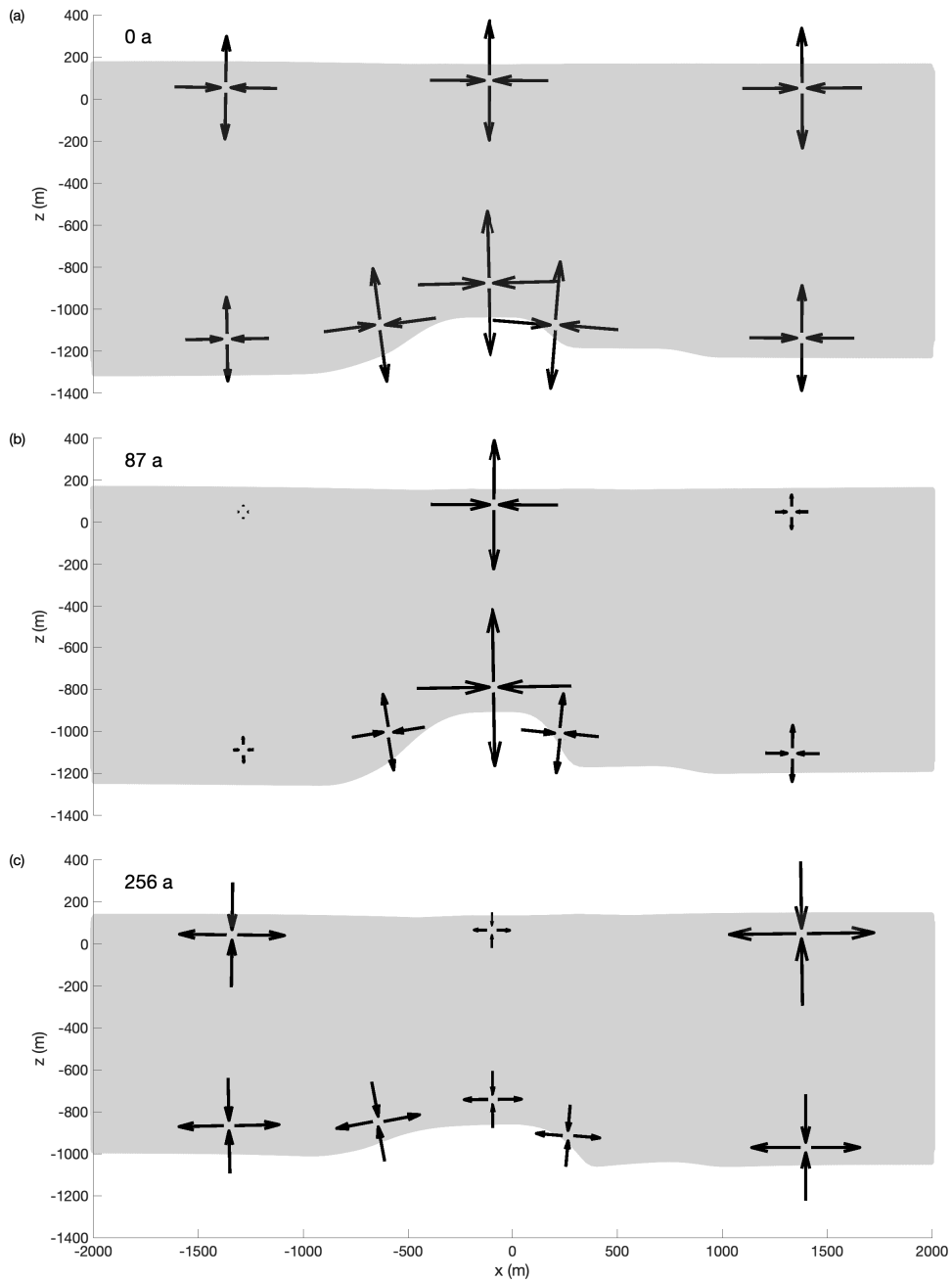
Figure B6. Schematic arrows with their length according to the simulated principal strain magnitude and the pointing direction fitting to principal strain directions at special points in the cross section for three different points in time (a) at $t = 0\,\mathrm{a}$ (after the spinup, maximum lateral compression), (b) $t = 87\,\mathrm{a}$ (small lateral displacement), (c) $t = 256\,\mathrm{a}$ (end of the simulation).

41
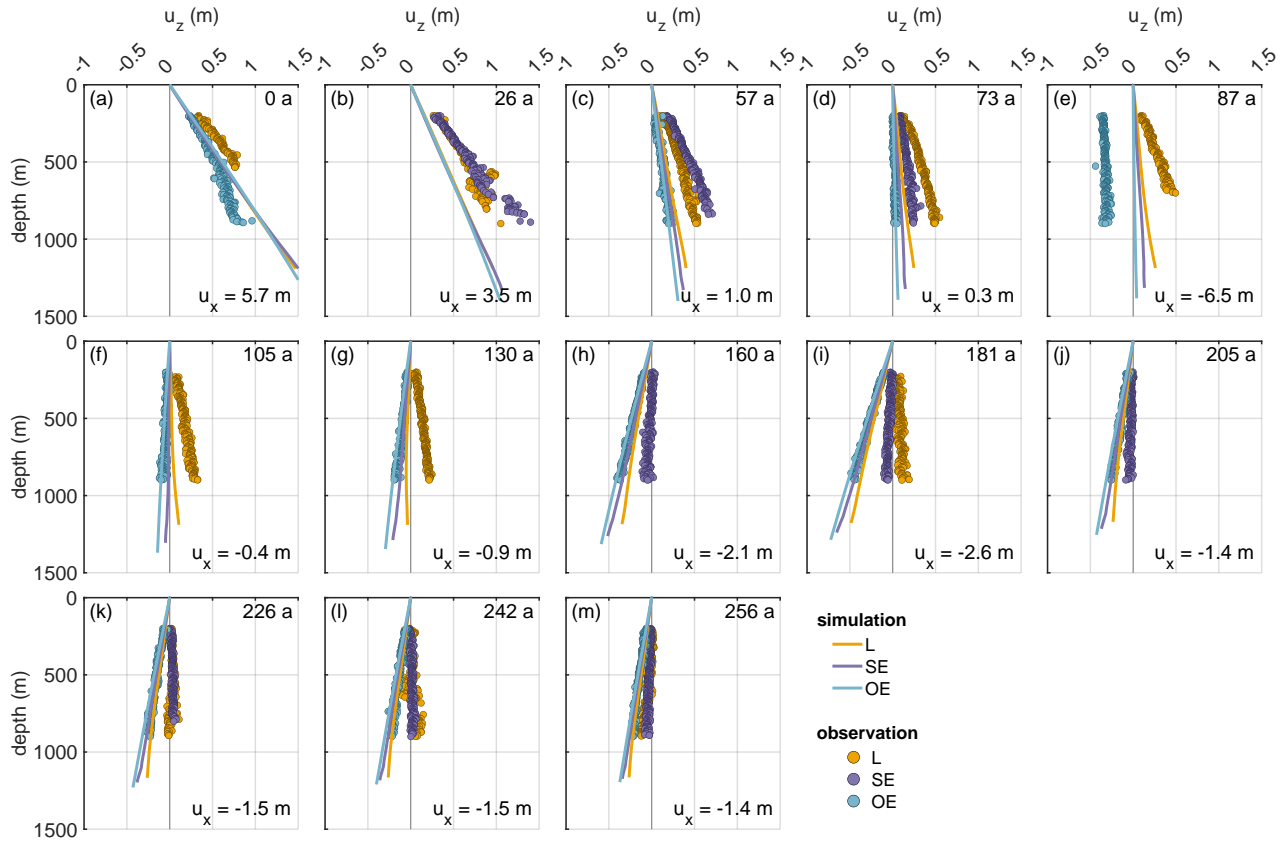
Figure B7. First experiment: comparison of displacements (u_z) derived from pRES measurements (dots) and from the simulations (lines). The different panels show the displacement for $\Delta t = 1\,\mathrm{a}$ allocated to the year of the model (number in upper right corner). The numbers in the lower right corners give horizontal displacement u_x derived from ε_{zz} of the pRES measurements outside the channel (OE) with positive values representing compression and negative values extension.
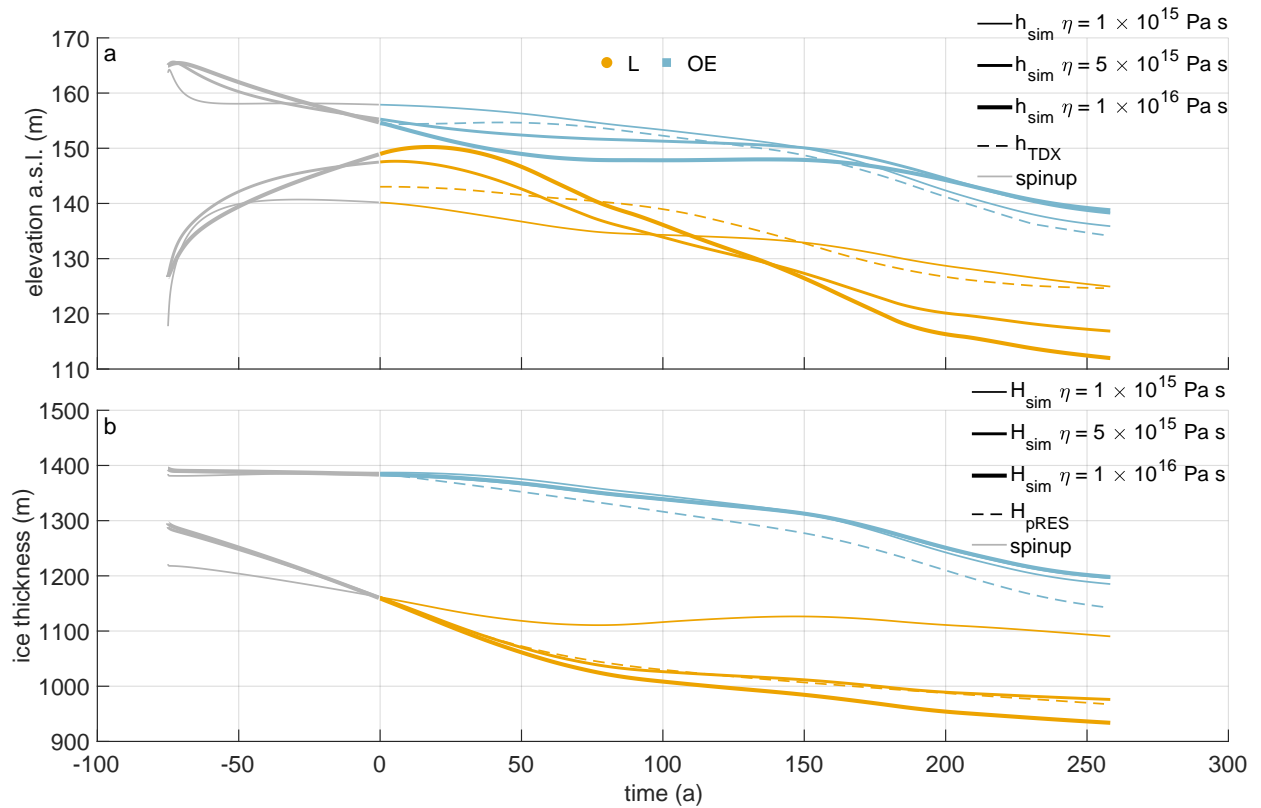
Figure B8. (a) Surface elevation above the channel (yellow) and outside the channel (blue) derived from the simulation (solid lines) and from TanDEM-X DLR (2020) (dashed lines). (b) Ice thickness above the channel (yellow) and outside the channel (blue) derived from the simulation (solid lines) and from pRES measurements (dashed lines). The thickness of the solid lines represents the different viscosities: $1 \times 10^{15}\,\mathrm{Pa\,s}$ (thin line), $5 \times 10^{15}\,\mathrm{Pa\,s}$ (medium line, same value as in the second experiment), $1 \times 10^{16}\,\mathrm{Pa\,s}$ (thick line). Gray lines represent values used in the spin-up and colored lines values used in the simulation of the evolution of the channel.
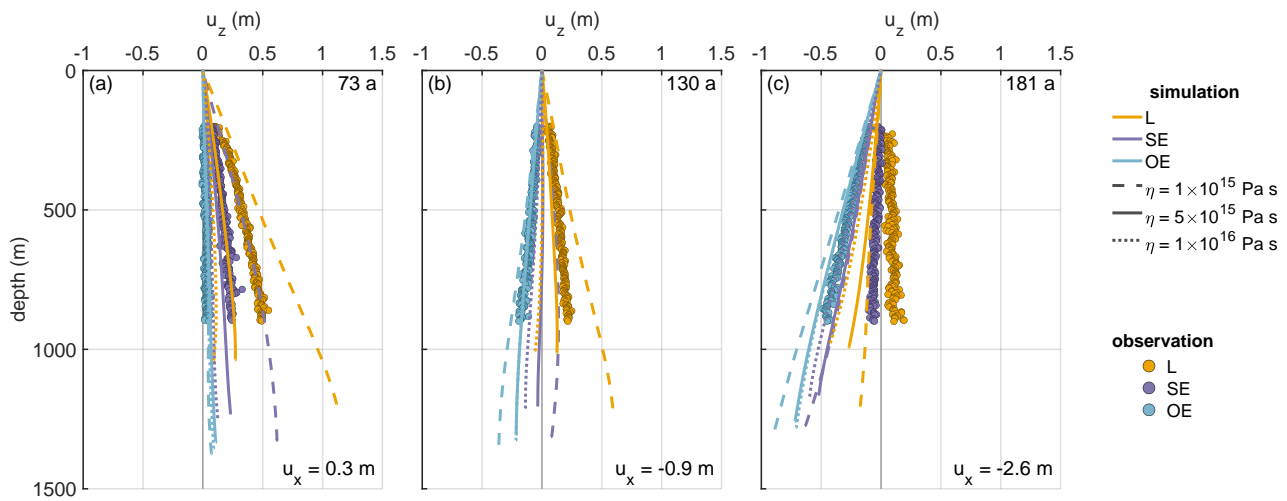
Figure B9. Second experiment: comparison of displacements (u_z) derived from observations (dots) and the simulations for different viscosities displayed by different line styles (lines). The different panels show the displacement for $\Delta t = 1\,\mathrm{a}$ allocated to the simulation time (upper right corner). The numbers in the lower right corners give horizontal displacement u_x derived from ε_{zz} of the pRES measurements outside the channel (OE) with positive values representing compression and negative values extension.
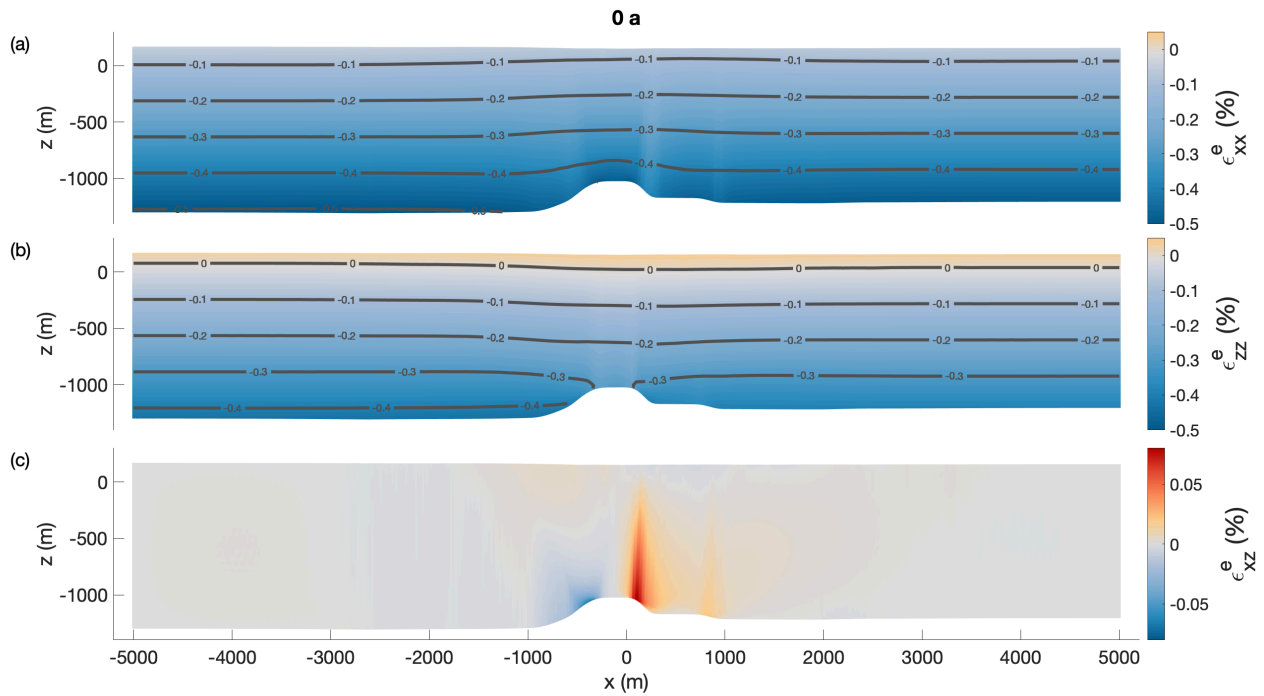
Figure B10. The simulated elastic part of Hencky strain (a) in across-flow direction, (b) in thickness direction and (c) the shear component for the second experiment using synthetic melt rates at $t = 0\,\mathrm{a}$ (after the spin-up, maximum lateral compression). The gray lines are contour lines of the elastic strain components. The normal components reach permille values (the blueish colors denote compression), while the shear component is one order of magnitude smaller.
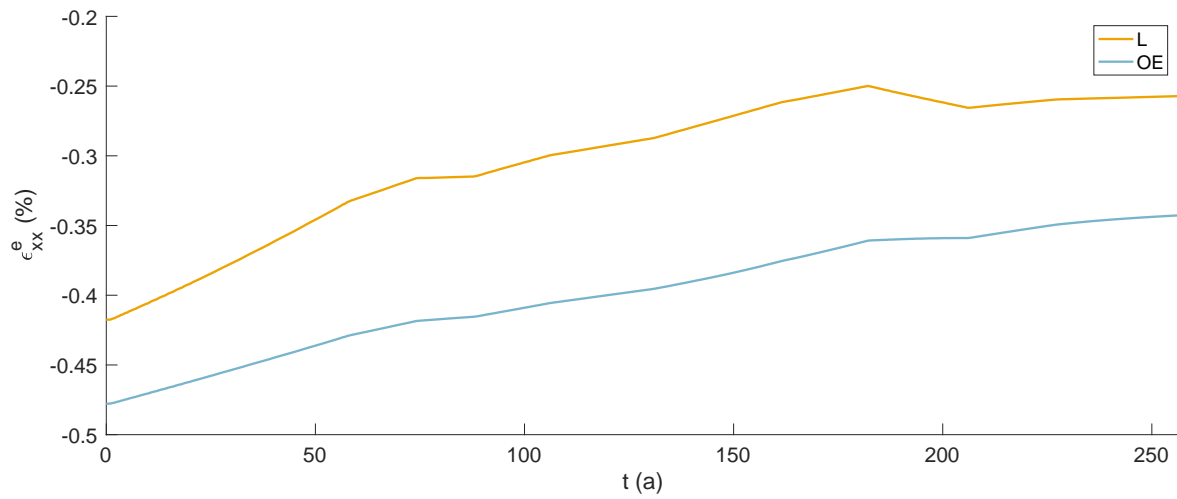
Figure B11. The evolution of the simulated elastic part of Hencky strain at the ice base inside and outside east the channel in percent over the simulation time of $256\,\text{a}$. The initial elastic response of the grounded ice becoming afloat has vanished as the grounding line to far upstream. The spinup of $75\,\text{a}$ leads to a continuous elastic transition at $t = 0\,\text{a}$ the start of the comparison between simulated results and observations.
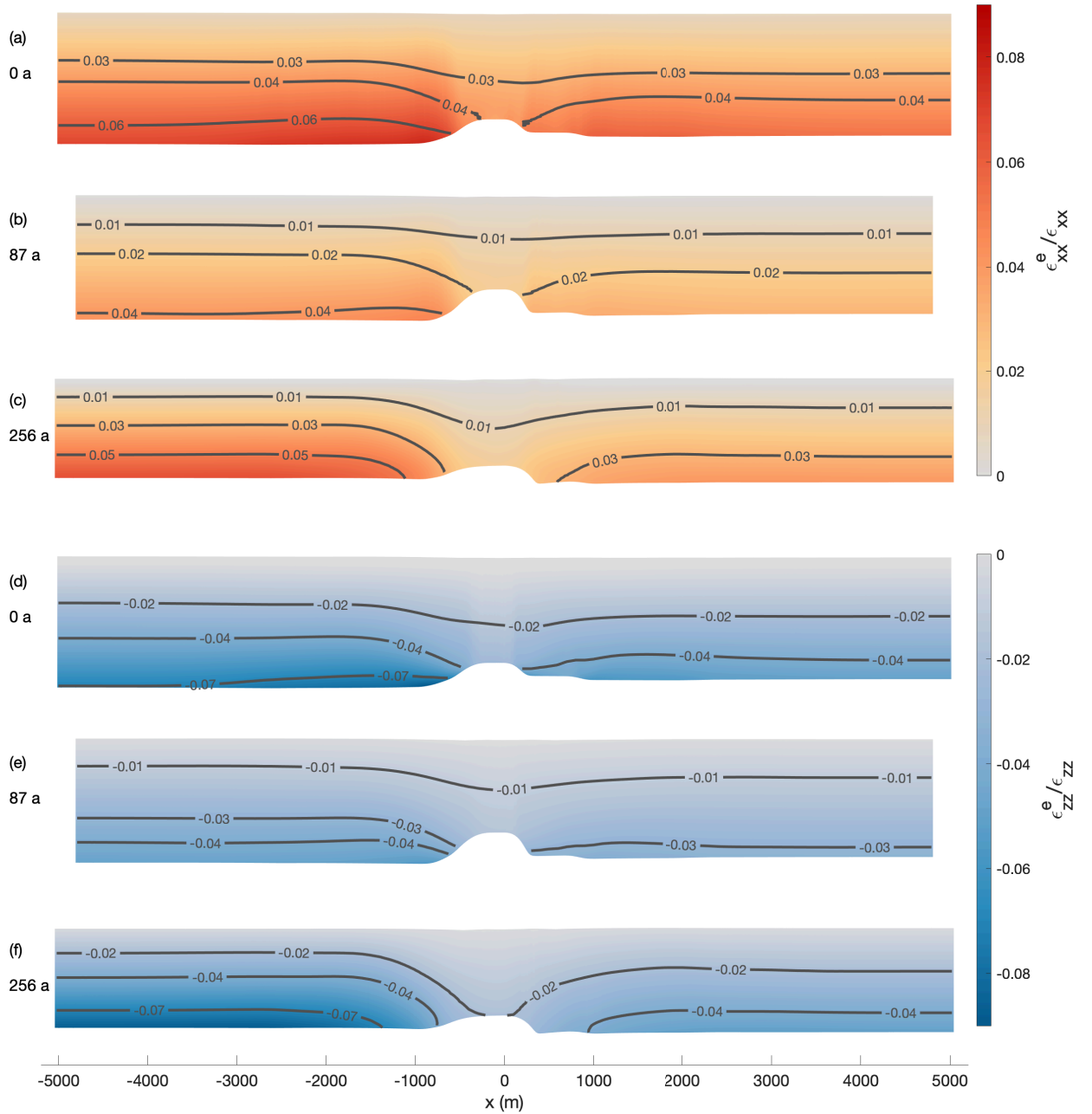
Figure B12. Relative contribution of elastic to total strain of the second experiment using synthetic melt rates for the simulation. The upper three panels show the relative elastic strain in across-flow direction $\epsilon^e_{xx}/\epsilon_{xx}$ for (a) $t = 0\,\mathrm{a}$ (after the spin-up, maximum lateral compression), (b) $t = 87\,\mathrm{a}$ (small lateral displacement), (c) $t = 256\,\mathrm{a}$ (end of the simulation). The lower three panels show the relative elastic strain in thickness direction $\epsilon^e_{zz}/\epsilon_{zz}$ for (d) $t = 0\,\mathrm{a}$ (after the spin-up, maximum lateral compression), (e) $t = 87\,\mathrm{a}$ (small lateral displacement), (f) $t = 256\,\mathrm{a}$ (end of the simulation). The negative values denote that the elastic and viscous strains have different signs. The elastic and viscous Hencky strain sum up to the total strain.

References

Alley, K. E., Scambos, T. A., Alley, R. B., and Holschuh, N.: Troughs developed in ice-stream shear margins precondition ice shelves for ocean-driven breakup, Science Advances, 5, eaax2215, https://doi.org/10.1126/sciadv.aax2215, 2019.

Blatter, H.: Velocity and stress fields in grounded glaciers: a simple algorithm for including deviatoric stress gradients, Journal of Glaciology, 41, 333–344, https://doi.org/10.3189/S002214300001621X, 1995.

Brennan, P. V., Lok, L. B., Nicholls, K., and Corr, H.: Phase-sensitive FMCW radar system for high-precision Antarctic ice shelf profile monitoring, IET Radar, Sonar & Navigation, 8, 776–786, https://doi.org/10.1049/iet-rsn.2013.0053, 2014.

Christmann, J., Plate, C., Müller, R., and Humbert, A.: Viscous and viscoelastic stress states at the calving front of Antarctic ice shelves, Annals of Glaciology, 57, 10–18, https://doi.org/10.1017/aog.2016.18, 2016.

Christmann, J., Müller, R., and Humbert, A.: On nonlinear strain theory for a viscoelastic material model and its implications for calving of ice shelves, Journal of Glaciology, 65, 212–224, https://doi.org/10.1017/jog.2018.107, 2019.

Christmann, J., Helm, V., Khan, S. A., Kleiner, T., Müller, R., Morlighem, M., Neckel, N., Rückamp, M., Steinhage, D., Zeising, O., and Humbert, A.: Elastic deformation plays a non-negligible role in Greenland's outlet glacier flow, Communications Earth & Environment, 2, 232, https://doi.org/10.1038/s43247-021-00296-3, 2021.

Corr, H. F., Jenkins, A., Nicholls, K. W., and Doake, C.: Precise measurement of changes in ice-shelf thickness by phase-sensitive radar to determine basal melt rates, Geophysical Research Letters, 29, 73–1 73–4, https://doi.org/10.1029/2001GL014618, 2002.

Cuitino, A. and Ortiz, M.: Computational modelling of single crystals, Modelling and Simulation in Materials Science and Engineering, 1, 225–263, https://doi.org/10.1088/0965-0393/1/3/001, 1992.

Dinniman, M. S., Asay-Davis, X. S., Galton-Fenzi, B. K., Holland, P. R., Jenkins, A., and Timmermann, R.: Modeling Ice Shelf/Ocean Interaction in Antarctica: A Review, Oceanography, 29, 144–153, https://doi.org/10.5670/oceanog.2016.106, 2016.

DLR: TanDEM-X - PolarDEM - Antarctica, 90m, https://doi.org/10.15489/9jhr18jepi65, 2020.

Dow, C. F., Lee, W. S., Greenbaum, J. S., Greene, C. A., Blankenship, D. D., Poinar, K., Forrest, A. L., Young, D. A., and Zappa, C. J.: Basal channels drive active surface hydrology and transverse ice shelf fracture, Science Advances, 4, https://doi.org/10.1126/sciadv.aao7212, 2018.

Drews, R.: Evolution of ice-shelf channels in Antarctic ice shelves, The Cryosphere, 9, 1169–1181, https://doi.org/10.5194/tc-9-1169-2015, 2015.

Drews, R., Pattyn, F., Hewitt, I. J., Ng, F. S. L., Berger, S., Matsuoka, K., Helm, V., Bergeot, N., Favier, L., and Neckel, N.: Actively evolving subglacial conduits and eskers initiate ice shelf channels at an Antarctic grounding line, Nature Communications, 8, 15 228, https://doi.org/10.1038/ncomms15228, 2017.

Dutrieux, P., Stewart, C., Jenkins, A., Nicholls, K. W., Corr, H. F., Rignot, E., and Steffen, K.: Basal terraces on melting ice shelves, Geophysical Research Letters, 41, 5506–5513, https://doi.org/10.1002/2014GL060618, 2014.

Eisen, O., Winter, A., Steinhage, D., Kleiner, T., and Humbert, A.: Basal roughness of the East Antarctic Ice Sheet in relation to flow speed and basal thermal state, Annals of Glaciology, 61, 162–175, https://doi.org/10.1017/aog.2020.47, 2020.

Foerste, C., Bruinsma, S., Abrykosov, O., Lemoine, J.-M., Marty, J. C., Flechtner, F., Balmino, G., Barthelmes, F., and Biancale, R.: EIGEN-6C4 The latest combined global gravity field model including GOCE data up to degree and order 2190 of GFZ Potsdam and GRGS Toulouse, https://doi.org/10.5880/icgem.2015.1, 2014.

Fujita, S., Matsuoka, T., Ishida, T., Matsuoka, K., and Mae, S.: A summary of the complex dielectric permittivity of ice in the megahertz range and its applications for radar sounding of polar ice sheets, in: Physics of ice core records, pp. 185–212, Hokkaido University Press, 2000.

Galton-Fenzi, B. K., Hunter, J. R., Coleman, R., Marsland, S. J., and Warner, R. C.: Modeling the basal melting and marine ice accretion of the Amery Ice Shelf, Journal of Geophysical Research: Oceans, 117, https://doi.org/10.1029/2012JC008214, 2012.

Gladish, C. V., Holland, D. M., Holland, P. R., and Price, S. F.: Ice-shelf basal channels in a coupled ice/ocean model, Journal of Glaciology, 58, 1227–1244, https://doi.org/10.3189/2012JoG12J003, 2012.

Gudmundsson, H.: Ice-stream response to ocean tides and the form of the basal sliding law, The Cryosphere, 5 (1), 259–270, https://doi.org/10.5194/tc-5-259-2011, 2011.

Gwyther, D. E., Kusahara, K., Asay-Davis, X. S., Dinniman, M. S., and Galton-Fenzi, B. K.: Vertical processes and resolution impact ice shelf basal melting: A multi-model study, Ocean Modelling, 147, 101 569, https://doi.org/10.1016/j.ocemod.2020.101569, 2020.

Haupt, P.: Continuum Mechanics and Theory of Materials, Springer, Berlin, https://doi.org/10.1007/978-3-662-04775-0, 2000.

Helm, V., Humbert, A., and Miller, H.: Elevation and elevation change of Greenland and Antarctica derived from CryoSat-2, The Cryosphere, 8, 1539–1559, https://doi.org/10.5194/tc-8-1539-2014, 2014.

Herron, M. M. and Langway, C. C.: Firn densification: an empirical model, Journal of Glaciology, 25, 373–385, https://doi.org/10.3189/S0022143000015239, 1980.

Hofstede, C., Beyer, S., Corr, H., Eisen, O., Hattermann, T., Helm, V., Neckel, N., Smith, E. C., Steinhage, D., Zeising, O., and Humbert, A.: Evidence for a grounding line fan at the onset of a basal channel under the ice shelf of Support Force Glacier, Antarctica, revealed by reflection seismics, The Cryosphere, 15, 1517–1535, https://doi.org/10.5194/tc-15-1517-2021, 2021a.

Hofstede, C., Beyer, S., Corr, H. F. J., Eisen, O., Hattermann, T., Helm, V., Neckel, N., Smith, E. C., Steinhage, D., Zeising, O., and Humbert, A.: Seismic reflection data of a basal channel and ocean cavity at the ice shelf-grounding line area of Support Force Glacier, Filchner Ice Shelf, Antarctica, https://doi.org/10.1594/PANGAEA.932278, 2021b.

Holland, D. M. and Jenkins, A.: Modeling Thermodynamic Ice–Ocean Interactions at the Base of an Ice Shelf, Journal of Physical Oceanography, 29, 1787 – 1800, https://doi.org/10.1175/1520-0485(1999)029<1787:MTIOIA>2.0.CO;2, 1999.

Holland, P. R. and Kwok, R.: Wind-driven trends in Antarctic sea-ice drift, Nature Geoscience, 5, 872–875, https://doi.org/10.1038/ngeo1627, 2012.

Howat, I., Morin, P., Porter, C., and Noh, M.-J.: The Reference Elevation Model of Antarctica, https://doi.org/10.7910/DVN/SAIK8B, 2018.

Howat, I., Porter, C., Smith, B. E., Noh, M.-J., and Morin, P.: The Reference Elevation Model of Antarctica, The Cryosphere, 13, 665–674, https://doi.org/10.5194/tc-13-665-2019, 2019.

Humbert, A., Steinhage, D., Helm, V., Hoerz, S., Berendt, J., Leipprand, E., Christmann, J., Plate, C., and Müller, R.: On the link between surface and basal structures of the Jelbart Ice Shelf, Antarctica, Journal of Glaciology, 61, 975–986, https://doi.org/10.3189/2015JoG15J023, 2015.

Humbert, A., Steinhage, D., Helm, V., Beyer, S., and Kleiner, T.: Missing evidence of widespread subglacial lakes at Recovery Glacier, Antarctica, Journal of Geophysical Research: Earth Surface, 123, 2802–2826, https://doi.org/10.1029/2017JF004591, 2018.

Jenkins, A. and Doake, C.: Ice-ocean interaction on Ronne Ice Shelf, Antarctica, Journal of Geophysical Research: Oceans, 96, 791–813, https://doi.org/10.1029/90JC01952, 1991.

Jenkins, A., Corr, H. F., Nicholls, K. W., Stewart, C. L., and Doake, C. S.: Interactions between ice and ocean observed with phase-sensitive radar near an Antarctic ice-shelf grounding line, Journal of Glaciology, 52, 325–346, https://doi.org/10.3189/172756506781828502, 2006.

Jeofry, H., Ross, N., Le Brocq, A., Graham, A. G. C., Li, J., Gogineni, P., Morlighem, M., Jordan, T., and Siegert, M. J.: Hard rock landforms generate 130 km ice shelf channels through water focusing in basal corrugations, Nature Communications, 8, 4576, https://doi.org/10.1038/s41467-018-06679-z, 2018.

Jourdain, N. C., Mathiot, P., Merino, N., Durand, G., Le Sommer, J., Spence, P., Dutrieux, P., and Madec, G.: Ocean circulation and sea-ice thinning induced by melting ice shelves in the Amundsen Sea, Journal of Geophysical Research: Oceans, 122, 2550–2573, https://doi.org/10.1002/2016JC012509, 2017.

Kovacs, A., Gow, A. J., and Morey, R. M.: The in-situ dielectric constant of polar firn revisited, Cold Regions Science and Technology, 23, 245 – 256, https://doi.org/10.1016/0165-232X(94)00016-Q, 1995.

Langley, K., von Deschwanden, A., Kohler, J., Sinisalo, A., Matsuoka, K., Hattermann, T., Humbert, A., Nøst, O., and Isaksson, E.: Complex network of channels beneath an Antarctic ice shelf, Geophysical Research Letters, 41, 1209–1215, https://doi.org/10.1002/2013GL058947, 2014.

Larour, E., Seroussi, H., Morlighem, M., and Rignot, E.: Continental scale, high order, high spatial resolution, ice sheet modeling using the Ice Sheet System Model (ISSM), Journal of Geophysical Research: Earth Surface, 117, F01 022, https://doi.org/10.1029/2011JF002140, 2012.

Le Brocq, A. M., Ross, N., Griggs, J. A., Bingham, R. G., Corr, H. F., Ferraccioli, F., Jenkins, A., Jordan, T. A., Payne, A. J., Rippin, D. M., et al.: Evidence from ice shelves for channelized meltwater flow beneath the Antarctic Ice Sheet, Nature Geoscience, 6, 945, https://doi.org/10.1038/ngeo1977, 2013.

Lee, E. H.: Elastic-plastic deformation at finite strains, Journal of Applied Mechanics, 36, 1–6, https://doi.org/10.1115/1.3564580, 1969.

MacAyeal, D. R.: Thermohaline circulation below the Ross Ice Shelf: A consequence of tidally induced vertical mixing and basal melting, Journal of Geophysical Research: Oceans, 89, 597–606, https://doi.org/https://doi.org/10.1029/JC089iC01p00597, 1984.

Marsh, O. J., Fricker, H. A., Siegfried, M. R., Christianson, K., Nicholls, K. W., Corr, H. F., and Catania, G.: High basal melting forming a channel at the grounding line of Ross Ice Shelf, Antarctica, Geophysical Research Letters, 43, 250–255, https://doi.org/10.1002/2015GL066612, 2016.

Martos, Y. M., Catalán, M., Jordan, T. A., Golynsky, A., Golynsky, D., Eagles, G., and Vaughan, D. G.: Heat Flux Distribution of Antarctica Unveiled, Geophysical Research Letters, 44, 11,417–11,426, https://doi.org/10.1002/2017GL075609, 2017.

Millgate, T., Holland, P. R., Jenkins, A., and Johnson, H. L.: The effect of basal channels on oceanic ice-shelf melting, Journal of Geophysical Research: Oceans, 118, 6951–6964, https://doi.org/10.1002/2013JC009402, 2013.

Morlighem, M.: MEaSUREs BedMachine Antarctica, Version 2. Boulder, Colorado USA. NASA National Snow and Ice Data Center Distributed Active Archive Center, Accessed 12 April 2021, https://doi.org/10.5067/E1QL9HFQ7A8M, 2020.

Morlighem, M., Rignot, E., Binder, T., Blankenship, D., Drews, R., Eagles, G., Eisen, O., Ferraccioli, F., Forsberg, R., Fretwell, P., Goel, V., Greenbaum, J. S., Gudmundsson, H., Guo, J., Helm, V., Hofstede, C., Howat, I., Humbert, A., Jokat, W., Karlsson, N. B., Lee, W. S., Matsuoka, K., Millan, R., Mouginot, J., Paden, J., Pattyn, F., Roberts, J., Rosier, S., Ruppel, A., Seroussi, H., Smith, E. C., Steinhage, D., Sun, B., Broeke, M. R. v. d., Ommen, T. D. v., Wessem, M. v., and Young, D. A.: Deep glacial troughs and stabilizing ridges unveiled beneath the margins of the Antarctic ice sheet, Nature Geoscience, 13, 132–137, https://doi.org/10.1038/s41561-019-0510-8, 2020.

Mouginot, J., Rignot, E., and Scheuchl, B.: MEaSUREs Phase-Based Antarctica Ice Velocity Map, Version 1. Boulder, Colorado USA. NASA National Snow and Ice Data Center Distributed Active Archive Center, Accessed 13 April 2021, https://doi.org/10.5067/PZ3NJ5RXRH10, 2019a.

Mouginot, J., Rignot, E., and Scheuchl, B.: Continent-Wide, Interferometric SAR Phase, Mapping of Antarctic Ice Velocity, Geophysical Research Letters, 46, 9710–9718, https://doi.org/10.1029/2019GL083826, 2019b.

Naughten, K. A., De Rydt, J., Rosier, S. H. R., Jenkins, A., Holland, P. R., and Ridley, J. K.: Two-timescale response of a large Antarctic ice shelf to climate change, Nature Communications, 12, 1991, https://doi.org/10.1038/s41467-021-22259-0, 2021.

845 Neff, P., Ghiba, I.-D., and Lankeit, J.: The exponentiated Hencky-logarithmic strain energy. Part I: constitutive issues and rank-one convexity, Journal of Elasticity, 121, 143–234, https://doi.org/10.1007/s10659-015-9524-7, 2015.

Nicholls, K. W.: Predicted reduction in basal melt rates of an Antarctic ice shelf in a warmer climate, Nature, 388, 460–462, https://doi.org/10.1038/41302, 1997.

Nicholls, K. W.: The study of ice shelf-ocean interaction—techniques and recent results, Advances in Polar Science, 3, 222–230,
850 https://doi.org/10.13679/j.advps.2018.3.00222, 2018.

Nicholls, K. W., Corr, H. F., Stewart, C. L., Lok, L. B., Brennan, P. V., and Vaughan, D. G.: A ground-based radar for measuring vertical strain rates and time-varying basal melt rates in ice sheets and shelves, Journal of Glaciology, 61, 1079–1087, https://doi.org/10.3189/2015JoG15J073, 2015.

Pattyn, F.: A new three-dimensional higher-order thermomechanical ice sheet model: Basic sensitivity, ice stream development, and ice flow
855 across subglacial lakes, J. Geophys. Res. Solid Earth, 108, https://doi.org/10.1029/2002JB002329, 2003.

Reeh, N., Mayer, C., Olesen, O. B., Christensen, E. L., and Thomsen, H. H.: Tidal movement of Nioghalvfjerdsfjorden glacier, northeast Greenland: observations and modelling, Annals of Glaciology, 31, 111–117, https://doi.org/10.3189/172756400781820408, 2000.

Rignot, E. and Steffen, K.: Channelized bottom melting and stability of floating ice shelves, Geophysical Research Letters, 35, https://doi.org/10.1029/2007GL031765, 2008.

860 Rizzoli, P., Martone, M., Gonzalez, C., Wecklich, C., Borla Tridon, D., Bräutigam, B., Bachmann, M., Schulze, D., Fritz, T., Huber, M., Wessel, B., Krieger, G., Zink, M., and Moreira, A.: Generation and performance assessment of the global TanDEM-X digital elevation model, ISPRS Journal of Photogrammetry and Remote Sensing, 132, 119–139, https://doi.org/10.1016/j.isprsjprs.2017.08.008, 2017.

Schultz, T.: Viskoelastische Modellierung der Dynamik eines Gletschers als Antwort auf basales Schmelzen und die Oberflächenmassenbilanz, Master thesis, 2017.

865 Sergienko, O.: Basal channels on ice shelves, Journal of Geophysical Research: Earth Surface, 118, 1342–1355, https://doi.org/10.1002/jgrf.20105, 2013.

Seroussi, H., Nakayama, Y., Larour, E., Menemenlis, D., Morlighem, M., Rignot, E., and Khazendar, A.: Continued retreat of Thwaites Glacier, West Antarctica, controlled by bed topography and ocean circulation, Geophysical Research Letters, 44, 6191–6199, https://doi.org/10.1002/2017GL072910, 2017.

870 Smith, B. E., Fricker, H. A., Joughin, I. R., and Tulaczyk, S.: An inventory of active subglacial lakes in Antarctica detected by ICESat (2003–2008), Journal of Glaciology, 55, 573–595, https://doi.org/10.3189/002214309789470879, 2009.

Stanton, T., Shaw, W., Truffer, M., Corr, H., Peters, L., Riverman, K., Bindschadler, R., Holland, D., and Anandakrishnan, S.: Channelized ice melting in the ocean boundary layer beneath Pine Island Glacier, Antarctica, Science, 341, 1236–1239, https://doi.org/10.1126/science.1239373, 2013.

875 Stewart, C. L., Christoffersen, P., Nicholls, K. W., Williams, M. J., and Dowdeswell, J. A.: Basal melting of Ross Ice Shelf from solar heat absorption in an ice-front polynya, Nature Geoscience, 12, 435, https://doi.org/10.1038/s41561-019-0356-0, 2019.

Timmermann, R. and Hellmer, H.: Southern Ocean warming and increased ice shelf basal melting in the twenty-first and twenty-second centuries based on coupled ice-ocean finite-element modelling, Ocean Dynamics, 63, https://doi.org/10.1007/s10236-013-0642-0, 2013.

van Wessem, J., Reijmer, C., Morlighem, M., Mouginot, J., Rignot, E., Medley, B., Joughin, I., Wouters, B., Depoorter, M., Bamber, J., et al.: Improved representation of East Antarctic surface mass balance in a regional atmospheric climate model, Journal of Glaciology, 60, 761–770, https://doi.org/10.3189/2014JoG14J051, 2014.

Vaňková, I., Nicholls, K. W., Corr, H. F., Makinson, K., and Brennan, P. V.: Observations of tidal melt and vertical strain at the Filchner-Ronne Ice Shelf, Antarctica, Journal of Geophysical Research: Earth Surface, 125, e2019JF005 280, https://doi.org/10.1029/2019JF005280, 2020.

Vaňková, I., Nicholls, K. W., and Corr, H. F. J.: The Nature of Ice Intermittently Accreted at the Base of Ronne Ice Shelf, Antarctica, Assessed Using Phase-Sensitive Radar, Journal of Geophysical Research: Oceans, 126, e2021JC017 290, https://doi.org/10.1029/2021JC017290, 2021.

Vaughan, D. G., Corr, H. F., Bindschadler, R. A., Dutrieux, P., Gudmundsson, G. H., Jenkins, A., Newman, T., Vornberger, P., and Wingham, D. J.: Subglacial melt channels and fracture in the floating part of Pine Island Glacier, Antarctica, Journal of Geophysical Research: Earth Surface, 117, https://doi.org/10.1029/2012JF002360, 2012.

Washam, P., Nicholls, K. W., Münchow, A., and Padman, L.: Summer surface melt thins Petermann Gletscher Ice Shelf by enhancing channelized basal melt, Journal of Glaciology, 65, 662–674, https://doi.org/10.1017/jog.2019.43, 2019.

Wearing, M. G., Stevens, L. A., Dutrieux, P., and Kingslake, J.: Ice-Shelf Basal Melt Channels Stabilized by Secondary Flow, Geophysical Research Letters, 48, e2021GL094 872, https://doi.org/10.1029/2021GL094872, 2021.

Xiao, H.: Hencky strain and Hencky model: extending history and ongoing tradition, Multidiscipline Modeling in Materials and Structures, 1, 1–52, https://doi.org/10.1163/1573611054455148, 2005.

Zeising, O. and Humbert, A.: Indication of high basal melting at the EastGRIP drill site on the Northeast Greenland Ice Stream, The Cryosphere, 15, 3119–3128, https://doi.org/10.5194/tc-15-3119-2021, 2021.

Zeising, O., Steinhage, D., Nicholls, K. W., Corr, H. F. J., Stewart, C. L., and Humbert, A.: Basal melt of the southern Filchner Ice Shelf, Antarctica, The Cryosphere, 16, 1469–1482, https://doi.org/10.5194/tc-16-1469-2022, 2022.

Authors point-to-point response on Editor comments

Line 11-12: What does "diminish" mean precisely in this context? That they are less frequent perhaps?
"Diminish" means that they decline in depth, width, they disappear, fade out.

Line 16: maybe "tend to occur less frequently"?
We think that "tend to occur less frequently" is not really representing what we aim to describe. However, it is correct that further downstream in ice shelves, they do appear less frequently, but we aim here to explain that they vanish with distance.

Line 25: are linked to incisions at the ice base due to buoyancy

Thanks, incisions is the perfect term here. We rephrased it accordingly for the revised version.

Line 26: This is not clear at all

We rephrase this and added another sentence for the revised version, so that it will read as 'Surface troughs on ice shelves are linked to incisions at the ice base, thus either to melt channels (citations) or to basal crevasses (citation). The surface troughs are formed by viscoelastic deformations in the transition to buoyancy and buoyancy equilibrium itself.'

Line 30: *the* lateral dimension

Done.

Line. 33-36: Tenses are inconsistent in this sentence and the next. Present tense seems more appropriate, but whatever the authors choose, please apply it consistently.
Thank you for this comment! In the revised version, we choose the present tense for the marked sentences.

Line 33: downstream?

Done.

Line. 37: It is unclear if the authors are referring to sub ice shelf channels in general or to the specific channel that is subject of the study. If the former, I would rephrase such channels -> sub ice shelf channels.
Yes, you are right. The wording "such channels" was misleading. So we changed it to "sub ice shelf channels", as you suggested.

Line 39: the lateral direction

Done.

Line 42: The mechanism described below is not specific to channels but to ice shelves in particular and was first (to my knowledge) described by A. Jenkins, A one-dimensional model of ice shelf-ocean interaction, JGR 1991, and even earlier by D. MacAyeal in the context of tidally induced melting.

This is correct. We have rephrased it and also cite Doug MayAyeal's work from 1994 in the revised version.

Line 44: Falling pressure due to what? I suppose that the authors are referring to decreasing hydrostatic pressure as one moves downstream along the ice shelf and the shelf draft decreases, but this should not be left to guessing.

This was mentioned also by the reviewers and is discussed below. We rephrased these sentences.

Line 51: Again, this comes out of the blue. It is understandable by a reader knowledgeable in ice sheet modeling, but it would be great if the authors could provide more context and avoid giving for granted concepts that are specific to a relatively small part of the audience.

Yes, we agree, this is like a jump into icy water and we rephrase this in the revised version.

Line 57: assessing in what regard? Can the authors be more specific?

We basically wanted to check with this simple computation if it is in hydrostatic equilibrium. Outside the hinge zone (which can be identified using interferograms), we have no other observational means to understand if the ice is in hydrostatic equilibrium. We rephrased 'assess' into 'understand' in the revised version.

Line 60: gradients in space?

To our knowledge, gradients are defined as derivatives in space. Therefore, it seems a bit odd, to add to each notion of gradients, spatial gradients.

Line 60: I believe "This process .." would work better

That is a very good suggestion, thank you.

Line 61: viscously

Line 67: engage with

Line 88: I suggest moving this back as "taking into account snow accumulation ..."

Line 95: obtained?

Line 110: again, tenses must be consistent throughout, whether it's present or past.

We apologise for that - in the revised version we will make sure that we correct this!

Line 123-125: I found this description hard to follow. It might be just because I am unfamiliar with the technique, but a schematic would certainly be helpful. If this is covered in the publication cited, then maybe the explanation is not even needed.

We think it is useful to be very specific here and the reason is that pRES and ApRES systems are more widely used in the recent past and one could potentially choose different settings for the windows for correlations. So, it is useful additional information for all who are doing themselves pRES and ApRES data processing.

Fig. 2: why does freezing correspond to zero melt rate?

We did not want to give freezing rates, therefore, we have chosen unfilled circles and placed them at zero melt rate. This is also mentioned in the text. It is interpreted as, freezing takes place, but the exact freezing rate is not known.

Line 216-217: provided no changes in the ice flux have occurred

This can be excluded by comparing to the measurements outside the channel, in which the advected ice thickness H_PDadv matches the observed well.

Line 241: shed

Line 241-242: beyond the scope of the project

Line 259: In my view the mathematical model should be fully stated, otherwise this description is confusing to the uninitiated

We are very much in favour of doing this and it was also mentioned by the reviewers. Our experience in the past was that, when we submitted a manuscript which included a

Line 272: no brackets needed (2x)

Line 303: years?

Line 329: notable

Line 404: they would be expected to

Line 423: is reduced

Authors point-to-point response on Referee Comment #1

Dear Reviewer,

We thank you for your detailed review and provide below point-to-point answers to all points raised. As you provided us with an additional attached file, our answers consist of two parts. Some of the comments were duplicated in/from the attached file, this is only answered once. To increase readability, our answers are presented in blue text and your original comments in black.

Your review considered many details very carefully and we want to express that we are very grateful for the time spent on the review!

Many thanks,

Angelika and co-authors

General Comments:

I found the paper quite difficult to read. There are many presentational issues that can be easily fixed and this would make a lot of difference to the reader. [...] I guess the main advice would be, do not assume the reader knows what you mean. Repetition is important.

Many thanks for pointing this out. The reviewer is definitely right and we will work through not only these examples, but will carefully revise all those unclear formulations.

Representativeness of the measurements:

It seems that primarily the eastern side of the channel was sampled. Where the western flank was sampled (2 locations), the melt rate there was much higher than at the eastern flank of the nearest cross-sections. In the southern hemisphere, Coriolis force deflects flows to the left, which in this case is westward. Therefore, it is not unreasonable to expect relatively higher melt rates on the western flank, and the two western flank measurements seem to go along with this. Can sampling bias explain the apparent discrepancy between observed melt rates and thickness profiles?

We expect that even with having both sides sampled similarly, we would find some difference between present day melt rates and melt rates needed to represent the channel evolution. However, with the data we obtained here, it becomes evident that a future campaign should sample both sides and it would make most sense to have an entire crossing with an airborne RES, to know exactly in which local topography the instrument is

placed. Indeed the influence of the Coriolis force could lead to higher melt rates on the western flank.

Could you get the correct channel geometry assuming asymmetric east west melt rate, higher on the western side?

Please keep in mind that it becomes a multi-dimensional parameter space problem if one goes that route. We do not have a symmetrical melt rate distribution, but we leave the melt rate on the western side constant in time, because we do not have observations there with which we could compare the simulated strain to, it would be all very vague. This is actually the really big advantage here, that we test imposed melt rates not only to geometry, but to strain. You can certainly 'burn' away ice to match a geometry, but it won't lead to the right vertical strain distribution. So conducting simulations with asymmetric time dependent melt rates on both sides need some pRES measurements on this side to be able to benchmark it against observed strain-rates. This is not achievable within this study.

Basal melting measurements, technique:

One thing I am missing in this paper are some figures of the basal return, how it changed between the two measurements, if at all, and what are the implications for the uncertainty in the basal melt rate. In particular, I am curious about how the basal melt rate at the steepest channel wall was derived (SW and SE). Is the first basal reflection that you consider from a flat base beneath? Or could it be off-nadir? Are there any ambiguities?

We are happy to present figures showing the basal return of different pRES measurements. First of all, we already excluded 5 of the 44 stations because the shape of the basal return changes significantly and thus prevented an unequivocally match. At the remaining stations, the shape of the basal reflector has not changed significantly enough to prevent a reliable determination of the change in thickness.

However, due to the steep ice base at the flanks of the basal channel, it is true that the first strong increase in amplitude originated from an off-nadir return. That this might have been the case at some stations is indicated by an increase in amplitude or a second, even stronger return at larger depth. How large the uncertainty caused by the interpretation of off-nadir returns is, depends on the off-nadir angle. From the seismic measurements, we figured out that the maximum off-nadir angle on the eastern side is about 20°, which results in an underestimation of roughly 6%. We will add the discussion and corrected melt rates in the revised version.

How was the basal melt rate time series derived? It seems quite jumpy all together. How robust is the time series? Why is the time series getting noisier with time (Fig 4 - blue high frequency oscillations get gradually higher amplitude)? Can you exclude the possibility of instrumental artifacts? - Are any of the jumps present in the internal reflector time series too? Do any of the jumps coincide with the changes in the character of the basal reflector? e.g. splitting/joining peaks as the reflector evolves? Or is the base just a simple, single peak that doesn't change its shape, in which case a lot of concerns would go away? I think this is something that should be discussed in the paper if the readers are to believe the presented time series.

Thank you for bringing up these points. Here, we want to address the above mentioned questions as well as those you wrote as a comment in the supplement.

<How was the basal melt rate time series derived?>
We derived the cumulative melt time series ΔH_b from the change in ice thickness (ΔH) and from the change in ice thickness due to vertical strain (ΔH_ε) and due to firn compaction (ΔH_f). ΔH was derived from the displacement of the basal return and ΔH_ε as well as ΔH_f from the linear fit of the internal displacements, which we derived similar to the method described for the single-repeated pRES measurements.

In the revised version, we will improve this description of the method, e.g. by adding the equation the cumulative melt time series is based on.

<It seems quite jumpy all together. How robust is the time series? Are any of the jumps present in the internal reflector time series too? Do any of the jumps coincide with the changes in the character of the basal reflector? e.g. splitting/joining peaks as the reflector evolves? Or is the base just a simple, single peak that doesn't change its shape, in which case a lot of concerns would go away?>
This is correct, the time series is jumpy, but we have identified the main reasons for that: The ApRES was located within the hinge zone where tides are bending the ice shelf. As a consequence, the vertical strain as well as the ice thickness are tidal dependent. Due to limitations arising from the noise-level depth, we couldn't retrieve the full displacement function of the strain down to the ice base. This means that we were not able to remove the full tidal dependent strain thinning/thickening (ΔH_ε) from the ΔH time series. This is the main reason for the jumps around the cumulative melt time series shown in Fig. 4a. To a smaller extent, this oscillation is observed in the displacement of the basal return.

However, the time series of the low-pass filtered cumulative melt is robust, as the basal return is always a simple, single peak that does not change its shape; we assume that the oscillation is a true change in ice thickness.

In the revised version, we will give more details on the robustness of the data.

<Why is the time series getting noisier with time (Fig 4 - blue high frequency oscillations get gradually higher amplitude)? Can you exclude the possibility of instrumental artifacts?>
The time series is getting noisier from September on, as a malfunction of the ApRES caused a change of the attenuation. As a consequence, the amplitude was reduced. Thus, the noise-level depth was shifted upwards and the influence of not being able to constrain the tidal influence in the ice mass below the noise-level depth is increasing. This caused the noisier time series.

<Fig 4: Should both of these be thinning time series? or is strain etc removed from the upper one (and therefore it is called cum. melt) but for some reason not from the lower one? Can you show melt rate time series instead of total thinning? This would make it easier to distinguish the sign of melting (melting vs freezing)>
Fig. 4a shows the cumulative melt (ΔH_b), as ΔH_ε and ΔH_f were removed from the time series of ΔH. The presence of the tidal induced signal prevents a robust analysis of the basal melt rate as a high resolution time series. To still investigate the occurrence of non-tidal melt anomalies, we analyzed the time series of ΔH by de-tiding the thinning rate to remove all

tidal induced signals. The result is shown in Fig. 4b. In this way, we could identify non-tidal melt events without estimating the correct amount of strain thinning/thickening. We will make this clearer in the revised version.

I have some more concerns about the melt rate time series now that I am looking at Fig 4 more carefully. The thinning rate doesn't show much seasonality (panel b). But then in panel a and also in Fig A3b it is indicated that the melt rate does have seasonality. Do the strain and melt time series have a seasonal variability that is equal but opposite? Such a result often indicates issues with the derivation of the melt rate time series. Or did you assume that vertical strain rate is constant in time, apart from tidal oscillations? But as before some of my confusion can be caused by mixing up terminology, specifically whether the time series shown are melt thinning or total thinning.

It is true that there is a seasonal cycle visible in Fig. 4a and Fig. A3b but not in Fig. 4b. The seasonality was observed in the time series of thinning more than in the time series of vertical strain. Consequently, it is still present in the cumulative melt time series. The reason that this is not visible in Fig 4b is that we show the de-tided thinning rate. As we used frequencies up to the solar annual constituent to de-tide the thinning rate, the seasonal cycle was removed, too.

In Fig. A3b, we show the same data as in Fig. 4a but linearly de-trended. Unfortunately, the label on the y-axis is not fully correct and so is the caption, as you have mentioned correctly - thank you very much. You are right, it is not the de-trended melt rate, but the de-trended cumulative melt time series. We will correct this in the revised version.

We hope this allays your concerns about the strain and the melt time series.

Model:

I think it would be useful to present the equations that are solved, as well as the boundary conditions written out mathematically. For those not used to the glaciology jargon, it can be hard to decode from the words (and not always so clear sentences) what system of equations is actually being solved.

The system of equations for finite viscoelasticity used in our manuscript as well as the boundary conditions are now written down in Appendix B1 in the revised version. As the theory for finite strain comes along with quite lengthy formulations, we originally aimed at only referring to Christman et al. (2019), but we are more than happy to present it here, too.

There are some viscosity sensitivity experiments briefly mentioned in the end. What I wasn't able to gather from the description is, whether any realistic rheological values could possibly account for the observed geometry and melt rate or not. And if so, at what expense would that be - presumably not a good fit of the vertical displacement profiles in Fig 8?

We discuss this more below, but it shall be mentioned here already, that the revised version will include more plots for the vertical displacement with other viscosities - another viscosity does not lead to better match between simulated to observed vertical displacement.

The authors optimize viscosity to match the channel thickness, but they don't optimize it to match the vertical strain rates. Why not? Could it be that a better fit to the vertical strain rates (especially in the middle of the channel) could yield a melt rate solution closer to that what was actually observed? It could be that an answer to this is already in the paper/experiments, but I wasn't able to find it.

We discuss that more below (there are a couple of locations where this comes up again). We include more figures in the revised version to show how simulated and observed u_z vary with viscosity. In short: the choice of viscosity does not solve the mismatch and the viscosity we have selected is overall a decent choice.

I am wondering why the authors do not find a strain rate structure similar to the modeling of Vaughan 2012, which promotes formation of basal crevasses. Is that because the ice here is so much thicker and the channel relatively shallow compared to the ice thickness? Or is this a fundamental difference between viscous and viscous-elastic rheology?

A large difference of our simulation to the one of Vaughan 2012 is that we compute a spin-up of 75 years to avoid unrealistic elastic responses to a channel that is created rapidly. By seismic measurements, we know that the basal channel for the Filchner Ice Shelf already appears in the grounded area, deepens until it reaches the grounding line, flattens a little bit but persists more than 60km downstream the grounding line. The elastic response in a viscoelastic Maxwell model occurs and gets important if the channel experiences changes in the forcing, in boundary conditions or in geometry changes (like melting or SMB) in the order of its characteristic Maxwell time (see our explanation of this to Reviewer 2). Vaughan 2012 stated that "if melting and relaxation occur on a similar timescale then rather lower stresses would be generated". The pRES observations additionally show that we have compression on the lateral boundary for the first 100 years of our simulation (the ice flows through a rather narrower part), which would compress the ice above the channel and not lead to the creation of basal crevasses. Afterwards, the horizontal displacements change their sign and the domain experiences horizontal tension, but this leads to a flattening of the channel as melting is low. However, also in the seismic measurements, we do not see any hint for basal crevasses forming for the Filchner melt channel. We will include deformation plots in the Appendix of the revised version of the manuscript to make this clear for the reader.

Is there any evidence of basal crevasses on this channel top?

There are no surface representations of basal crevasses similar to the ones on Fimbulisen (Humbert & Steinhage, 2011) and on Jelbartisen (Humbert et al. 2015). However, only ice penetrating radar surveys covering the entire channel, rather than point measurements, can answer that. We hope to be able to do that in future. It is worth to note, that Hofstede et al. (2021) did not find any indication of surface cracks or basal crevasses in the seismic profiles.

Discussion:

There is some comparison with a study from Ross Ice Shelf, but it is not clear what the purpose of the discussion is. The authors are citing high melt rate values observed elsewhere but those were measured much closer to the grounding line than in the current

study. So what is the purpose of this comparison? To state that elsewhere people measure higher melt rates in channels? Or that it is possible that had you measured closer to the grounding line, you might have found higher values of melting?

Data on basal melt rates within melt channels is very sparse, so we think it is worth comparing our results with other findings and we expected reviewers to criticise if we hadn't done so. Now we have done it, and it is also not well received. While it is true that the comparison with the melt rates measured in the Ross Ice Shelf is not perfect, we nonetheless feel that a comparison with the few other extant measurements of basal melt rates within melt channels adds necessary context to this paper.

I think the first paragraph of the discussion should be rewritten.

It seems to us that the reviewer is unhappy about us discussing our findings in relation to other studies and it remains unclear why this is the case. We are happy to follow the advice if we are given more insight on what is not adequate in that paragraph.

Another point regarding the main conclusion of the paper, which is that melt rates must have been higher in the past. Have you consider whether melt rate on side walls, which can be 10 times higher than on the base (Dutrieux et al 2014), could explain the maintenance of the channel without having to evoke a major change over the past 250 years?

We have done observations on the 'side walls', which we denoted 'steepest east = SE' and they are shown in Fig. 2. They are not higher at all, they are almost everywhere lower than outside the channel, although slightly higher then in the thinnest part of the channel. Based on these observations, we do not have any indications for that, therefore we do not carry out simulations with extreme melt rates on the flanks. While developing our experiments here, we actually did carry out some test runs in this direction and found that we would need unreasonable low viscosity if melting on the flank should be high and this leads to strain profiles not matching the observations of vertical strain. So we conclude, from both observation and from these test runs, that there are no extreme melt rates on the flanks here.

Naughten et al 2021 does idealized abrupt change experiments. I don't think that paper can be used as a supporting evidence for the hypothesis that melt rates in the channel decreased over the past 250 years.

We do not agree entirely. Naughten and co-workers conduct a number of experiments of which one is a piControl with a pre-industrial level (no abrupt change), one is an abrupt change (4xCO2 and then constant) and one is a 1% increase. Thus, only one of the experiments is an abrupt change experiment.

We also think that it is worth mentioning that our results are consistent with some findings of Naughten et al. (2021). This could also stimulate further studies in the future.

Some more comments (page/line):

Again, need to differentiate between melting and total thickness change. On 11/225 you claim 1 cm tidal melt amplitude, but on 12/235 you say you were unable to get tidal melt rate.

We agree that the results and the discussion of the tidal melt amplitude is not clearly written and will improve this in the revised version. At the beginning, the unfiltered cumulative melt rate time series indicated a 1 cm tidal melt amplitude. However, the further analysis revealed that this is due to the inaccuracy in the determination of the strain thinning/thickening. In the revised version, we will restructure this section.

6/130:

How does the tidal bending at daily or so timescales (so presumably mainly elastic response) translate into long term vertical strain rate that is depth dependent (primarily viscous response)? Is that just coincidental, or is that expected from theory?

First of all: this is our observation. Secondly, that tidal modulation of ice motion is not 'offsetting', but leads to asymmetric distribution as shown by Gudmundson (2011) already and is expected to be driven by the non-linearity of the sliding law. That is nothing that we focus on here, because our study is not intending to discuss the effect of bending of the hinge zone, it just happens to be the case that these measurements were taken in a hinge zone.

I would draw different conclusions than the authors from some of the provided figures, e.g. Fig. 2c.

This is answered below in detail.

8/200:

My interpretation of this figure would be that except for a few outliers (very high melt rates) the melt rate pretty much lies on a line, increasing with increasing draft. And it doesn't matter whether you measure melt inside or outside the channel.

Well, if we exclude outliers AND the points of freezing, one could see a linear trend. But one cannot draw any conclusions if it matters if it is inside or outside the channel, as the measurements do not cover areas of similar ice thickness inside and outside the channel.

13/265:

The authors you Poisson's ratio of 0.325. Jenkins 2006 found this to be 0.5 near Rutford Ice Stream, which is relatively nearby. How sensitive are the simulations to this parameter?

It is not easy to understand how Jenkins et al. (2006) come to their value of 0.5 (at the surface), in particular as 0.5 is a singularity. There have also been laboratory experiments supporting 0.325: Gammon, P., Kiefte, H., Clouter, M., & Denner, W. (1983). Elastic Constants of Artificial and Natural Ice Samples by Brillouin Spectroscopy. *Journal of Glaciology, 29*(103), 433-460. doi:10.3189/S0022143000030355. They may come to that value, because they disregard the viscous components, or due to assumptions on the load situations or boundary conditions that may not represent the system well. If an ice stream is nearby or not shouldn't matter, as this is a material parameter - unless the reviewer wants to hypothesise that impurities are actually influencing Poissons's ratio strongly and that similar snow deposition regimes would lead to similar values and may lead to other Poisson's ratios elsewhere. But there is no indication for that. The effect on our results is minor and will not lead to any other conclusions, so the sensitivity is low.

Related to that, there has been some discussion recently on n in glen's flow law being closer to 4 than to 3 (e.g. Milstein 2021), in which why would you expect that to influence the result, if at all? - I am just curious about that one, I am not really asking you to run more simulations.

There have been other papers on n=4, too, and in the history of deriving a Norton-Hoff type flow law for ice n=3 was rather an agreement than an evidence based decision as the range in lab experiments was n = 2.5 to 4.2. From our perspective, we would be happy with each flow law, for which also the rate factor including the activation energy has been adjusted to match lab experiments - even if it could only be inverted numerically. Having said that, we do not expect n=3 versus n=4 to make a difference here at all and in general, it would be worth it to compare simulations using the standard Glen's flow law with n=3 to a new n=4 with a suite of benchmark experiments. Because if the parameters for both flow laws are adjusted to lab experiments representing the 'true' material behaviour, it may well be that there is not such a big difference between the simulations at the end. But this is more of a speculation and certainly a completely different project.

Authors response on comments:

5/92: "After collecting the data, each chirp was correlated with every other chirp in order to reject those which had a low correlation coefficient on average. The remaining chirps were stacked." Is this referring to the chirps within each burst? I would assume that. Are you basically saying that for a given burst, you are removing anomalous chirps and averaging the rest? I am not sure I would understand that from the way it is written.

Yes, this is right. To make this more clearer, we will rewrite these sentences as follows: "After collecting the data, anomalous chirps within each burst were removed and the remaining chirps were stacked. Anomalous chirps were identified by correlating each chirp with every other chirp of the burst. Those with a low correlation coefficient on average were rejected."

5/109: "Snow accumulation/ablation, firn compaction but also changes in radar hardware (and settings) can cause an vertical offset near the surface that cannot be distinguished from one another." Do you mean that these can occur between repeat visits? e.g. using a different instrument for the revisit?

Yes, this is correct. We used a different pRES instrument for the revisit. We will change the sentence as follows:

"Snow accumulation/ablation, firn compaction but also changes in radar hardware or settings (a different pRES instrument was used for the revisit) can cause an vertical offset near the surface that cannot be distinguished from one another. "

6/127: "Since noise prevents the reliable estimation of the vertical displacement from a certain depth on, we calculated the depth at which the averaged correlation of unstacked chirps undercuts the empirical value of 0.65." Not that I would know better, but I am curious to know why you picked 0.65.

The correlation coefficient in the upper part of the ice column is close to 1 and drops rapidly from a certain depth. This drop often occurs from values above 0.8 to below 0.4, which

remain low for deeper parts. Therefore, the noise-level depth limit is not very sensitive to the value of 0.65. However, higher values, e.g. 0.8, are partly undercut in upper layers, which leads to an early cutoff. Therefore, 0.65 has emerged as a reliable limit.

6/143 "This leads to uncertainties in the melt rate of more than 0.2 m/a for locations in the hinge zone, while at other locations the uncertainty is predominantly in the range of < 0.05 m/a." How much more? perhaps give the full range of uncertainties?

The uncertainties in the hinge zone were up to 0.26 m/a. We will change the sentence by giving this number.

15/333 Is the spin-up initial state and forcing the same for both experiments? If yes, can you say that explicitly?
No, the initial geometry is not the same for both experiments as the melt rate is different. In both experiments, the melt rate is kept constant during the spin-up. But in the first experiment, that value is the observed melt rate at t=0 (a_b(0)) and in the second experiment, it is the larger synthetic melt rate at t=0 (a_b^syn(0)). Hence, the initial geometry has to be different for both experiments as the geometry after the spin-up should be the same and, more precisely, the one of the seismic observation. We added some additional formulation to make this clear.

Comments of Reviewer#1 in the pdf attachment:

Line 16: "However" suggests some contradiction, what is the contradiction of surprise in this statement?

The sentence before that one, stating 'Melt channels in ice shelves have been hypothesized to destabilize ice shelves and were often linked to enhanced basal melt'

Line 37: This is a common issue in the presentation. You use the attribute but don't include the object, assuming the reader is following. But if the reader is not following it can be really difficult to figure out what the authors mean.

It was difficult to understand which sentence this refers to, but it is a more general statement, so we take it as advice to go through the entire text to check for such occurrences and correct it.

Line 40: Is this also from pRES? From the context it seems like it.

Yes, it is done using the same type of pRES as we use, but we probably mislead the reader by starting the paragraph with mentioning the pRES system, because it actually does not matter which system you use unless it would be not an adequate system. We correct this by leaving out the first sentence of this paragraph.

Line 49: I don't think this reference is relevant for channels, so it doesn't seem to be relevant here?

It is indeed not relevant for channels, but it is very relevant for studying temporal variations of basal melt and this is what the prior sentences already have as a topic.

Line 54: Maybe emphasize that this is a horizontal resolution issue?

Well, unstructured grids could solve this issue and a number of ocean models use unstructured meshes, also some of the models of the publications we cited here. In the revised version we will emphasize that it requires high horizontal resolution.

Line 57/58: would "these types of modeling results" make it clearer?

Yes, that certainly will make it clearer and we will rephrase it accordingly in the revised version.

Line 68: do you mean "provide constraints"? Even without these you could probably use modeling to gain some insights about the evolution of the feature

That is true. 'Provide constraints' is by far better and is included in the revised version.

Line 92/93: Is this referring to the chirps within each burst? I would assume that. Are you basically saying that for a given burst, you are removing anomalous chirps and averaging the rest? I am not sure I would understand that from the way it is written.

This was answered above in detail.

Line 108/109: do you mean that these can occur between repeat visits? e.g. using a different instrument for the revisit?

This was answered above in detail.

Line 116: what was the ambiguity?

We rejected stations at which the correlation of the surrounding depths resulted in ambiguous alignments. We will improve the corresponding sentence in the revised version.

Line 128: Not that I would know better, but I am curious to know why you picked 0.65

This is answered above in detail.

Line 132: How does the tidal bending at daily or so timescales (so presumably mainly elastic response) translate into long term vertical strain rate that is depth dependent (primarily viscous response)? Is that just coincidental, or is that expected from theory?

This is answered above in detail.

Line 133: It seems that you believe that nonlinear feature - would it be then appropriate to reconsider the 0.65 correlation cutoff?

In many cases, the 0.65 correlation cutoff turned out to be a robust threshold. However, at some of these six stations, the correlation values fell below this value and then remained in a similar range for deeper layers. Based on our threshold, we excluded them from the strain

analysis. However, if the estimated displacements of the lower layers are correct, then this would lead to an overestimation of the melt rate. Since we wanted to avoid this, we made a second, depth-dependent estimate of the strain. Because of this, some stations have a larger error of up to 0.29 m/a.

Line 134: probably should cite Jenkins et al 2006 here

It is cited in Sect. 2.2.1.

Line 134: lower limit on what?

Well spotted, thank you, |Delta H_epsilon| - is included in the revised version.

Line 135: By the displacement do you mean delta H_epsilon?

No, displacement is denoted by the vector field u(x,y,z,t) and in this sentence the displacement in vertical direction u_z as mentioned above.

Line 143: how much more? perhaps give the full range of uncertainties?

This is answered above.

Line 149: in time or in space?

In time and in space - will be included in the revised version.

Line 149: You do this along a flowline right?

Yes, indeed, along the flow line and we include this in the revised version.

Line 158: as opposed to Hi as in the case of pRES?

Yes, this is correct.

Line 166: Is that what you use or not? I don't think that is elaborated on later, so is the first guess the final guess?

Yes, this is what we use. We have deleted the notion of first guess.

Line 168: do you mean strain?

We mean melt. The sentence is improved for the revised version and we also stated the equation.

Eq 8: How did you derive the total thickness timeseries?

We derived the change in ice thickness similar to the change in ice thickness of the single-repeated measurements. In the revised version, we will add a sentence to the manuscript making this clearer.

Line 172: you started talking about melt rate and now you are talking about thinning rate, please make this clear. & Line 175?: I am really confused here. You start talking about investigating tidal basal melt, but then you just describe the process of detiding the signal?

Yes, you are right. The way the corresponding sentences could have been written more clearly. We will improve the sentences in the revised version:

"Subsequently, we used the time series of Delta H(t) to investigate the occurrence of melt events. We de-tided Delta H(t) by subtracting a harmonic fit based on frequencies up to the solar annual constituent and calculated the thinning rate afterwards."

Line 191: How certain is that? That is, is the uncertainty small enough to make the sign of melting definitive? Is freezing significant enough that it comes even from amplitude correlation alone without having to rely on the phase measurement, which is more complicated in the freezing case?

At all four stations that we attribute to indicate basal freezing, we observed an increase in ice thickness after correcting for snow accumulation and firn compaction. This increase can also be derived from the amplitude correlation alone, although it is rather small with ~ 0.1 m/a. However, we found strain thinning at three of the four stations. Thus, we concluded that freezing caused the increase in ice thickness, although the rate is only slightly above the measurement uncertainty.

Fig 2c: My interpretation of this figure would be that except for a few outliers (very high melt rates) the melt rate pretty much lies on a line, increasing with increasing draft. And it doesn't matter whether you measure melt inside or outside the channel.

This is answered above in detail.

Line 223: [displacement] of what?

Vertical displacement of the ice, u_z(z).

Line 223: where is this presented? I don't see this immediately below, so perhaps give the section?

Thanks! We linked section 3.2.2 to this sentence.

Line 229: only qualitative right? I assume no quantitative assessment is possible with a single gps?

We agree that the sentence was not well written. What we meant was that we compared the tidal constituents we found with the ApRES and the GPS measurements. We will rewrite this sentence in the revised version:

"The spectral analysis of the unfiltered cumulative melt time series shows all main diurnal and semi-diurnal constituents, which is in accordance with the frequencies observed from the GPS station."

Line 229: of what, melt? total thickness?

Line 230: now, do you mean "melt rate time series"?

This point is answered in the general comment section.

Fig 4: Should both of these be thinning time series? or is strain etc removed from the upper one (and therefore it is cold cum. melt) but for some reason not from the lower one?

This point is answered in the general comment section.

Fig4: Can you show melt rate time series instead of total thinning? This would make it easier to distinguish the sign of melting (melting vs freezing)

This point is answered in the general comment section.

Line 234: how much, lower half? Third?

Of roughly the lower half. We added this to the sentence.

Line 235: a few lines before you said 1 cm amplitude tidal melt

We answered this already above.

Line 237: looking at the dependency of the result on the centre frequency might be a more robust way of assessing this

It is true that accretion characteristics depence on the centre frequency. However, if there is no change in amplitude of the basal reflection, then there is no reason to suspect freezing, independent of the centre frequency.

Line 242-245: How did you arrive at the 1000 m cutoff? Maybe at other locations (less damaged ice/better layering) the signal could be fine even at greater ranges, no?

Yes, you are right. We will remove the "1000 m" cutoff and write the sentence more generally:

"With melt channels being located (or initiated) in the hinge zone, any kind of ApRES time series performed at thick ice columns might be affected by the unclear strain-depth profile in the lower part of the ice column."

Line 257: This paragraph suggests that had you had observations further upstream all the way inland you wouldn't need a spin up. Is that true? I would imagine that there still would be some transient response because observations are always imperfect, so you would still need it.

This is a good point. It depends what we would want to analyse then. With measurements up to the grounding line and the goal to analyse the simulated vertical displacement field at, let's say, 100km away from the grounding line, one would not need a spin-up as one could

‘discard’ the first tenth of kilometers of simulations (years) without depending on it. But in general, one would indeed want to conduct spin-ups, in particular if dealing with a viscoelastic model.

We have added this sentence to make more clear why a spin-up is required here: To fit best to the stress-state at the first cross-section, we conduct a spin-up.

Line 266: Jenkins 2006 found this to be 0.5 near Rutford Ice Stream, which is relatively nearby. How sensitive are the simulations to this parameter?

This is answered in detail above.

Line 268: Just curious, why would you choose (a priori) the upper limit and not some kind of mean value?
As shown in Fig. B7, we need a relatively high viscosity value for ice so that the basal channel can stay open. If we take a mean value, this channel will close faster because of a larger viscous flow of ice from outside into the channel. If we want to omit this and keep the channel open, we have to increase basal melt inside this channel or prevent large amounts of ice that flow into the channel by a higher viscosity. To support our magnitude of the viscosity, we present the discussion with the inversion that those high viscosity values occur in the Filchner-Ronne Ice Shelf. They are not absurdly high and we can assume such a value for our simulation

Line 275: This is glaciological jargon, can you just write what that means mathematically?

This is not really glaciological jargon, rather common in any form of technical mechanics and continuum mechanics, but we agree that the reader might not be aware of this and give the mathematical description in the revised version.

Line 275: what do you mean by "it" the domain? So do you essentially have periodic boundary conditions along y?

Shape and loading do not vary in y-direction.

Line 284: and also upstream? so would along-flow or simply y, since you already defined that, be clearer?

Yes, indeed, along-flow would definitely be clearer here.

Line 284: do you mean realistic?

This is indeed a better wording!

Line 285: transform?

Done.

Line 287: From where it is obvious that -epsilon_zz = 2 u_x /W?

Thank you for this comment! You are absolutely right, the explanation of how we computed this relation was missing. We added a few sentences in the revised version to make our consideration and the assumptions we made clear to the reader.

Line 288: do you mean that they are depth-independent or constant in time?

Depth-independent - we include this in the revised version.

Line 292: Presumably RACMO is not very well observationally constrained in this region. How well do you expect it to perform here? Are the results sensitive to this forcing or not too much, compared to other factors?

It is not in the scope of this study to assess the performance of RACMO. The results are moderately sensitive to the SMB.

Line 297: Why would the melt rate be symmetric between east and west? Wouldn't you expect rotational effects? The data also seem to suggest higher melt on the western side.

The melt rate is not assumed to be symmetric between east and west. The wording was misleading here and we try to make it more clear in the revised version. Nevertheless, we just don't have enough data points on the western side to constrain a temporal evolution of the melt rate there, so we set it constant in time. And you are right, for a time larger than twenty years after the spin-up, we have higher melt rates on the western than on the eastern side. With the knowledge of this study and the experience of time needed to make a survey really across to the western side, we would certainly plan differently in future, whereas in 2015 we were just happy to have made it to record that much data as you see here.

Line 298: That is not true, units of distance and time are different. Explain better what you mean.

Many thanks. We have rephrased the sentence to make it clearer.

Line 300: That is for all times or t=0 or when?

The comparison is done for the whole simulation interval of 250 a. We include this in the revised version.

Fig 5: The simulations are 2D, so the graphic should probably also be 2D

Please note, that our simulations have a small extension in 3D, the along-flow direction, for the purpose of applying boundary conditions. The geometry that is sketched here represents this very well.

Line 301: I wasn't able to understand from the description what is the model geometry that you start with at the beginning of the spin up. Is it that of IV or that of the geometry at the grounding line? I would have thought that IV, but I am not sure.

We do not start with the geometry at seismic IV for the spin-up, we aim to end with the geometry of seismic IV at the end of the spin-up. It actually does not really matter, with which geometry one exactly starts the spin-up, as here the only purpose is to avoid an

instantaneous elastic response to be falsely interpreted. In our case we have chosen a more or less arbitrary geometry, but we end with a geometry very close to seismic IV. Imagine it to be a synthetic geometry that has the only purpose to allow the model to relax to the geometry of seismic IV and having a stress state that represents the stress at seismic IV.

Line 302: to what?

To geometry changes, for instance, caused by basal melt rates. We include this in the revised version.

Line 327: than what? than the simulated one or than at t0?

We added 'than the simulated one'.

Line 333: Is the spin-up initial state and forcing the same for both experiments? If yes, can you say that explicitly?

This is answered in detail above.

Fig 8: What is the source of the mismatch between the observed and modeled u_z? Is it the constants in the rheology?

This is very, very difficult to assess! It could be due to our boundary conditions on the western side, the plain strain assumption, due to the melt rates along the western steep slope, but also due to viscosity (see second answer to 'line 381' below) not representing the real world perfectly. Which of that is governing is not possible to assess from our simulations. But one can also take a different perspective on it: so many things could go wrong in such a complicated setting, we are doing surprisingly well here!

Line 380: This is a very confusing sentence. Can you just clearly give the viscosity and channel heights for all the sensitivity experiments?

You mean 'two times higher' and 'five times smaller' is not precise enough? We do still think that 'A two times higher viscosity leads to an ice thickness in the channel that is 42 m smaller after 250 a, while a five times lower viscosity results in 116 m thicker ice above the channel due to more viscous flow into the channel.' is sufficiently compact and informative. But on advice of the editor, we are happy to change it.

Line 381: than what?

'Than' with the best matching viscosity.

Line 381: How does the viscosity play into the u_z comparison? is the "best" one for reproducing thickness also the best one for reproducing u_z evolution?

This is a very good point. We have prepared a new figure for the revised version which shows this. The viscosity does (unfortunately) not solve all issues - all viscosities which we used for the sensitivity tests lead to discrepancies, but the one we selected as best is leading to best match 'on average'. This supports also that other factors than the fluidity prohibit obtaining better matches with observed u_z.

Line 384: This is not a very good comparison. You are citing high melt rate values elsewhere but those were near the grounding line, were you do not have measurements. So what is the purpose of this comparison? To state that elsewhere people measure higher melt rates in channels? Or that it is possible that had you measured closer to the grounding line, you might have found higher values of melting?

The purpose of this comparison is (a) to indeed show what the sparse data at other locations showed and (b) to compare downstream of the grounding line the data inside and outside of the channel at this location on the Ross Ice Shelf. We do think that this is of interest for the reader, therefore we do not really get the point why this shall not be cited here.

Line 387: lower than what?

We changed it to 'We also find that the melt rates decrease by a factor of five ....'.

Line 388: same as what

Thanks, we agree that this sentence has been confusing and rephrased it entirely.

Line 388: I don't understand what you are trying to say here and why

Again, you are correct, this was confusing and we improved this sentence in the revised version.

Line 400: Another assumption is that the melt rate is the same on both sides of the channel. And also that melt on vertical side walls is negligible.

We did not assume a symmetrical melt rate distribution at all. We are not sure what the reviewer means with vertical side walls? The only vertical walls are the lateral margins of the modelling domain and they are not prone to melt at all. If the steep slopes are meant here, it is to mention that they are not vertical at all - it is important to keep the scale in mind - they are about 26° not 90°!.

Line 409: These are idealized abrupt increase in CO2 experiments, so not supporting evidence for your claim of decreased melt rates in the past 250 years.

The reviewer is certainly right in criticising that the simulations in Naugthen et al. (2021) are not exactly comparable to our situation here, in particular as no geometry of a melt channel was taken into account in that study. However, it is actually very interesting to compare it with their findings. We suggest keeping the citation, but to clarify this comparability in the revised version.

Line 420: why is the sediment relevant to the melt rates?

This is correct, we deleted that part of the sentence.

Line 427: Different topic so new paragraph

Good point, thank you. We included this for the revised version.

Line 429: The situation here is a bit different than at Site 5 now? There the melt rate anomalies go both ways, but here there appears to be only the "warm" anomaly? So not sure how comparable the sites are.

Still, the time scale is consistent with eddies passing through and even if one site has melt rate anomalies in both directions, the warm anomaly here can be explained by eddies.

Line 439/440: I missed where you showed this. Can you separate these effects from your simlations?

We include in the revised version a new part, in which we show the elastic and viscous effect separated.

Line 440/441: Why is that obvious? Can you provide some simple explanation?

With the new figures that we incorporate in the revised version this will become easier to understand. It is basically that the viscous component is due to the high viscosity rather slow, while the elastic response to the change in geometry, and hence load, is instantaneous. In the new figures, this can be seen quite well.

Line 442: high compared to what? They didn't compare viscous with viscoelastic simulations, right? I don't think their setup is directly comparable with yours, is it?

High compared the melt rates in our case to be required to keep the channel open. It is correct, their setup is not directly comparable to ours, but they do simulate a melt channel in with a viscous Stokes model and we think it is indeed worth to mention and discuss this.

One actually should not compare viscous to viscoelastic simulations, but the viscous component in the viscoelastic simulation to the elastic component in the viscoelastic simulations. In a purely viscous simulation all response to load is taken up by the damper, while in a viscoelastic the damper takes less response to load, because some of the load is taken up by the spring.

Line 449: can you be specific about what weaknesses you mean? Do you mean the limited knowledge of rheological parameters?

The limited knowledge of lateral boundary conditions and rheological parameters. We will include that in the text in the revised version.

Line 471: Again, I missed where you showed an analysis of the role of the different components of the rheology (viscous vs elastic)

Indeed, this has not been included in the original submission, but the revised version shows here by far more information.

Table A1: can you include units for each variable?

Yes, we will do that.

Fig. A3: I am a bit confused why this time series shows so much seasonal variability compared to that in Fig 4b. Is that seasonal variability also present in the vertical strain rate?

This is answered in detail above.

Fig A3 caption: again, what precisely is this quantity? The units are m, so it is not rate, and there are a lot of tides so it is probably detrended total thickness time series?

Thank you! This was a typo, it is a melt rate indeed. This will be corrected in the revised version.

Fig B6: The colormap suggests that there is a switch from negative to positive, because of the white in the middle, so this choice is quite deceiving, given all strain values are actually positive. Use smooth colormap without sharp gradients?

This is a good point. The intention to use this colormap was to show in white what the average strain is, but we will choose the colormap for the revised version better in order not to mislead the reader.

Authors point-to-point response on Referee Comment #2 to tc-2021-350

Dear Reviewer,

We are very grateful for this review! The comments of the reviewers are so extremely well thought through, that we as authors are delighted that the reviewer took the time to get into the details of the system and our ideas.

Below, we do answer point to point all comments, but we also refer to things that are discussed as an answer to Reviewer 1.

In addition to the review, we also got comments in the pdf as an attachment. Many of the comments below were in the pdf comments, too, so we answer them here. The remaining ones we added to the list here too.

Many thanks,

Angelika and co-authors

Overall comments:

The manuscript is well organised and fairly well written. I have included some suggested edits in the attached PDF to improve the clarity of the text and the ease of reading.
Thank you very much. Your suggested edits were very helpful to improve our manuscript! We commented on a few of those edits below or revised the manuscript according to your advice in most cases.

It would be informative to show more results from the viscoelastic modelling. At the moment I don't feel the reader can appreciate the modelling without seeing more results.
The point is made that it is important to consider elastic effects, but this is not demonstrated in any of the results.
We are delighted to present the elastic effects in more detail! Many thanks for raising this! As we are dealing with nonlinear strain theory, it is far more tricky to extract the elastic component, as in the present configuration only multiplicative terms of elastic times viscous deformation appear. This is different from linear strain theory, in which strain is composed additively of elastic and viscous strain components. A comparison with a purely elastic simulation or a comparison with a purely viscous simulation would not represent the spring in the spring-dashpot rheological model, or the dashpot in the spring-dashpot system. Therefore, we have to introduce a new strain measure here, that is anyway only rarely applied in material and engineering science, and has never been used before in glaciology to our knowledge. The so-called Hencky strain is a logarithmic strain measure and the logarithm leads then to an additive composition of elastic and viscous strain components. This is far more complicated than in the linear strain theory, but it is a really nice way to

It would be good to explicitly state the Maxwell Time. Normally it is assumed to be on the order of hours to days (Gudmundsson 2011, Ultee et al., 2020), so on short time periods, such as the tidal cycle or large hourly fluctuations in the melt rate, elastic effects will be important, but here you are considering approximately steady melt rates over long time periods (decades to centuries).

The characteristic time of a Maxwell material is proportional to the viscosity. In a 1D approach, it is eta/E and analogously for 2D/3D it is eta/mu with the Lamé constant mu=E/(2*(1+nu)), Young's modulus E and Poisson's ratio nu. With the material values of our manuscript of nu=0.325, E=1 GPa and eta= 10^15 Pa s we get a characteristic Maxwell Time tau=153 days. The elastic effects are important if we have changes of the order of several times the Maxwell time. This is the case for nearly all boundary conditions, as melt rates, SMB and horizontal displacement are changing permanently and this is taken into account in our simulations. We include the characteristic time in the revised version of the manuscript (also see our answer to your individual comment on this below).

I'm not an expert on the role the tidal signal plays on controlling ice-shelf melt rates and deformation. It would be helpful to provide more details on these processes and how they can be linked to the findings here. At present this section (2.3.2) is confusing.

We understand that the physical processes that might be impacting melt rates are of interest. However, in this study we found that what initially appeared to be tidal melt was caused by tidal bending. But still, we are happy to add a few sentences on the oceanographical processes that cause the melt rates:

"For an ice shelf such as the Filchner we expect the principal drivers of basal melting to be the water speed and its temperature above the in situ freezing point (e.g. Holland and Jenkins, 1999). For much of the ice shelf the water speed is dominated by tidal activity (Vanková et al., 2020), but near the grounding line of SFG we expect the tidal currents to be low, consistent with the evidence from the ApRES thinning rate time series. It is likely that the anomalously high melting events seen in the record result from the passage of eddies, with their associated water speed and temperature anomalies."

Furthermore, we understand that section 2.3.2 was confusing. We will improve this section in the revised version.

Imposed melt rate in numerical modelling: looking at Figures B2 and B3 the width of the channel seems to grow considerably downstream between seismic line IV and V, but this is no reproduced in the simulation, particularly on the right flank. This feature isn't addressed. Would a different spatial distribution of the imposed melt be required to reproduce it? And if so, what does this imply?

Yes, you are right. If we want to shift the channel or widen it up, we have to adapt ('optimize') the spatial distribution of the melt rate. For this, we would need a melting rate that is not only varying in time but also in space (in across flow direction) and therefore, we need observations of the thickness distribution as a dense grid, as we otherwise have no way to constrain it.

For example with a transition of 800m between the melting outside east and lowest, we will get this evolution of the base:
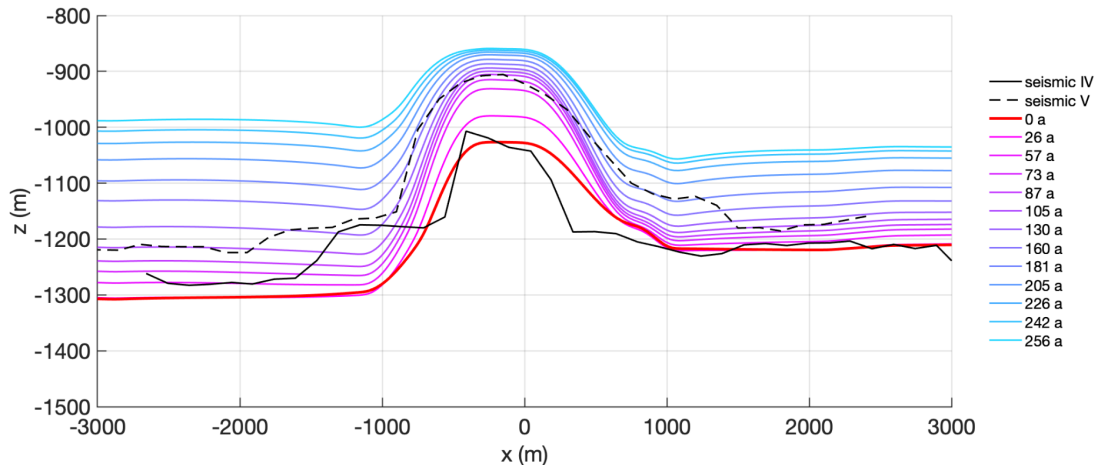
However, we wanted to appropriately model the slope at seismic IV and hence we take a smaller transition between melting at L and OE. But this is a very good point and we will shortly discuss this in the revised version of the manuscript. Thank you.

The current set of figures are well presented and informative. It would be good to include some more figures showing results from the viscoelastic modelling.
We agree and as stated above we will include more figures of the viscoelastic modelling in the revised version, in particular we will show which role the elastic versus the viscous contribution has.

The work is of interest to many in the scientific community: oceanography, glaciology, geophysics, numerical modelling.

Individual Comments:

Line 11-12: *"The type of melt channel in this study diminishes with distance from the grounding line and are hence not a destabilizing factor for ice shelves."* I agree that channels that close towards the calving front are not destabilizing in the way that they may breakthrough the ice shelf, but unless they close completely, these areas of thinner ice may be the initiation sites for fracturing due to extension perpendicular to the ice front, as in Dow et al., (2018).

This comes up again below at Line 397-398, where we answer this in great detail.

Line 33: *"The channel increases in height close to the grounding line and widens afterwards."* Have you thought about the processes that lead to the widening of the channel?

Here (line 33), we refer to the channel geometry found by Hofstede et al (2021a) up to the location where our study starts. It would indeed be very interesting to know more about melt rates and stresses in this area, however, we do not have any observations there. As

Hofstede has been able to traverse even upstream the grounding line, we hope to deploy instruments in this area and tackle exactly this question in future.

Line 39-40: *"In lateral direction, the melt rate is only 0.82ma−1 demonstrating enhanced melt inside the channel."* I'm not sure what you mean here. Initially I thought you were suggesting that the horizontal melt rate is 0.82 m/a (i.e. channel is growing wider). But when you mention enhanced melt inside the channel it suggests you mean that outside of the channel the melt rate is 0.82 m/a?

Yes, indeed. They found that the melt rate outside the channel is only 0.82m/a, whereas inside the channel it was 22.2m/a at the grounding line and 2.5m/a inside the channel at a 40km distance. We rephrased this, to draw a clearer picture in the revised version.

Line 43-44: *"At some point, it becomes super-cooled due to the falling pressure. Thus, the melt rate decreases and could even change to refreezing."* I think these sentences need rewriting. If the water is super-cooled it can no-longer melt?

Yes, indeed, super-cooled water typically leads to the formation of frazil ice that rises to the ice base and also direct freeze-on will appear. We have rephrased this to make it clearer.

Line 49-50: *"M2 tidal constituent"* Maybe add detail of the related time period here for those unfairly with tides. (i.e. approximately 12.5 hr or semi-diurnal).

Thanks! We will add "semi-diurnal".

Lines 61-66: Is it possible to calculate the corresponding Maxwell Time?
Yes, of course. Please see our answer to your overall comment on the Maxwell Time. We include this characteristic time at the position you point out here and its derivation at the beginning of the model chapter in the revised manuscript.

Line 81-82: *"A GPS station was also in operation at this point from December 24, 2015 to May 5, 2016."* This is prior to the time period in which the pRES was deployed. It would be good to acknowledge this and note what the purpose of the GPS data is here to avoid confusion.

Thanks! We will make clear that the GPS recorded one year before the ApRES and what the purpose of the data is. The new sentence will be:

"One year earlier, a GPS station was also in operation at this point from December 24, 2015 to May 5, 2016, the data of which we use for tidal analysis."

Lines 132-137: This is an interesting observation. Has this been observed elsewhere? It would be good to include some references if so. Also why would e_zz decrease to 0 at the base? Is there a physical process behind this idea?

Yes, this was found by e.g. Jenkins et al. (2006) or Vankova et al. (2020) for other locations on the Filchner-Ronne Ice Shelf.

We are happy to add the sentence that the tidal dependency referred to tidal bending.

"A depth-dependent tidal vertical strain caused by tidal bending near the grounding line was also found by Vankova et al. (2020), although the long-term vertical strain was found to be depth independent."

Jenkins et al. (2006) conclude that buoyancy forces of a non-isostatic ice shelf result in a "neutral surface" separating horizontal compression and expansion. Thus, the distribution of the vertical strain switches sign ($e\_zz = 0$) at the neutral surface. The depth of the neutral surface depends on the external pressure conditions. However, that the neutral surface is at the ice base is certainly a special case. This requires an extension regime over the whole ice column, which means that there is no change of sign and that the horizontal compression from the buoyancy forces equals the extension at the ice base.

However, we have no indication that there has been a change of sign in the vertical strain distribution over depth which means that there is no change from extension to compression. As the observations indicate a strain at least close to zero near the ice base, we used $e\_zz = 0$ in order to find the lower boundary of the strain thinning/thickening.

Line 146: *"interpolated the ab, $\hat{a}$ †Hε and $\hat{a}$ †Hs along the distance of the channel"* What method of interpolation did you use?

We used a linear interpolation that was smoothed with a moving average window of 14 km.

We will update the corresponding sentence as follows: "First, we linearly interpolated a_b, ΔH_ε and ΔH_s along the distance of the channel to get continuous values between the cross-sections and smoothed the results in order to obtain a trend for each process."

Line 155-156: Good to remind the reader here that ApRES measures are taken every 2 hours.

Thanks! We will update the sentence as follows: "The processing of the autonomous measured time series with a 2-hour measurement interval differs slightly from the single-repeated measurements."

Line 170-174: How do you expect tides to impact melt rates? It would be good to give the reader an insight into the physical process you think might be impacting melt rates.

We answered this point above in the Overall Comments.

Line 203-204: *"inside the channel (L) the melt rates decrease with reduced draft."* Here we observe a big jump in melt rate at around 750m – what could be causing this?

Is the reviewer referring to Fig2c and means 950m instead of 750m?

It is true that there is a big jump in the melt rate at a draft of about 950 m. Here, the melt rate increases from <0.5 m/a to >1.5 m/a. However, this jump only occurred in the centre of the channel. An explanation for this jump can be the reduced basal slope in the channel and with that a reduced flow velocity of the plume. At the locations where the high melt rates

occurred, the ice thickness above the channel decreases by 100 m within 10 km. Within the next 14 km, the ice thickness thinned by only 25 m.

Line 205: *"The distribution of â˘†Hε shows a significant thickening of more than 1ma−1 at the most upstream cross-section at L and OE"* It would be good to see the along-flow and transverse-to-flow components of strain in this region – is thickening due to along-flow compression or lateral compression?

We fully understand that this would be interesting to see, but actually, our measurements cannot show that. We only measure vertical strain and with the assumption of incompressibility, we know the sum of horizontal strain, but we cannot assign it in flow direction or transverse to the flow direction. The satellite remote sensing products are unfortunately not of an accuracy to allow us to do that, too. In the future, in another expedition, one could imagine measuring this via strain-rate networks of GPS/GNSS stations like pentagons with an ApRES in center, but that would be really a large effort.

Line 228-229: *"cumulative melt shows a tidal signal with amplitudes of ~ 1cm within 12h around the low-pass filtered cumulative melt."* Can you distinguish how the melt rate is related to the tidal signal? When is the largest melt rate?

This has been answered above already.

Line 233-234: "*We found evidence for a clear accordance of the strain in the upper ice column with the tidal signal as recorded by GPS measurements.*" How does the tide impact strain within the ice column? These datasets are from different time periods – how are they compared?

You are right that the data sets are from different time periods. The accordance we found was based on the frequency spectrum in both datasets and not on the direct comparison of the signals itself.
The tides impact the strain due to tidal bending as the site was located near the grounding line. Unfortunately, noise prevents a clear analysis of the strain distribution over depth.

Line 238-239: *"Consequently, we infer that strain in the lower part compensates the one in the upper part and there is only a small variation of basal melt on tidal time scales."* I don't understand this. What is happening within the ice column? What is the sign of the strain in the upper and lower portions? What physical processes lead to these values?

The sign in the upper and lower portion is opposite, if one extends, the other contracts. We suggest bending to be the mechanism behind.

Line 260-261: *"there is no justification to expect a priori the deformation to be small for simulation times of more than 200a."* The deformation is induced by melt rate and accumulation only? Therefore this is limited by the magnitude of these terms?
No, the term "deformation" here also includes the viscous flow of ice. We rephrased the termination to make it clear for all readers to:
The model comprises non-linear strain theory, as there is no justification to expect a priori the simplified, linearized strain description for simulation times longer than 200a (Haupt 2000).

Line 275: y-direction – what does this correspond to? Along-flow? Vertical?

y-direction is the direction along flow. We rephrase this sentence to make the assumption of plane strain more clear.

Line 306: *"After the spin-up, the width W(t0) of the simulated geometry is 10km."* Is the initial width something you vary as part of the spin up process? Assuming that the width is not fixed, how does this change during the simulation? Is it similar to the width of the embayment?

That is correct, the width of the computational domain is not fixed. We prescribe a certain horizontal displacement (see eq.11) computed by the observed vertical displacement assuming incompressibility and a nearly constant ice thickness. Yes, your explanation is right, the flow of ice through the embayment is represented by this. We reformulated the paragraph explaining the derivation of the horizontal displacement and hope that it will be more clear to the reader in the revised version.

Line 309-310: *"Short-term forces like the time-varying climate forcing as well as the lateral extension or compression demand the usage of a viscoelastic instead of a viscous model to simulate the temporal evolution of the basal channel."* In your model are these short-term forcings? The change in the imposed melt rate is fairly slow (maximum melt from 3 m/yr to 0 m/yr in 250 yr). You're not using the annual variability from your time series of ApRES measurements as forcing?

No, we do not use an annual variability from the ApRES. However, the characteristic Maxwell time is nearly half a year in our case and hence forces changing every year would require a viscoelastic consideration as the elastic response is not negligible for the temporal evolution of the basal channel. We want to emphasise that we do not intend to represent seasonality in our simulations.

Line 322-323: *"the ice thickness OE increases due to the prescribed displacement at the lateral boundaries."* Is this due to the fact that the flow regime is compressive here and that the lateral boundaries are moving towards the centre of the channel? If so, it would be clearer to say this explicitly.

Yes, the prescribed displacement leads to compression meaning that the lateral boundaries move towards the centre of the channel.

Line 330-331: *"This match confirms that present day melt rates would not lead to the observed channel evolution over 250a."* How different is this result using the viscoelastic model to that using the simple advection assumption, eq (5)?

This is shown in Fig. 3 and discussed in line 211-219.

Line 343-344: *"Above the channel, the surface elevation is first overestimated by 4m at the end of the spin-up."* On first reading I thought; you can't really say that this is an over estimation as your spin up produced this initial geometry, and therefore couldn't you change your spin up to more closely match this initial geometry? On closer reading I realised you have made a distinction between surface elevation and ice thickness. It would be good to make this clear. i.e. "While ice thickness is in good agreement, surface elevation..."

Thank you for this suggestion, we do that in the revised version.

Line 356-357: *"At the position of the furthest upstream pRES observations we can see from the seismic IV profile that the influence of the grounding line has not completely vanished."* What exactly do you mean by this? What features are you referring to? Could this also be a result of incorrect assumption for density?
Is this based on the height of the ice surface above sea level and buoyancy? If so, can the ice density here be different too?

This is not only due to uncertainties in density, but that this location is still in the hinge zone, which is confirmed by interferometry, too. For comparison, in Hofstede et al. (2021) the location of seismic IV is shown superimposed on an interferogram. However, we agree that our text is confusing and we rephrase the text accordingly in the revised version.

Line 359-360: *"Hence, simulations carried out using a higher SMB within the channel would result in better agreement with the observed values of hTDX."* Because higher SMB implies a larger firn column and reduced mean density?

It is not the mean density, but just simply the effect of the motion of the upper surface. If in each time step that is computed the correct/real SMB would be added, the entire ice thickness would evolve more realistically. But the SMB forcing from the regional climate does not resolve the melt channel (which is understandable), whereas in reality, snow drift may easily lead to higher SMB within such a topographic feature.

Line 367-368: *"The generally good agreement of the simulated displacements outside the channel comes from tuning ux at the lateral boundary to match uz from the pRES measurements at OE.*" Is it possible to investigate the influence of gradients in both ux and uy, (i.e. exx and eyy) seeing as compressive exx would increase closure of the channel, while extensive/compressive eyy would thin/thicken whole shelf.
Unfortunately, we do not have any strain observations in the along-flow direction. Surface velocities derived from remote sensing are not accurate enough to get the information of extension or compression in the flow direction. For the viscoelastic model, we assume plane strain conditions, thus no compression or extension in the y-direction and hence we can convert the vertical strain into horizontal strain in the across-flow direction. The thickness of the modelled ice shelf fits quite well to the observed ice thickness for each cross-section, therefore, we feel confirmed that the ice thickness does not change much due to the along flow regime.

Line 397-398: *"We thus do not find any evidence that such channels are a cause for instabilities of ice shelves as suggested by Dow et al. (2018)."* Dow et al., (2018) suggests thinner ice, at along-flow channels, may act as initiation sites for fractures perpendicular to flow, which would still be the case unless the channel completely closes.

We think there are several points to be discussed here: (i) do we find evidence that this channel could lead to instabilities, (ii) can such channels initiate cracks along their flanks, (iii) do cracks along the flanks lead to instability.

(i) We did not find any cracks in the area of the melt channel, neither in high resolution SAR imagery in ascending and descending mode, nor while driving twice with a skidoo traverse over this area.

(ii) The initiation of cracks on flanks is definitely possible and has been found at many occasions that are associated with basal crevasses. In that view, both are topographic features meaning if the ice is thinner due to a basal crevasse or a melt channel does not matter for looking at cracks at the surface for a moment. Depending on the stresses at these flanks cracks do appear.

(iii) Does that mean that any basal crevasse leading to cracks on the surface at the flanks lead to instability? A clear no to that. We have ice shelves like Jelbartisen that contain numerous such features (to mention just one) and they are not a sign of instability. Actually, not even every calving event is initiated by those cracks. Furthermore, most shear margins create massive crevasse zones - which do have different orientations to flow than a cracks at a melt channel - but none of those is the cause for ice shelf instability. Fimbulisen is a really nice example here.

So to summarize, we do not find evidence that such cracks are existing in our study area, we are aware of many other incidences where cracks are formed that also do not lead to instability. However, if there is an oceanographic mechanism, or surface melt, or whatever, that not only keeps such a feature open, but enhances and widens it, this could possibly be a weak zone and may lead to instability, we just found no evidence for that.

Line 399 – 402: I agree. It would be good to note somewhere that generally ice shelves comprise of mainly extensive ice flow regimes. The compressive regime within this study area seems to stem from the fact that the ice from Support Force Glacier runs into the main body of the Filchner-Ronne Ice Shelf directly opposite to the pinning point of Berkner Island.

Yes, that is a good point and we incorporate this into the revised version. It may be the case in numerous other locations, too, with similar settings, but there are also numerous extensive flow regimes right from the grounding line on.

Line 410-411: *"However, our model results suggest that the mismatch between the past melt rates needed to explain the observed channel geometry and those that were observed applies only to the channel, and not to the ambient ice."* Ocean conditions at the grounding line may trigger melting and formation of plume/focused melting in the channel. What is the along-flow profile in ice thickness from the grounding line? Seismic 1? Is the grounding line considerably deeper? Could we expect variability there to impact just the channel and not the ambient ice downstream?

As we stated before, we do not have a radar or seismic profile that goes along the channel. All seismic data is presented in Hofstede et al. (2021) and we will refer the reader more often to that paper in the revised version.

It remains unclear what the reviewer means with 'grounding line' deeper. The ice base having a higher draft than in our survey area? The channel to be deeper? The channel was narrower and deeper incised into the ice at the grounding line, see Hofstede et al. (2021), Figure 6.

Subglacial discharge could definitely play a role in a change of the channel geometry upstream, but this would have an impact on the melt rates and melt rate change is what we infer from our results.

Line 439-441: *"The simulated geometry change is mainly due to the elastic response to thinning by basal melt and ice accumulation. Any purely viscous simulation would overrate the deformation."* It would be good to highlight this result with a figure that demonstrates this. Can this difference be quantified?

Yes, we can quantify this (now), and we will show this in more detail in the revised version. This was also a point made by the other reviewer and we have answered there in more detail. It is not as simple to do as for linear strain theory, but we found a way.

Line 444-445: *"The elevation difference is most likely caused by the constant density that we used for the simulations, as the ice thickness matches well."* Does this geometry mismatch lead to a difference in stresses?

It is fair to assume that a mismatch in ice thickness is always leading to a stress change, as thickness matters for any volume forces, such as gravity.

Line 452-453: *"first few cross-sections still being influenced by the hinge zone."* This is also where highest channel melt rates are. Would this have an impact?

At the moment, the melt rates are constant for the spin-up. If the melt rates would be higher at the grounding line we would need a thicker initial ice shelf. This is necessary to counteract the higher basal melt rates and reach the observed seismic geometry profile IV after the spin-up. But it is worth to note, that still this is 'only' a spin-up. It would matter, if we would want to draw conclusions on stresses, deformation, melt-rates etc between the grounding line and our first cross-section of measurements, but we only do a spin-up to have a good initial state.

Line 456-461: Also necessary to know spatial variation in ice density to infer thickness from surface elevation.

Yes and we think it would be best, if we could survey ice thickness and surface elevation with an airborne campaign and to derive the mean density from that. But we would also be curious how the density-depth profile is different inside the channel than outside, so two shallow firn cores would also be nice, actually.

Line 466-467: *"The channel diminishes because the reduced melt rate is unable to maintain the channel geometry against viscoelastic deformation."* It would be good to include a figure that demonstrates this.

You raised this point in the conclusion section. But there, we do not think we should include references to figures. We, therefore, incorporate more references to figures of the viscoelastic modelling in the discussion section and added an additional sentence to capture your remark already in the discussion.

Points from the attached pdf document of Reviewer#2

Many, but not all, of these points were also included in the text above. Where we answer the exact same point above, we only write 'Answered above'. The two remaining points are answered in detail below.

Line 11/12: Good point! Does this channel completely close? If not, it may still act as an initiation site for fracturing (Dow et al., 2018)

Answered above.

Line 39/40: I'm not sure what you mean here. Initially I thought you were suggesting that the horizontal melt rate is 0.82 m/a (i.e. channel is growing wider). But when you mention enhanced melt inside the channel it suggests you mean that outside of the channel the melt rate is 0.82 m/a.

Answered above.

Line 44: In relation to the previous sentence, once water is super-cooled it can no-longer melt? Maybe just need to rewrite this and previous sentence so that it is consistent.

Answered above.

Line 49/50: Maybe add detail of the related time period here for those unfairly with tides. (i.e. approximately 12.5 hr)

Answered above.

Line 65/66: What is the corresponding Maxwell Time?

Answered above.

Line 82/83: Separate time periods? How are we meant to interpret these data?

Answered above.

Line 155/156: Good to remind reader here that measurements are taken every 2hr.

Answered above.

Line 203: big jump around 750 m

Answered above.

Fig. 2: Only first two locations at centre of channel have larger melt rates than outside channel. Maximum melt outside channel.

We are not sure what exactly the reviewer expects from us here.

Line 233/234: But this is from a different time period? More specifically, what is the nature of this agreement?

Answered above.

Line 238/239: I don't really understand this, in terms of what is actually going on within the ice column. What is the sign of the strain in the upper and lower portions? What physical processes lead to these values?

Answered above.

Line 261: Deformation is induced by melt rate and accumulation? Therefore this is limited by the magnitude of these terms?

Answered above.

Line 323/324: Or rather that the along-flow regime is compressive.

Answered above.

Line 330/331: How different is this to the simple advection assumption, eq (5) ?

Answered above.

Line 343/344: Can't really say that this is an over estimation as your spinning up to reproduce this initial geometry. Could you change your spin up to more closely match this initial geometry?

Answered above.

Line 352/353: I don't understand this sentence

Yes, we agree this was phrased confusing. In the revised version we make this clearer.

Line 356/357: Is this based on the height of the ice surface above sea level and buoyancy? If so, can the ice density here be different too?

Answered above.

Line 359/360: Because higher SMB implies a larger firn column and reduced mean density?

Answered above.

Line 392: New paragraph here

Very good suggestion - will be followed for the revised version.

Line 398: Dow et al., (2018) suggests thinner ice, at along-flow channels, may act as initiation sites for fractures perpendicular to flow.

Answered above.

Line 400: I agree. It would be good to note somewhere that generally ice shelves comprise of mainly extensive ice flow regimes. The compressive regime within this study area seems to stem from the fact that the ice from Support Force Glacier runs into the main body of the Filchner-Ronne Ice Shelf directly opposite to the pinning point of Berkner Island

Answered above.

Line 410/411: Ocean conditions at grounding line may trigger melting and formation of plume/focused melting in the channel. What is the along-flow profile in ice thickness from the grounding line? Seismic 1?

Answered above.

Line 435: What difference does the elastic component make to the results?

We will include in the revised version a detailed figure and discussion of it and what difference the elastic component makes. The contribution of the elastic component changes with time and is likely to be most important between the grounding line and where our study area starts, but we will show in detail how large the contribution is along the distance we simulate here.

Line 439-441: It would be good to highlight this result with a figure that demonstrates this. Can this difference be quantified?

Answered above.

Line 444/445: Does this geometry mismatch lead to a difference in stresses?

Answered above.

Line 452/453: This is also where highest channel melt rates are. Would this have an impact?

Answered above.

Line 459: Also need to know ice density to infer thickness from surface elevation.

Answered above.

Line 466/467: It would be good to include some more results/figures that highlight this point.

Answered above.